

**Missions towards NEAs  
with Departure from Lagrangian Points L4 and L5**

Trajectory Optimization



Candidate:  
**Stefano De Santi**

Supervisor:  
**Prof. Lorenzo Casalino**

Co-Supervisor:  
**Prof. Michèle Lavagna**



# Acknowledgement

My deepest gratitude to my *Mom and Dad*, for having supported me in all the possible ways a person can be supported during these years.

A heartfelt thanks to *prof. Lorenzo Casalino*, for his disponibility and priceless advices, without whom I would not have managed to accomplish this work.

Let me thank *Andrea, Edoardo, Fabio* and *Giacomo*, my travel companions, without whom my experience at PoliTo would have been much more boring.



# Contents

<b>Introduction</b>	<b>1</b>
<b>1 Near-Earth Asteroids</b>	<b>3</b>
1.1 Classification . . . . .	3
1.2 Hazard . . . . .	6
1.2.1 The Torino Scale . . . . .	6
1.2.2 The Palermo Scale . . . . .	7
1.2.3 Projects to Minimize the Risk . . . . .	8
<b>2 Orbital Mechanics Elements</b>	<b>9</b>
2.1 The Two-Body Problem . . . . .	9
2.1.1 Constants of Motion . . . . .	10
2.1.2 Orbital Elements . . . . .	11
2.2 The Restricted Three-Body Circular Problem . . . . .	13
2.2.1 Lagrangian Points . . . . .	16
2.3 Interplanetary Missions . . . . .	20
2.3.1 Fly-by . . . . .	21
<b>3 Space Propulsion Elements</b>	<b>25</b>
3.1 Overview . . . . .	25
3.1.1 Classification . . . . .	26
3.1.2 Relevant Entities . . . . .	26
3.1.3 Tsiolkovsky Equation . . . . .	29
3.2 Electrical Propulsion . . . . .	30
3.2.1 Generalities . . . . .	30
3.2.2 Electrostatic Propulsion . . . . .	31
<b>4 Indirect Methods for Space Trajectories Optimization</b>	<b>37</b>
4.1 Optimal Control Theory . . . . .	37
4.2 Boundary Value Problem . . . . .	43

<b>5</b>	<b>Problem Definition</b>	<b>49</b>
5.1	Spherical Coordinates . . . . .	50
5.2	State and Adjoint Variables . . . . .	52
5.3	Dimensionless Quantities . . . . .	54
5.3.1	Dimensionless Distance . . . . .	54
5.3.2	Dimensionless Time . . . . .	54
5.3.3	Dimensionless Velocity . . . . .	54
5.3.4	Dimensionless Acceleration and Mass . . . . .	55
5.4	Boundary Conditions . . . . .	55
5.4.1	Departure . . . . .	55
5.4.2	Fly-By . . . . .	56
5.4.3	Arrival . . . . .	57
5.5	Initial Conditions . . . . .	57
5.5.1	Tentative Solution Definition . . . . .	58
5.6	Choice of the Target Asteroids . . . . .	59
5.7	Spacecraft Characteristics . . . . .	61
<b>6</b>	<b>Results</b>	<b>63</b>
6.1	Asteroid 2014 FZ . . . . .	66
6.2	Asteroid 2004 FN8 . . . . .	75
6.3	Asteroid 2012 UE34 . . . . .	80
6.4	Asteroid 2008 TS10 . . . . .	85
6.5	Asteroid 2015 XA379 . . . . .	90
6.6	Asteroid 2016 YE . . . . .	95
6.7	Asteroid 2017 BN93 . . . . .	100
6.8	Final Assessment . . . . .	105
	<b>Conclusion</b>	<b>109</b>

# List of Figures

1.1	Cumulative discoveries of NEAs . . . . .	4
1.2	Classification of NEAs . . . . .	5
1.3	The Torino scale . . . . .	7
2.1	Conic sections . . . . .	11
2.2	Orbital elements . . . . .	12
2.3	The three-body problem frame . . . . .	14
2.4	Lagrangian points . . . . .	19
2.5	Trailing side fly-by . . . . .	22
3.1	Momentum conservation scheme . . . . .	26
3.2	Electric forces acting on different species . . . . .	32
3.3	Gridded ion thruster's scheme . . . . .	35
5.1	Spherical coordinates . . . . .	50
5.2	Velocity components in the horizon plane . . . . .	51
6.1	Asteroid 2014 FZ, major semiaxis evolution: SX departure from L4, DX departure from L5 . . . . .	67
6.2	Asteroid 2014 FZ, eccentricity evolution: SX departure from L4, DX departure from L5 . . . . .	67
6.3	Asteroid 2014 FZ, inclination evolution: SX departure from L4, DX departure from L5 . . . . .	69
6.4	Asteroid 2014 FZ, switching function evolution: SX departure from L4, DX departure from L5 . . . . .	69
6.5	Asteroid 2014 FZ, trajectory: Departure from L4 . . . . .	71
6.6	Asteroid 2014 FZ, trajectory: Departure from L5 . . . . .	71
6.7	Asteroid 2014 FZ, aphelion distance evolution: SX departure from L4, DX departure from L5 . . . . .	73
6.8	Asteroid 2014 FZ, perihelion distance evolution: SX departure from L4, DX departure from L5 . . . . .	73
6.9	Asteroid 2004 FN8, major semiaxis evolution: SX departure from L4, DX departure from L5 . . . . .	76

6.10 Asteroid 2004 FN8, eccentricity evolution: SX departure from L4, DX departure from L5 . . . . .	76
6.11 Asteroid 2004 FN8, inclination evolution: SX departure from L4, DX departure from L5 . . . . .	77
6.12 Asteroid 2004 FN8, switching function evolution: SX departure from L4, DX departure from L5 . . . . .	77
6.13 Asteroid 2004 FN8, aphelion distance evolution: SX departure from L4, DX departure from L5 . . . . .	78
6.14 Asteroid 2004 FN8, perihelion distance evolution: SX departure from L4, DX departure from L5 . . . . .	78
6.15 Asteroid 2004 FN8, trajectory: Departure from L4 . . . . .	79
6.16 Asteroid 2004 FN8, trajectory: Departure from L5 . . . . .	79
6.17 Asteroid 2012 UE34, major semiaxis evolution: SX departure from L4, DX departure from L5 . . . . .	81
6.18 Asteroid 2012 UE34, eccentricity evolution: SX departure from L4, DX departure from L5 . . . . .	81
6.19 Asteroid 2012 UE34, inclination evolution: SX departure from L4, DX departure from L5 . . . . .	82
6.20 Asteroid 2012 UE34, switching function evolution: SX departure from L4, DX departure from L5 . . . . .	82
6.21 Asteroid 2012 UE34, aphelion distance evolution: SX departure from L4, DX departure from L5 . . . . .	83
6.22 Asteroid 2012 UE34, perihelion distance evolution: SX departure from L4, DX departure from L5 . . . . .	83
6.23 Asteroid 2012 UE34, trajectory: Departure from L4 . . . . .	84
6.24 Asteroid 2012 UE34, trajectory: Departure from L5 . . . . .	84
6.25 Asteroid 2008 TS10, major semiaxis evolution: SX departure from L4, DX departure from L5 . . . . .	86
6.26 Asteroid 2008 TS10, eccentricity evolution: SX departure from L4, DX departure from L5 . . . . .	86
6.27 Asteroid 2008 TS10, inclination evolution: SX departure from L4, DX departure from L5 . . . . .	87
6.28 Asteroid 2008 TS10, switching function evolution: SX departure from L4, DX departure from L5 . . . . .	87
6.29 Asteroid 2008 TS10, aphelion distance evolution: SX departure from L4, DX departure from L5 . . . . .	88
6.30 Asteroid 2008 TS10, perihelion distance evolution: SX departure from L4, DX departure from L5 . . . . .	88
6.31 Asteroid 2008 TS10, trajectory: Departure from L4 . . . . .	89
6.32 Asteroid 2008 TS10, trajectory: Departure from L5 . . . . .	89
6.33 Asteroid 2015 XA379, major semiaxis evolution: SX departure from L4, DX departure from L5 . . . . .	91

6.34 Asteroid 2015 XA379, eccentricity evolution: SX departure from L4, DX departure from L5 . . . . .	91
6.35 Asteroid 2015 XA379, inclination evolution: SX departure from L4, DX departure from L5 . . . . .	92
6.36 Asteroid 2015 XA379, switching function evolution: SX departure from L4, DX departure from L5 . . . . .	92
6.37 Asteroid 2015 XA379, aphelion distance evolution: SX departure from L4, DX departure from L5 . . . . .	93
6.38 Asteroid 2015 XA379, perihelion distance evolution: SX departure from L4, DX departure from L5 . . . . .	93
6.39 Asteroid 2015 XA379, trajectory: Departure from L4 . . . . .	94
6.40 Asteroid 2015 XA379, trajectory: Departure from L5 . . . . .	94
6.41 Asteroid 2016 YE, major semiaxis evolution: SX departure from L4, DX departure from L5 . . . . .	96
6.42 Asteroid 2016 YE, eccentricity evolution: SX departure from L4, DX departure from L5 . . . . .	96
6.43 Asteroid 2016 YE, inclination evolution: SX departure from L4, DX departure from L5 . . . . .	97
6.44 Asteroid 2016 YE, switching function evolution: SX departure from L4, DX departure from L5 . . . . .	97
6.45 Asteroid 2016 YE, aphelion distance evolution: SX departure from L4, DX departure from L5 . . . . .	98
6.46 Asteroid 2016 YE, perihelion distance evolution: SX departure from L4, DX departure from L5 . . . . .	98
6.47 Asteroid 2016 YE, trajectory: Departure from L4 . . . . .	99
6.48 Asteroid 2016 YE, trajectory: Departure from L5 . . . . .	99
6.49 Asteroid 2017 BN93, major semiaxis evolution: SX departure from L4, DX departure from L5 . . . . .	101
6.50 Asteroid 2017 BN93, eccentricity evolution: SX departure from L4, DX departure from L5 . . . . .	101
6.51 Asteroid 2017 BN93, inclination evolution: SX departure from L4, DX departure from L5 . . . . .	102
6.52 Asteroid 2017 BN93, switching function evolution: SX departure from L4, DX departure from L5 . . . . .	102
6.53 Asteroid 2017 BN93, aphelion distance evolution: SX departure from L4, DX departure from L5 . . . . .	103
6.54 Asteroid 2017 BN93, perihelion distance evolution: SX departure from L4, DX departure from L5 . . . . .	103
6.55 Asteroid 2017 BN93, trajectory: Departure from L4 . . . . .	104
6.56 Asteroid 2017 BN93, trajectory: Departure from L5 . . . . .	104
6.57 Final mass of the missions as a function of: SX major semiaxis, DX inclination . . . . .	106
6.58 Final mass of the missions as a function of: SX $V_\infty$ at fly-by, DX duration . . . . .	106



# List of Tables

- 2.1 Orbits shape . . . . . 13
  
- 6.1 Chosen asteroids . . . . . 63
- 6.2 Missions towards 2012 UE34, departure from L5 . . . . . 64
- 6.3 Asteroid 2014 FZ, optimal mission characteristics . . . . . 66
- 6.4 Asteroid 2004 FN8, optimal mission characteristics . . . . . 75
- 6.5 Asteroid 2012 UE34, optimal mission characteristics . . . . . 80
- 6.6 Asteroid 2008 TS10, optimal mission characteristics . . . . . 85
- 6.7 Asteroid 2015 XA379, optimal mission characteristics . . . . . 90
- 6.8 Asteroid 2016 YE, optimal mission characteristics . . . . . 95
- 6.9 Asteroid 2017 BN93, optimal mission characteristics . . . . . 100
- 6.10 Missions performance summary . . . . . 108



# Introduction

This thesis aims to describe the physical and numerical aspects of the optimization of missions that, starting from the *Earth-Sun equilateral Lagrangian points  $L_4$  and  $L_5$* , rendezvous with *Near-Earth Asteroids*. An indirect method, based on the *Optimal Control Theory*, is adopted to maximize the payload fraction, thus minimizing the propellant consumption. The analyzed missions use electrical propulsion and leverage an Earth gravity assist manoeuvre, to bring the satellite to the Near-Earth Asteroid orbit with the smallest propellant throughput. The reference mission considers CubeSats that could be left at the starting Lagrangian point as a piggyback of a larger primary spacecraft. Leveraging the advantageous starting position and its inherent stability, the satellites could wait for the optimal time to begin their mission.

The interest in space missions involving the equilateral Lagrangian points is expected to grow in the near future. In fact, these points represent a strategic location both for space observation and, as considered in this thesis, for missions towards Near-Earth Asteroids departure. Among these small bodies there is a huge number of *Potentially Hazardous Objects* —PHOs—, which may impact the Earth with serious consequences. The study of such objects is the first crucial step for the risk mitigation of such an undesired event. The rendezvous with a PHO is essential to study the properties of the body and to monitor its orbit characteristics. Only with the aforementioned inspections it is possible to evaluate the risk connected to the eventual impact of the object and to define the necessity for an active intervention to modify its orbit. It comes without saying that the optimization of trajectories towards Near-Earth Asteroids is of extreme importance, given the considerations highlighted. In this thesis the absolute importance of missions towards Near-Earth Asteroids has been combined with the trend of exploiting the advantageous location of the equilateral Lagrangian points.

Firstly, an overview of the characteristics of Near-Earth Asteroids is carried out. In second place, the essential elements of orbital mechanics and space propulsion, necessary to fully understand the analyzed problem, are recalled. Then, the general characteristics of indirect methods of space trajectories optimization, exploiting the Optimal Control Theory, are described. Thus, it is possible to formulate the problem and how such theory can be applied to its solution. In the end, the results are reported.



# Chapter 1

## Near-Earth Asteroids

*"We used to look up at the sky and wonder at our place in the stars, now we just look down and worry about our place in the dirt"*  
— Interstellar

Since this work concerns the optimization of trajectories that rendezvous with Near-Earth Asteroids, it is crucial to give an overview of such bodies. In this Chapter will be introduced the characteristics of these small objects, from their physical and orbital properties to the danger they represent, which is the main reason for the relevance of missions towards them.

*Near-Earth Asteroids*, or NEAs, are particular asteroids whose orbit is relatively close to the Earth's one. Some of these asteroids represent a threat as their orbit intersects the one of our planet, creating the risk for celestial impact. Most of these asteroids are relatively small, with diameter inferior to one kilometer, but they are a huge number: more than twenty thousands are the ones known up to now, as it can be inferred looking at Fig. 1.1.

From a statistical point of view, these objects can exist in their near-Earth orbit only for some tens of millions of years. As a matter of fact, sooner or later they either collide with one of the inner planets or are drifted out of the solar system through gravitational interaction — swing-by — with the same planets. Nonetheless, the number of NEAs does not substantially change over time since it is continuously increased with a supply of new asteroids coming from the main belt.

### 1.1 Classification

As already introduced, NEAs are asteroids drifted away from the main belt by gravitation interactions with Jupiter. Four main categories of NEAs exist, and they are classified on the basis of the characteristics of the orbit. The four classes are:

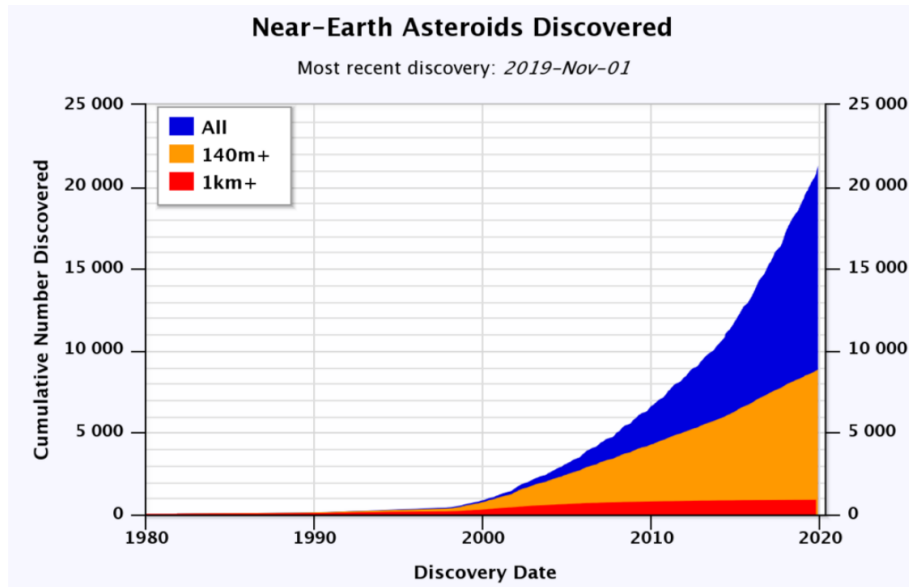


Figure 1.1: Cumulative discoveries of NEAs

- *Atras*

Atras are asteroids with orbit completely internal to the Earth's one. In particular, if  $a$  is the major semiaxis of the NEA's orbit and  $r_A$  is the aphelion distance, Atras' orbits are characterized by:

$$r_A < 0.983 \text{ AU} \quad \longrightarrow \quad a < 0.983 \text{ AU}$$

- *Atens*

Atens are characterized by:

$$r_A > 0.983 \text{ AU} \quad \text{and} \quad a < 1 \text{ AU}$$

Thus, their orbit is smaller than the Earth's one and crosses it.

- *Apollos*

Apollos are characterized by:

$$r_P < 1.017 \text{ AU} \quad \text{and} \quad a > 1 \text{ AU}$$

where  $r_P$  is the perihelion distance. It is worth highlighting that 1.017 AU is the Earth's orbit aphelion distance.

- *Amors*

Amors are asteroids whose major semiaxis lies between the Earth's one and the Mars's one. Mathematically:

$$1.017 \text{ AU} < r_P < 1.3 \text{ AU} \quad \longrightarrow \quad a > 1.017 \text{ AU}$$

thus, Amors' orbits do not cross the Earth's one. Since, Amors often cross Mars's orbit, Mars's satellites —Demos and Foibos— may be Amor asteroids captured by the red planet's gravity field.

A graphical representation of typical orbits of Atens, Apollos and Amors is reported in Fig. 1.2.

Since Atiras and Amors do not intersect Earth's orbit, they do not represent a threat for mankind. The biggest risk of impact comes from asteroids belonging to Aten and Apollo categories. These could be *Potentially Hazardous Objects* since their orbit crosses the Earth's one. To be regarded as PHOs their *Minimum Orbit Intersection Distance* —MOID— shall be lower than 0.05 AU and their diameter has to be greater than 140 m. Clearly, not all the PHOs have the same degree of dangerousness, thus it is necessary to evaluate it, introducing a measuring scale.

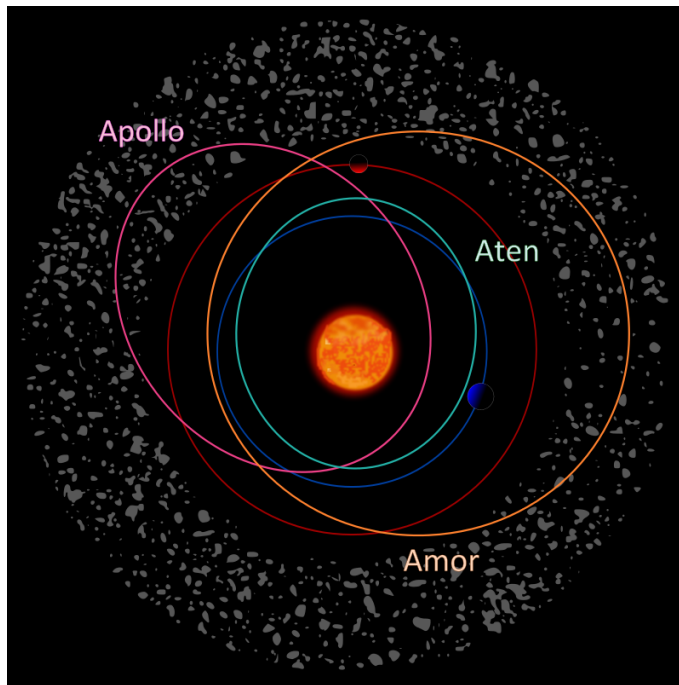


Figure 1.2: Classification of NEAs

## 1.2 Hazard

The attention to the possibility of a catastrophic impact with an asteroid, did rapidly grow after the formulation of the hypothesis that a similar impact caused the mass extinction of the Cretaceous-Paleogene. Such an event may find its cause in the impact of a 10 km asteroid in the Yucatan peninsula, 66 millions years ago, thus resulting in the extinction of dinosaurs, who had been dominating Earth for more than 180 millions years.

Statistically, asteroids impacts are not such rare events, but fortunately they rarely are catastrophic. In particular:

- *Small impacts*: impacts characterized by energy inferior to 1 kiloton happen almost once a month. For comparison, the asteroid that probably caused the extinction of dinosaurs had an energy equal to 190,000 gigatons.
- *1 km impacts*: impacts with asteroids with diameter up to 1 km statistically happen every million years.
- *5 km impacts*: impacts with asteroids with diameter up to 5 km statistically happen every 10 million years.

### 1.2.1 The Torino Scale

The Torino scale is a method for the classification of the impact danger related to NEAs and near-Earth comets. It combines statistical probability with the entity of the potential damage—connected to the kinetic energy of the object—, in order to convey immediately the dangerousness of an eventual impact. Given its inherent qualitative nature, the Torino scale is useful for conveying the concept to public opinion, but it is not used by astronomers. As a matter of fact, in the scientific community it is largely replaced by the Palermo scale, which is more complex and technical.

As can be inferred looking at Fig. 1.3, the Torino scale is based on values ranging from 0 to 10: only natural numbers are used, thus no decimal appears in the levels of hazard. A NEA designed with the level 0 has either too little associated kinetic energy to create any sort of damage or too low probability to impact. On the other hand, a 10 level NEA is certain to impact and the consequences would be catastrophic. In particular:

- *White: Level 0*

**No hazard:** The likelihood of impact is zero, or the body is so small that it would be burnt up in the atmosphere.

- *Green: Level 1*

**Normal:** Usual event corresponding to routine discoveries.

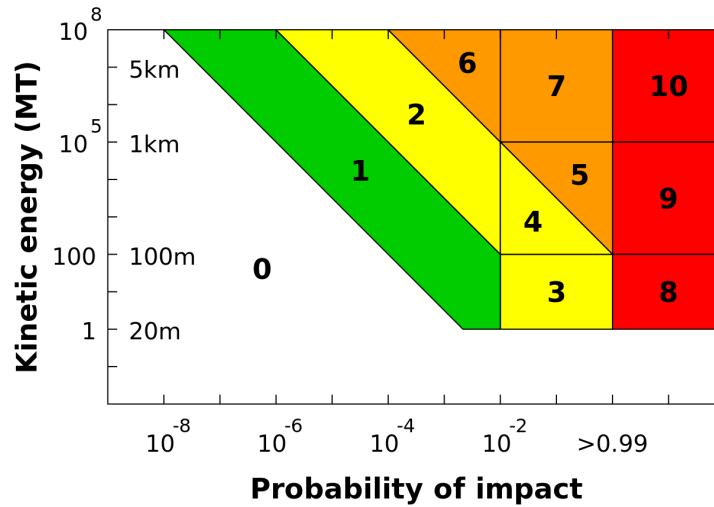


Figure 1.3: The Torino scale

- *Yellow: Levels 2 3 4*

**Meriting astronomers' attention:** NEAs that shall be monitored and, if no threat is highlighted, they may be de-classified as Level 1 objects.

- *Orange: Level 5 6 7*

**Threatening:** Close encounter with relatively big objects with still not certain probability of impact.

- *Red: Level 8 9 10*

**Certain collision:** The impact is certain, and the consequences may range from tsunamis — if close offshore— to a global catastrophe that may destroy civilization and the world as we know it.

No object has ever been ranked with a Level higher than 4 and, up to now, there is not a single object with a Level different from 0.

### 1.2.2 The Palermo Scale

The Palermo scale is a logarithmic scale that, as already introduced, is used by astronomers to evaluate the threat deriving from an impact with a near-Earth object. In fact, it is more quantitative and technical than the already described Torino scale.

The value connected to an asteroid is  $P$  and is derived as follows:

$$P = \log \frac{p_i}{T f_B}$$

where  $\log$  is the logarithm with base 10,  $p_i$  is the probability of collision,  $T$  is the time in years and  $f_B$  is the background impact risk defined as:

$$f_B = \frac{3}{10} E^{-\frac{4}{5}}$$

where  $E$  is the energy related to the impact, measured in megatons.

Thus, a value  $P = 0$  is related to a risk equivalent to the background risk, while  $P = 1$  indicates a risk ten times higher than the background one. Clearly, the Palermo scale uses indexes in all the domain of Real numbers.

### 1.2.3 Projects to Minimize the Risk

The fact that an impact with a 1 km NEA would be a catastrophic event for mankind, guided the scientific community to develop a possible system of defence against this possibility.

The first step is the individuation of all the objects big enough to represent a serious threat. Then, different means of defence have been identified, some more feasible than others:

- *Nuclear weapons*

A nuclear bomb may be installed on the surface of the impacting NEA, hence its explosion would deviate the asteroid on another orbit. As a matter of fact, this method is a sort of non-canonic nuclear propulsion. Nevertheless, since some asteroids are no more than an aggregate of several debris, such a method would result in a division of the main asteroid in many meteoroids. Thus, the hazard would only be changed from a single impact, to a rain of meteors—that may cause even more damage to mankind—.

- *Mass driver*

These devices, installed on the surface of the NEA, would collect material from the same in order to throw it away. Thus, the thrust provided by these sort of catapults would drag the NEA away from its impact orbit.

- *Solar sails*

If solar sails are installed on the NEA, their interaction with the solar pressure would change the asteroid's orbit.

- *Surface powder coating*

If the NEA is covered with a powder, the orbit would be deviated leveraging Yarkovsky effect.

- *Rocket*

Perhaps, this is the simplest solution in terms of concept. A rocket may intercept the NEA and then drive it away.

## Chapter 2

# Orbital Mechanics Elements

*"Or perhaps we've just forgotten that we are still pioneers. And we've barely begun.  
And that our greatest accomplishments cannot be behind us, because our destiny lies  
above us"*

— Interstellar

Before entering the core topic of the thesis, it is important to summarize some concepts that will be the basis of the analyzed problem. In this Chapter, are presented the basic knowledge and the physical aspects of the space flight mechanics, which further in this work will be taken for granted. In particular, the principal concepts concerning the Two-Body Problem and the Three-Body Circular Problem will be introduced. Then an overview of interplanetary missions will be given, with a focus on the heliocentric phase and the fly-by manoeuvre.

### 2.1 The Two-Body Problem

The *Two-Body Problem* is the starting point of every orbital mechanics problem. As can be inferred from its definition, it describes the motion of two bodies due uniquely to their mutual gravitational interaction. The nature of this interaction has been already defined by Newton in its masterpiece: *'Philosophiae Naturalis Principia Mathematica'*, back in 1687. The gravitational force is a central and attractive interaction, proportional to the product of the two involved masses and indirectly proportional to the square of the distances of the two bodies:

$$\mathbf{F} = G \frac{mM}{r^2} \frac{\mathbf{r}}{r} \quad (2.1)$$

where  $G = 6.67 \cdot 10^{-11} \frac{m^3}{kg s^2}$  is the *gravitational constant* and  $\mathbf{r}$  is the distance vector from the mass  $M$  to the mass  $m$ .

This problem is here presented in its simplified form, based on the assumption that the smaller body has a negligible mass if compared to the bigger one. Thus, the new

problem is often defined as the *Restricted Two-Body Problem*, and can be applied to systems such as Earth-Satellite or Sun-Earth. The R2BP's hypothesis can be summarized as follows:

- *Spherical Symmetry* of the mass distribution
- *Homogeneity* of the mass distribution
- *Punctiform masses* concentrated in the centers of the bodies
- Only gravitational forces
- $M \gg m$

These assumptions lead to the definition of the following equation of motion:

$$\ddot{\mathbf{r}} = -\frac{\mu}{r^2} \frac{\mathbf{r}}{r} \quad (2.2)$$

where  $\mu = GM$  is the *gravitational parameter* of the principal body. This equation is not solved here for brevity, but leads to the following expression for the distance between the two bodies:

$$r = \frac{h^2}{\mu} \frac{1}{1 + e \cos \nu} \quad (2.3)$$

The physical quantities in the expression above will be defined in the next paragraph. It is important to highlight that the equation above generates trajectories which follow the shape of conic sections. These are represented in Fig 2.1.

### 2.1.1 Constants of Motion

In the R2BP, it can be demonstrated that some physical quantities are constant throughout all the motion, if no further interactions arise. In particular, the two constants of motion are:

- *Angular Momentum*

$$\mathbf{h} = \mathbf{r} \wedge \dot{\mathbf{r}} \quad (2.4)$$

Since the angular momentum is constant both in module and orientation, the motion followed by the smaller body around the primary one in the R2BP is a planar trajectory.

- *Mechanical Energy*

$$E = \frac{v^2}{2} - \frac{\mu}{r} \quad (2.5)$$

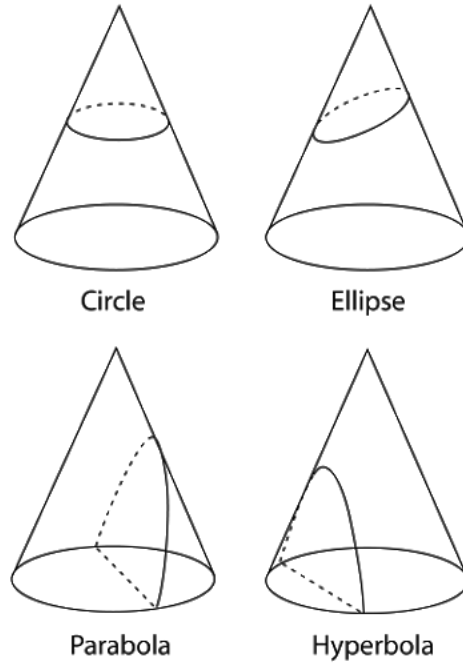


Figure 2.1: Conic sections

### 2.1.2 Orbital Elements

The orbit and the position of a body, in the R2BP, can be completely defined through 6 parameters, known as the *Classical Orbital Elements*. There are other means for the representation of the trajectory of a body, but they fall outside the purposes of this work. The orbital elements are the following:

- *Eccentricity*  $e$

Which is connected to the form of the orbit. In particular, it can be demonstrated through the analysis of the conic sections' geometry, that the Tab. 2.1 describes the families of trajectories divided by the value of their eccentricity.

- *Major Semiaxis*  $a$

Which is connected to the dimension of the orbit. More precisely, the major semiaxis is directly connected to the energy of the orbit. In particular, it can be demonstrated, unifying the energetic analysis to the geometric one that:

$$E = -\frac{\mu}{2a} \quad (2.6)$$

Tab. 2.1 describes also the relation between  $a$  and the trajectory.

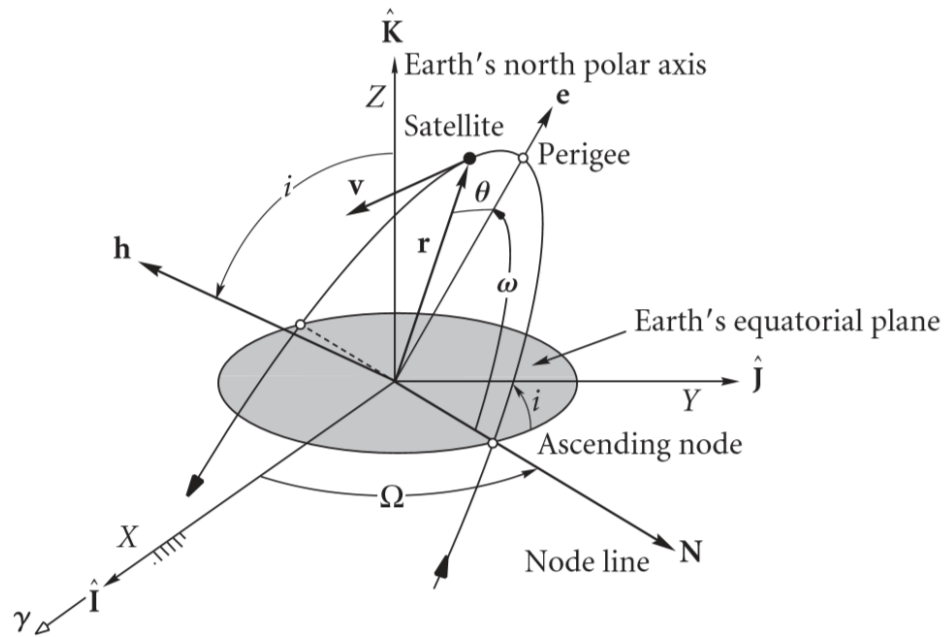


Figure 2.2: Orbital elements

- *Argument of Periapsis  $\omega$*

Which defines the position of the periapsis, which is the closest point of the trajectory to the principal body.

- *Right Ascension of Ascending Node  $\Omega$*

The RAAN gives the position of the ascending node of the trajectory: the point where the secondary body enters the region of the positive values of the coordinate  $z$ .

- *Inclination  $i$*

It is obviously the inclination of the orbit's perifocal plane, with respect to a fixed direction.

- *True Anomaly  $\nu$*

It gives the angular position of the secondary body, along the orbit, from the periapsis. In the R2BP, this is the only variable element, while all the others are constant.

It is easier to understand the orbital elements looking at Fig. 2.2. In the figure the orbital elements are defined for a satellite orbiting around Earth. Nonetheless, their definition can be broadened to any secondary body in revolution around a primary one much bigger.

$E$	$a$	$e$	Orbit
$< 0$	$> 0$	$e = 0$	Circle
$< 0$	$> 0$	$0 < e < 1$	Ellipsis
$0$	$0$	$e = 1$	Parabola
$> 0$	$< 0$	$e > 1$	Hyperbola

Table 2.1: Orbits shape

## 2.2 The Restricted Three-Body Circular Problem

Since the scope of this thesis is to analyze a trajectory which has the departure in a Lagrangian Point, it is crucial to define such an entity. In order to explain what a Lagrangian point is, the *Restricted Three-Body Circular Problem* has to be defined. The hypothesis on which the described model relies are the following:

- *Three Bodies*: two of which are principal bodies, while the third is negligible, in terms of mass. Thus, the third body does not affect the other two with its gravitational interaction.
- *Circularity*: the principal bodies are characterized by circular orbits around the center of mass of the system.

Systems that can be modeled under the hypothesis of the R3BCP are Earth-Moon-Satellite or, as considered in this thesis, Sun-Earth-Satellite. The R3BCP scheme is represented in Fig. 2.3. It is useful, to define two new constants:

$$M = m_1 + m_2$$

$$\mu = \frac{m_2}{M}$$

The positions of the principal bodies, with respect to the center of mass of the system, can be easily derived:

$$m_1 = \begin{bmatrix} -\mu r_{12} \\ 0 \\ 0 \end{bmatrix}$$

$$m_2 = \begin{bmatrix} (1 - \mu)r_{12} \\ 0 \\ 0 \end{bmatrix}$$

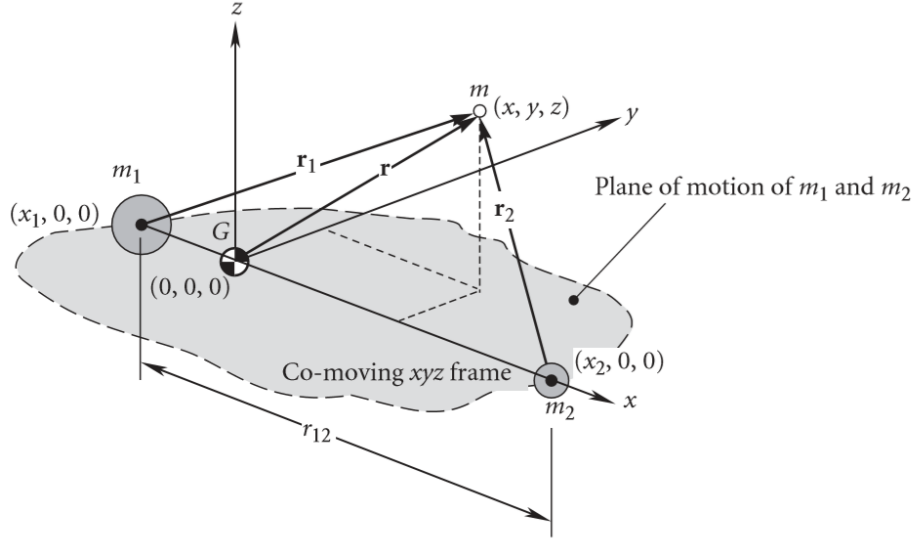


Figure 2.3: The three-body problem frame

Thus, the positions of the secondary body, with respect to the primary ones, can be defined as follows:

$$\mathbf{r}_1 = \begin{bmatrix} x + \mu r_{12} \\ y \\ z \end{bmatrix} \quad (2.7)$$

$$\mathbf{r}_2 = \begin{bmatrix} x - (1 - \mu)r_{12} \\ y \\ z \end{bmatrix} \quad (2.8)$$

The angular velocity of the system can be defined as well:

$$\omega = \sqrt{\frac{GM}{r_{12}^3}} \quad (2.9)$$

Since the reference frame is rotating, it is not inertial. Thus, to write down the equations of motion, it is important to take into account the Coriolis acceleration and the centripetal one. The vectorial form of the *Equations of motion* is:

$$\ddot{\mathbf{r}} + \boldsymbol{\omega} \wedge (\boldsymbol{\omega} \wedge \mathbf{r}) + 2\boldsymbol{\omega} \wedge \dot{\mathbf{r}} = \frac{1}{m} (\mathbf{F}_1 + \mathbf{F}_2) \quad (2.10)$$

where:

$$\mathbf{F}_1 = -G \frac{(1 - \mu)Mm}{r_1^3} \mathbf{r}_1$$

$$\mathbf{F}_2 = -G \frac{\mu Mm}{r_2^3} \mathbf{r}_2$$

The equations of motion can be written in the scalar form, expliciting the components on the three coordinates:

$$\ddot{x} - \omega^2 x - 2\omega\dot{y} = -GM\frac{1-\mu}{r_1^3}(x + \mu r_{12}) - GM\frac{\mu}{r_2^3}[x - (1-\mu)r_{12}] \quad (2.11)$$

$$\ddot{y} - \omega^2 y + 2\omega\dot{x} = -GM\frac{1-\mu}{r_1^3}y - GM\frac{\mu}{r_2^3}y \quad (2.12)$$

$$\ddot{z} = -GM\frac{1-\mu}{r_1^3}z - GM\frac{\mu}{r_2^3}z \quad (2.13)$$

the equations of motion can be expressed in a *dimensionless form*, adopting the following substitutions:

$$\boldsymbol{\rho} = \frac{\mathbf{r}}{r_{12}} \quad \longrightarrow \quad \xi = \frac{x}{r_{12}} \quad \eta = \frac{y}{r_{12}} \quad \zeta = \frac{z}{r_{12}} \quad (2.14)$$

$$\tau = t\omega \quad \longrightarrow \quad \frac{d}{dt} = \omega \frac{d}{d\tau} \quad (2.15)$$

Thus, the dimensionless expression is:

$$\xi'' - \xi - 2\eta' = -(1-\mu)\frac{\xi + \mu}{\rho_1^3} - \mu\frac{\xi - (1-\mu)}{\rho_2^3} \quad (2.16)$$

$$\eta'' - \eta + 2\xi' = -(1-\mu)\frac{\eta}{\rho_1^3} - \mu\frac{\eta}{\rho_2^3} \quad (2.17)$$

$$\zeta'' = -(1-\mu)\frac{\zeta}{\rho_1^3} - \mu\frac{\zeta}{\rho_2^3} \quad (2.18)$$

In the Three-Body Problem, the *gravitational potential function* has the following formulation:

$$U = G\frac{m_1}{r_1} + G\frac{m_2}{r_2} + \frac{1}{2}(x^2 + y^2)$$

that can be expressed in the dimensionless form:

$$u = \frac{1-\mu}{\rho_1} + \frac{\mu}{\rho_2} + \frac{1}{2}(\xi^2 + \eta^2) \quad (2.19)$$

Derivating the potential function with respect to the dimensionless coordinates, and substituting the derivatives in the system of the equation of motion, a new form for the equations themselves can be easily derived:

$$\xi'' - 2\eta' = \frac{\partial u}{\partial \xi} \quad (2.20)$$

$$\eta'' + 2\xi' = \frac{\partial u}{\partial \eta} \quad (2.21)$$

$$\zeta'' = \frac{\partial u}{\partial \zeta} \quad (2.22)$$

### 2.2.1 Lagrangian Points

The *Lagrangian Points* are particular positions in the space where gravitational interactions and inertial forces are at equilibrium. Thus, they are characterized by the following set of equalities:

$$\begin{aligned}\xi' &= 0 & \xi'' &= 0 \\ \eta' &= 0 & \eta'' &= 0 \\ \zeta' &= 0 & \zeta'' &= 0\end{aligned}$$

If a spacecraft is in a Lagrangian point, it rotates solidally with the system. Since the center of mass of the system Sun-Earth-Satellite lies underneath the surface of the Sun, the Earth and the spacecraft — if it is in a Lagrangian point — have the same angular velocity around the star, which is actually fixed.

Given the definition of Lagrangian point, the equations of motion for these points become:

$$\frac{\partial u}{\partial \xi} = 0 \tag{2.23}$$

$$\frac{\partial u}{\partial \eta} = 0 \tag{2.24}$$

$$\frac{\partial u}{\partial \zeta} = 0 \tag{2.25}$$

thus, the Lagrangian points are the minimum of the potential function of the Three-Body System.

The only condition that allows to satisfy equation (2.25) is:

$$\zeta = 0$$

Thus, all the Lagrangian points lie in the same plane.

#### Collinear Points

These points are obtained under the following conditions:

$$\zeta = 0 \tag{2.26}$$

$$\eta = 0 \tag{2.27}$$

As can be inferred from their name, these points lie on the same line, which corresponds to the  $x$  axis. There are three collinear points:

- *Lagrangian Point  $L_1$*

It is found imposing:

$$-\mu < \xi < (1 - \mu)$$

and solving the system:

$$\begin{cases} \xi - (1 - \mu) \frac{\xi + \mu}{\rho_1^3} - \mu \frac{\xi - (1 - \mu)}{\rho_2^3} = 0 \\ \rho_1 + \rho_2 = 1 \end{cases}$$

It is characterized by:

$$\rho_2 = \sqrt[3]{\frac{\mu}{3}} \quad (2.28)$$

- *Lagrangian Point  $L_2$*

It is found imposing:

$$\xi > (1 - \mu)$$

and solving the system:

$$\begin{cases} \xi - (1 - \mu) \frac{\xi + \mu}{\rho_1^3} - \mu \frac{\xi - (1 - \mu)}{\rho_2^3} = 0 \\ \rho_1 - \rho_2 = 1 \end{cases}$$

It is characterized by:

$$\rho_2 = \sqrt[3]{\frac{\mu}{3}} \quad (2.29)$$

clearly in the other direction with respect to  $L_1$ .

- *Lagrangian Point  $L_3$*

It is found imposing:

$$\xi > -\mu$$

and solving the system:

$$\begin{cases} \xi - (1 - \mu) \frac{\xi + \mu}{\rho_1^3} - \mu \frac{\xi - (1 - \mu)}{\rho_2^3} = 0 \\ \rho_2 - \rho_1 = 1 \end{cases}$$

It is characterized by:

$$\rho_2 = 2 \quad (2.30)$$

$$\rho_1 = 1 \quad (2.31)$$

The collinear points are spots of unstable equilibrium. Thus, if an external disturbance displaces the satellite from one of these points, it continues to move away from the Lagrangian point itself.

### Equilateral Points

These points are obtained under the following conditions:

$$\zeta = 0 \quad (2.32)$$

$$\rho_2 = \rho_1 = 1 \quad (2.33)$$

As can be deduced by their definition, these points have the same distance from the two masses. They can be retrieved, solving the system:

$$\begin{cases} \xi - (1 - \mu)(\xi + \mu) - \mu[\xi - (1 - \mu)] = 0 \\ \eta - (1 - \mu)\eta - \eta\mu = 0 \end{cases}$$

Therefore, the equilateral points are:

- *Lagrangian Point  $L_4$*

$$\xi = \frac{1}{2} - \mu \quad (2.34)$$

$$\eta = \frac{\sqrt{3}}{2} \quad (2.35)$$

- *Lagrangian Point  $L_5$*

$$\xi = \frac{1}{2} - \mu \quad (2.36)$$

$$\eta = -\frac{\sqrt{3}}{2} \quad (2.37)$$

Thus, they form two equilateral triangles with the two principal masses. As a matter of fact,  $L_4$  rotates around  $m_1$  on the same orbit as  $m_2$  but preceding it of  $60^\circ$ . On the other ends,  $L_5$  follows  $m_2$  of the same angular distance.

The equilateral points are spots of stable equilibrium. If a disturbance arises, the spacecraft moves back to its position.

The position of the Lagrangian points can be better understood looking at Fig. 2.4. In the reality of astrodynamics, if the real system is analyzed — without the hypothesis adopted to simplify it — the Lagrangian points are not punctiform. In fact, they represent an area in which the third body is at equilibrium.

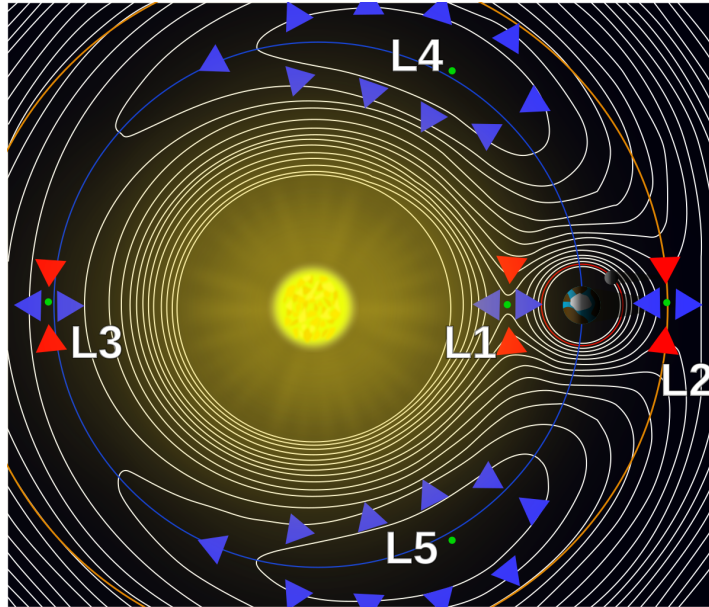


Figure 2.4: Lagrangian points

Considering the three-body system *Sun-Earth-Satellite*:

- $L_1$ : Lies between the Sun and the Earth
- $L_2$ : Lies on an orbit external to the Earth's one and is characterized by the same distance as  $L_1$  from the blue marble.
- $L_3$ : Is the symmetrical position of Earth with respect to the Sun
- $L_4$ : Precedes Earth of  $60^\circ$  on its orbit
- $L_5$ : Chases Earth of  $60^\circ$  on its orbit

The advantages of starting the rendezvous mission from an equilateral Lagrangian point, lie in the possibility of waiting for the most favourable moment for departure, without the need of station-keeping and with the possibility to carry out deep space observations in the meanwhile. Moreover, being already outside the sphere of influence — a concept that will be defined right after — there is no need for an escape manoeuvre, that would be necessary if the departure point was on an Earth orbit.

## 2.3 Interplanetary Missions

In order to study missions towards Near-Earth Asteroids, it is necessary to introduce some basic notions about interplanetary transferts. These are studied under the hypotheses of the *patched conics* method. The interplanetary mission is split into three phases:

- *Escape* from the sphere of influence of the departure body
- *Heliocentric trajectory*
- *Arrival* in the sphere of influence of the target body

The *sphere of influence* of a body is the portion of space around it, in which the spacecraft can be supposed to interact only with the body itself. Thus, when into the sphere of influence of the Earth, the satellite can be studied under the hypothesis of the R2BP, with the planet as the principal body. On the other hand, during the heliocentric trajectory, the spacecraft is outside the sphere of influence of any planet. Thus, the Sun is the principal body, and the spacecraft is subject only to its gravitational interaction. The radius of the Earth's sphere of influence can be calculated as follows:

$$r \simeq \left( \frac{m_{\oplus}}{m_{\odot}} \right)^{\frac{2}{5}} r_{\oplus-\odot} \simeq 10^6 km$$

where  $r_{\oplus-\odot}$  is the mean distance between the Sun and the Earth and  $m_{\oplus}$  and  $m_{\odot}$  are respectively the masses of the Earth and of the Sun.

This dimension, if compared to the extension of the solar system, is negligible. Thus, the patched conics approximation is a relatively accurate model. The crucial aspect of the study of interplanetary trajectories with the patched conics approximation is the relation of the physical quantities at the interface of the three legs, thus when passing out and in the spheres of influence.

The description of the departure phase lies outside the scope of this thesis. As a matter of fact, since the mission's departure point is one of the Lagrangian points, the spacecraft's initial position is already outside the Earth's sphere of influence.

As far as the heliocentric trajectory is concerned, it is strongly affected by the manoeuvre effectuated during its duration. Thus, it is impossible to describe it in a general way. In many pieces of literature, the heliocentric phase is studied as a coasting arc — thus with no propulsion — of a *Hohmann Transfer* between the two bodies. As a matter of fact, this description only fits the approximation of impulsive manoeuvres, that are not considered in this work.

The only point of interest is the phase of arrival at the target body. In fact, since the mission studied in this thesis relies on the *gravity assist manoeuvre*, its definition is crucial.

### 2.3.1 Fly-by

When entering the sphere of influence of a planet, the spacecraft can follow two different scenarios. These are defined by the *impact parameter* of the spacecraft. Its expression, considering an arrival into the Earth's sphere of influence, is:

$$B = \frac{R_{\oplus}}{V_{\infty}} \sqrt{V_{\infty}^2 + 2 \frac{\mu_{\oplus}}{R_{\oplus}}} \quad (2.38)$$

where  $R_{\oplus}$  and  $\mu_{\oplus}$  are respectively the Earth's radius and gravitational parameter, and  $V_{\infty}$  is the spacecraft's *hyperbolic excess velocity*. This is the velocity of the spacecraft at an infinite distance from the planet, thus when the gravitational potential energy is null. Given the dimension of the Earth's sphere of influence with respect to its radius, such velocity is the velocity relative to the Earth, when entering its sphere of influence.

It is important to highlight that a spacecraft with an elliptic orbit around the Sun, when entering the sphere of influence of a planet, has a high relative velocity with respect to the planet itself. Thus, in the sphere of influence, it is characterized by a hyperbolic orbit around the planet. Thus, if  $d$  is the minimum distance of the spacecraft's hyperbolic trajectory around the target body, the possible scenarios are:

- $d < B$

The trajectory leads the spacecraft to impact the target body.

- $d > B$

The spacecraft trajectory does not collide with the target body.

In the second case, the spacecraft can perform two main activities:

- *Capture*

The spacecraft operates a manoeuvre to decrease its velocity, in order to enter an elliptic orbit around the planet.

- *Fly-by*

The spacecraft leverages the velocity of the planet to change its heliocentric velocity, therefore changing its orbit around the Sun. This manoeuvre can be operated without the use of the propulsive system.

As far as the topic of this thesis is concerned, the interest is focused on the fly-by manoeuvres. As a matter of fact, these missions are used to change the heliocentric velocity of the satellite —both in module and direction—, at expense of the velocity of the planet. However, since the satellite's mass is negligible if compared to the mass of a planet, the change of velocity in the planet is totally negligible.

Since NEAs are generally objects with an orbit at an higher energy than the Earth, the focus of this work is on fly-bys connected to a velocity increase.

## Earth gravity assist

The mechanism of the gravity assist fly-by is easily understandable looking at Fig. 2.5. Without going deep into the mathematical aspects, two main changes can be pointed out:

- *Flight path angle*

The angle that the velocity forms with the horizon at the escape is different from the one at the arrival. Thus, the gravity assist manoeuvre allows to change the direction of the velocity, and therefore the inclination of the orbit. This is a crucial aspect since inclination change manoeuvres are very expensive from a propulsive point of view. Leveraging the fly-by of the planet, it is possible to reach the orbit of the NEA —which, in general, is inclined with respect to the Earth’s orbit— saving propellant.

- *Velocity module*

The heliocentric velocity at the escape is higher, allowing to get closer to the NEA’s orbit, which have an higher energy than the Earth’s one.

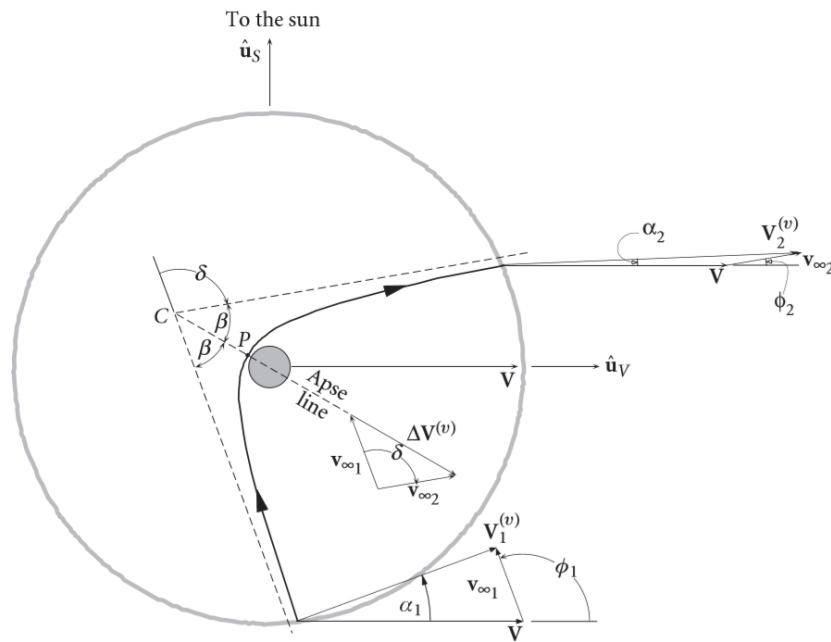


Figure 2.5: Trailing side fly-by

As already said, gravity assist manoeuvres allow to increase and rotate the heliocentric velocity of the spacecraft, and therefore the energy of its heliocentric orbit, with little or no propellant throughput. Looking at Fig. 2.5, one can appreciate that the

hyperbolic excess velocity across the fly-by is constant in the module:  $V_{\infty 1} = V_{\infty 2}$ . In fact, if the engine is not switched on, the fly-by only consists in a rotation of the hyperbolic excess velocity. Since this velocity is vectorially added to the planet's heliocentric velocity to form the heliocentric velocity of the spacecraft, the rotation of  $V_{\infty}$  results in a change in both verse and module of this last quantity across the fly-by. Thus:  $V_1 \neq V_2$ , as can be inferred from the figure.

It is important to highlight that, being the sphere of influence negligible if compared to the heliocentric trajectory, the duration of a fly-by is negligible as well. As a matter of fact, fly-bys will be treated as discontinuities in terms of velocity — but not in mass and position —.



## Chapter 3

# Space Propulsion Elements

*"Newton's Third Law. The only way humans have figured out how to move forward is to leave something behind"*  
— Interstellar

In this Chapter are presented the basic concepts of space propulsion, which are essential for the understanding of the missions analyzed. First a global overview of the principles shared by all the propulsive systems is given, then an insight on electrical thrusters—which are the ones considered for the analyzed missions—is carried out.

As it has been introduced in the preceding Chapter, if no external force is applied to a body in the space, its trajectory is a conic section and is completely defined by the position and velocity of the body itself at a certain time.

As a matter of fact, propulsion can be defined as the capability to generate a force to change the velocity of the spacecraft, thus modifying — or maintaining — the trajectory.

### 3.1 Overview

Although they are based on different physical phenomena, to generate thrust all types of propulsors leverage the *Newton's third law of motion*:

*"When one body exerts a force on a second body, the second body simultaneously exerts a force equal in magnitude and opposite in direction on the first body"*

also known as the action-reaction principle.

Thus, since the space is a vacuum, the only possibility to generate thrust — besides concepts of advanced space propulsion, such as solar and magnetic sails — is to carry onboard something to exchange momentum with: the *propellant*. Clearly, this strongly hinders the capability of motion in space, since the spacecraft can carry only a limited amount of propellant. Once it has run out there is no possibility for the spacecraft to acquire different orbits.

### 3.1.1 Classification

It is possible to categorize space propulsors following different criteria. The first type of classification is based on the purpose of the propulsor itself:

- *Primary propulsion*: it is designed and used in order to change the trajectory of the spacecraft.
- *Auxiliary propulsion*: it is designed and used in order to maintain the desired trajectory, withstanding and contrasting external disturbance actions.

On the other hand, it is possible to classify propulsor on the basis of the energy source used to accelerate the propellant. In particular, three different classes exist:

- *Chemical propulsion*: it exploits a chemical propellant or the reaction between two propellants — a fuel and an oxidizer — to generate thrust.
- *Electrical propulsion*: it exploits electromagnetic phenomena to accelerate the propellant.
- *Nuclear propulsion*: it leverages nuclear power to generate thrust.

### 3.1.2 Relevant Entities

Since all the propulsors leverage the action-reaction principle, it is possible to describe in a general way their behaviour and to introduce some particularly relevant quantities, without specifying the class of the propulsor itself.

It is considered a body on which no external force is applied, thus its behaviour can be studied as a closed system. If this hypothesis is respected, the global momentum must be constant over time.

In a first moment, the body of mass  $m$  is moving with a velocity  $v$ . After an infinitesimal interval of time, the body has expelled a part of its mass: the propellant mass  $dm_p$ . Thus, the body loses a part of its mass but increases its velocity. The increment in velocity is related to the velocity with which the propellant infinitesimal mass is expelled:  $c$ . This is the *effective discharge velocity*. It is worth highlighting that  $c$  is defined with respect to the spacecraft, thus the global velocity of the propellant is  $c - v$ . The scheme of the problem is shown in Fig. 3.1.

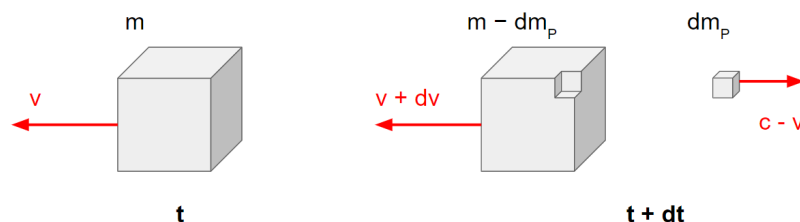


Figure 3.1: Momentum conservation scheme

This said, it is possible to impose the conservation of the total momentum of the system:

$$mv = (m - dm_P)(v + dv) - dm_P(c - v)$$

Carrying out the mathematical operations and neglecting the second degree infinitesimal terms, it is possible to obtain:

$$m dv = dm_P c$$

Taking into account that the propellant is expelled in a continuous and not discrete way, it is possible to define the *propellant flow*:

$$\dot{m}_P = \frac{dm_P}{dt} \quad (3.1)$$

The preceding considerations yield to:

$$m \frac{dv}{dt} = \dot{m}_P c$$

Since the term on the left is the product of mass and acceleration of the body, the term on the right must be the force applied to the body itself, according to *Newton's second law of motion*. This force is nothing but the *thrust*:

$$T = \dot{m}_P c \quad (3.2)$$

with which is possible to express the *thrust power*:

$$P_T = \frac{1}{2} T c = \frac{1}{2} \dot{m}_P c^2 \quad (3.3)$$

which is the power necessary to accelerate the propellant at the velocity that generates a thrust of intensity  $T$ .

It is worth highlighting that the exit velocity is not, in general, equal to the effective discharge velocity. This is due to the fact that, when accelerated in the nozzle the propellant is subjected also to pressure forces. In particular, the portion of propellant that is still inside the nozzle — and therefore still belongs to  $m$  — exchanges a pressure force with the propellant that is already outside. The entity of this force, referred to as *static thrust*, depends on the difference between the exit pressure and the ambient pressure. Thus, the thrust is divided in two terms: a dynamic one — depending on the exhaust velocity — and a static one:

$$T = \dot{m}_P u_e + A_e (p_e - p_0)$$

where,  $u_e$  is the exhaust velocity,  $A_e$  is the exit section of the nozzle,  $p_e$  is the pressure in the exit section and  $p_0$  is the ambient pressure — equal to null in space —. Anyway, from the point of view of the mission analysis there is no interest in knowing how the thrust is divided between dynamic and static. This is the reason why the effective discharge

velocity is defined. As a matter of fact, it is  $c$  that is defined once that the thrust is known — and not vice versa —.

In general, for space propulsors the exit velocity is almost equal to the *effective exhaust velocity*:

$$c = \frac{T}{\dot{m}_P} \quad (3.4)$$

At this point it is worth introducing some other relevant quantities that describe the performances of the propulsor. The first one is the *total impulse*:

$$I_t = \int_{t_0}^{t_f} T dt \quad (3.5)$$

which indicates the total propulsive power of the system. The bigger the total impulse, the higher is the propulsive cost of the mission that the spacecraft may carry out.

With the total impulse it is possible to define the *specific impulse*:

$$I_s = \frac{I_t}{m_P g_0} \quad (3.6)$$

where  $m_P$  is the total propellant mass onboard and  $g_0$  is the gravity acceleration on the Earth's surface. If the thrust is constant:

$$I_t = T \Delta t$$

where  $\Delta t$  is the functioning time of the propulsor.

Considering that if  $T$  and  $c$  are constants, also the propellant flow is:

$$m_P = \dot{m}_P \Delta t$$

Substituting these two expressions in equation (3.6), it is easy to obtain:

$$I_s = \frac{c}{g_0} \quad (3.7)$$

This equation means that, neglecting a constant,  $c$  and  $I_s$  have the same value. As a matter of fact, both the specific impulse and the effective discharge velocity are a measure of the efficiency with which the propellant is used to generate thrust. The higher the value, the more performant the thruster is.

Perhaps, it is easier to understand this crucial concept if the following example is introduced. If a propulsor which generates a thrust of an entity equal to the weight of its propellant mass on Earth is considered, its operative time is exactly the specific impulse. In fact:

$$T = m_P g_0 \quad \longrightarrow \quad I_t = T \Delta t = m_P g_0 \Delta t \quad \longrightarrow \quad I_s = \frac{I_t}{m_P g_0} = \Delta t$$

This means that if two thrusters with the same propellant mass but different specific impulses are compared, the one with the highest specific impulse may:

- Function for the same time but with a higher thrust level
- Generate the same thrust but for a longer time

needless to say it is important to have a high specific impulse. This consideration is even more important if the concepts introduced in the following paragraph are considered.

### 3.1.3 Tsiolkovsky Equation

The Tsiolkovsky equation is perhaps the most important and surely the most iconic equation of space propulsion. As a matter of fact it is often referred to as the *rocket equation*. It relates the ideal propulsive cost of a manoeuvre with the propellant mass it needs to be carried out. The term '*ideal*' means that no losses or external disturbances are taken into account.

The starting point is the definition of the propulsive cost, or more precisely the *characteristic velocity*:

$$\Delta V = \int_{t_0}^{t_f} \frac{T}{m} dt \quad (3.8)$$

which is the variation of the velocity of the body across the manoeuvre. Using equation (3.2), it is possible to express the characteristic velocity as:

$$\Delta V = \int_{t_0}^{t_f} c \dot{m}_P \frac{dt}{m}$$

Considering that  $\dot{m}_P = -\dot{m}$  — the spacecraft's mass decreases as the propellant is expelled — and taking into account equation (3.1):

$$\Delta V = - \int_{t_0}^{t_f} c \dot{m}_P \frac{dm}{m}$$

the integral is easy to determinate, if the assumption of constant  $c$  is adopted. In general, the effective discharge velocity is not constant, but an opportune average value is always possible to estimate. Anyway, solving the integral, the *Tsiolkovsky equation* is retrieved and expressed in its two forms:

$$\Delta V = c \ln \frac{m_0}{m_f} \iff m_f = m_0 e^{-\frac{\Delta V}{c}} \quad (3.9)$$

Since the propellant consumption and the propulsive cost are connected through an exponential relation, it is crucial to have an effective discharge velocity which is at least comparable with the characteristic velocity. If the specific impulse is too low the final mass is negligible if compared to the initial one, thus there is no possibility of carrying any payload. The exponential relation highlights a crucial concept. When accelerating a payload, the propulsor is not only accelerating the payload itself, but it is also accelerating the propellant that is needed to accelerate that payload. Thus, if the payload is increased, the propellant mass needed does not increase linearly but

exponentially, since the propulsor does not only have to accelerate extra payload, but to accelerate extra propellant.

Hence the need for a high specific impulse. The higher  $c$ , the less propellant is needed to accomplish the manoeuvre: this strongly hinders the vicious cycle of mass increasing.

## 3.2 Electrical Propulsion

As far as unmanned space missions are concerned, electrical propulsion is the state of the art. Electrical thrusters rely on electrical power—in general generated exploiting solar arrays—in order to accelerate a propellant gas. Nonetheless, different categories of electrical propulsors exist, on the basis of how this energy is used to create thrust: that is to say on the basis of the physical principle they rely on. In particular:

- *Electrothermal propulsion*: uses electrical power to heat the propellant. Then the same is accelerated in a nozzle where the thermal energy is converted—with losses and non-ideal effects—in kinetic energy, thus generating thrust.
- *Electrostatic propulsion*: uses electrical power to ionize the propellant and accelerate it leveraging electrical forces. Thus, the gas is ionized—creating ions and electrons—the ions are accelerated through an electric field and then the exit beam is neutralized.
- *Electromagnetic propulsion*: uses electrical power to create electric and magnetic fields. These generate forces that accelerate the propellant, creating thrust. It is worth highlighting that also electrostatic thrusters seldom use magnetic fields, but the acceleration is only created by the electric field. On the other hand, electromagnetic acceleration is created by both electric and magnetic forces.

Besides the classification on the physical principle there is a parallel categorization on the basis of the characteristic power of the thruster. In particular:

- *Microthrusters*: used, in general, for precision attitude control.
- *1 kW*: used for station keeping or orbit injection—or deorbit—of small satellites.
- *5-10 kW*: used for GEO insertion or deorbit of big satellites.
- *100+ kW*: are under development concepts that could be implemented in human exploration missions.

### 3.2.1 Generalities

Independently on the physical principle they exploit to accelerate the propellant, all the electrical thrusters share some common behaviours. As a matter of fact, in the end they all convert an *electrical power* in the final useful effect, which is *thrust*. This conversion process is not ideal: in fact it is characterized by a certain *global efficiency*. The value of

this performance index is much different depending on the thruster category, but for now there is no interest in fixing the numbers. Therefore, in general, the important concept is that it is not possible to neglect the global efficiency, independently of its value.

Mathematically, what has been said is:

$$\eta P_E = \frac{1}{2} T c \quad (3.10)$$

where  $\eta$  is the global efficiency,  $P_E$  is the electrical power consumption and the term on the right —recalling equation (3.3)— is the thrust power.

It is therefore possible to invert the relation in equation (3.10), to express the effective discharge velocity:

$$c = \frac{2\eta P_E}{T}$$

This relation highlights a crucial concept. As far as electrical propulsion is concerned, it is possible to increase  $c$ —in the limits imposed by the current technologies— accepting a disadvantage in terms of thrust or power source’s mass.

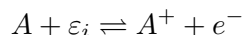
As a matter of fact, if compared to chemical rockets, electrical thrusters are characterized by higher specific impulse and lower thrust. The high values of specific impulse come at the price of low thrusts — 10  $\mu\text{N}$  - 1 N— or heavy power generation systems. With the current technology, electrical thrusters can not provide accelerations higher than  $\frac{g}{100}$ . Thus, there is no possibility for electrical propulsion to be applied to launchers. On the other hand, the characteristics of electrical thrusters perfectly fit the requirements of long and efficient missions, exactly as the ones analyzed in this thesis.

### 3.2.2 Electrostatic Propulsion

Electrical thrusters accelerate the propellant through electrostatic forces, thus exploiting electrical fields. In general, also a magnetic field is generated, but it is used for other purposes different from the propellant acceleration. Since they rely on electrical forces, electrostatic thrusters operate with ionized propellants. As a matter of fact, ionization is just the first of the three processes which make up electrostatic propulsion:

- *Ionization*

The ionization of a propellant is the process through which it is possible to separate some atoms from one of their electrons, thus creating a ion —and the electron itself—. Such a process requires energy. In particular, each atom of the periodic table is characterized by a *first ionization energy*:  $\varepsilon_i$ . This can be provided in different ways, but in general the following reaction happens:



where  $A$  and  $A^+$  are respectively the propellant’s atom and ion and  $e^-$  is the free electron. It is crucial to highlight that not all the propellant’s atoms are ionized.

As a matter of fact, only a fraction of atoms receives the energy sufficient to lose an electron and become an ion. Therefore, the *ionization ratio* is not equal to 1.

Now that ions and electrons are created, it is necessary to separate them. In fact, applying an electric field to both electrons and ions would generate a null thrust. This happens because electrons and cations have the same charge in terms of module, but different signs. Thus, recalling the basic equation of electrostatic physics:

$$\mathbf{F} = q\mathbf{E}$$

electrons and ions are subject to equal opposite force, which mutually neutralize themselves. In fact,  $\mathbf{F}$  is the force on the considered particle,  $\mathbf{E}$  is the electric field and  $q$  is the elementary charge.

The phenomenology of what has been previously described is shown in a graphic way in Fig. 3.2.

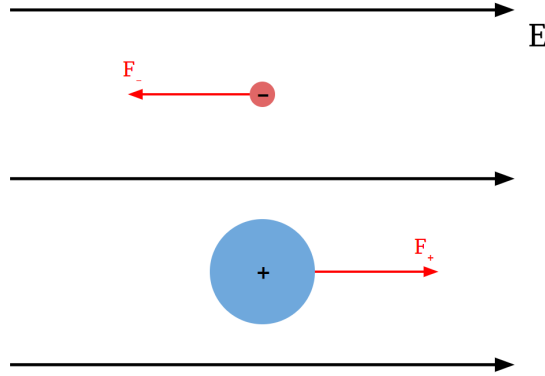


Figure 3.2: Electric forces acting on different species

The separation of the two species may be carried out exploiting different means, depending on the thruster type. One of these methods is exploiting a magnetic field that, without entering the particular description of the electromagnetic interactions, confines the electrons in the propulsor and allows to accelerate only the ions.

- *Acceleration*

As it has been already said, the acceleration is generated through the application of an electric field that acts on the ions. In particular, being the electric field a conservative field, it is connected to an electric potential. The potential connected to the acceleration is referred to as the *net accelerating potential*, and indicated with the symbol  $V_N$ . With an analogy, if the electric field is compared to the gravitational one, the potential is a difference in altitude. Thus, as a ball accelerates down a slope, the ions are accelerated by the net accelerating potential.

Mathematically, this means that the electrical potential energy is converted into kinetic energy. Neglecting the efficiency of the conversion process, it is possible to impose the conservation of the total energy. In the propulsor there is only electric potential energy —the propellant is globally static, there is only the chaotic thermal agitation velocity, which is globally null— and at the exit it only has kinetic energy:

$$qV_N = \frac{1}{2}m_+u_+^2$$

where  $q$  and  $V_N$  have been already defined,  $m_+$  is the atomic mass of the ion — that, being electrons far more lighter than neutrons and protons, is equal to the mass of the propellant atom itself— and  $u_+$  is the exit velocity. On the basis of the considerations in paragraph 3.1.2, this is almost equal to the effective exhaust velocity. Hence its expression is easily derivable:

$$u_+ = \sqrt{\frac{2qV_N}{m_+}} \quad (3.11)$$

Clearly, the only modifiable parameters are the net potential and the atomic mass of the propellant.

- *Neutralization*

The last but not least step is to neutralize the accelerated beam of ions. As a matter of fact, it is crucial to maintain the global neutrality of the propulsor. If the ions were just accelerated, the propulsor itself would grow an inner negative charge, due to the expulsion of a positive flow of charges. To avoid the insurgence of such an undesired event, the ion beam is neutralized with an equal current of electrons. This *neutralizing current* is not accelerated, since it does not have to concur in producing thrust. In general, a sort of electron cloud is created at a certain distance from the thruster's exit. The high speed ions pass through this cloud and for electrostatic interaction tie to an electron and get neutralized. Each ion takes an electron and in the end what exits is a neutral beam of atoms —as the propellant was before ionization—.

## Ion Thrusters

Ion thrusters are certainly the more diffused and established electrostatic propulsors. As can be inferred from their name, they accelerate ions, created ionizing a propellant. In general, this is a high atomic mass gas, such as Xenon. Being this a noble gas, it has an extremely high first ionization energy, since its external electronic level is complete. Thus, in order to have a propellant easier to ionize, the Xenon is mixed with other elements. This process, called *seeding*, requires a little injection —1-5%— of an alkaline metal —which only has one external electron, thus is easy to ionize—. This allows to have a smaller *ion production energy*. In fact, the electrical power is not only used to accelerate the propellant, but in the first place it is necessary to spend some energy to

create the ions. This means that, even in the more ideal case, the process has not 100% efficiency, but there is an *ideal efficiency*:

$$\eta_{id} = \frac{\frac{1}{2}m_+u_+^2}{\frac{1}{2}m_+u_+^2 + \varepsilon_B}$$

where  $\varepsilon_B$  is the production cost of one ion. The ionization process can be carried out leveraging different physical principles:

- *Electron Bombardment*

An electron gun injects electrons at high energy —and therefore speed— in the same chamber of the propellant. The electrons are subjected to both an electric field —that accelerates them— and a magnetic field —that confines them to stay in the chamber for the longest possible time—. Thus the electrons move between the two electrodes at different potential —that generate the electric field— of the ionization chamber and impact with the propellant atoms. These collisions lower the velocity of the electrons and may ionize the atoms of propellant.

- *Radiofrequency*

A radiofrequency coil creates electromagnetic waves that provides the energy necessary for the ionization.

Independently on the ionization method, the process is not ideal. Thus, not all the propellant atoms are ionized.

The acceleration of the fraction of the propellant atoms that are ionized is, in general, carried out in a limited region between two grids. This is why most ion thrusters are defined as *gridded*. The ions are accelerated between a *screen grid* and an *acceleration grid*, which are at different potential levels. These grids are nothing but curved plates of molybdenum, with millimetric holes in them.

This solution is chosen, instead of one single bigger exit section, in order to have a more focused beam. In fact, being all positively charged, the ions would tend to repulse each other. This effect is magnified by a single beam with more ions, and is strongly hindered by the gridded geometry that separates the ions in different beams. These, if the grids are well designed, do not interact with one another.

The grids themselves are posed at a millimetric distance. Nonetheless, it is necessary to not exceed in having too close grids with a high potential difference. In general, to avoid the insurgence of sparks:

$$\frac{V_G}{d} < 2 \frac{kV}{mm}$$

is the limit, being  $V_G$  the difference of potential between the grid and  $d$  their distance. Grids are made in molybdenum because it is easy to manipulate. As a matter of fact, grids are the critical components of ion thrusters, being expensive, complex and delicate. In particular, the erosion of the grids —mainly the accelerating one— is the dimensioning

factor of ion thrusters life. Moreover, grids need to be curved so that, when under thermal loads, their buckling direction is known. If they were planar, it would be impossible to forecast their behaviour when expanding due to temperature rise. Also their dimension has to be limited, in general:

$$\frac{D}{d} < 600$$

where  $D$  is the grids' diameter.

Perhaps, it is easier to understand the functioning of an ion thruster looking at Fig. 3.3, where a gridded ion thrusters leveraging electron bombardment is shown.

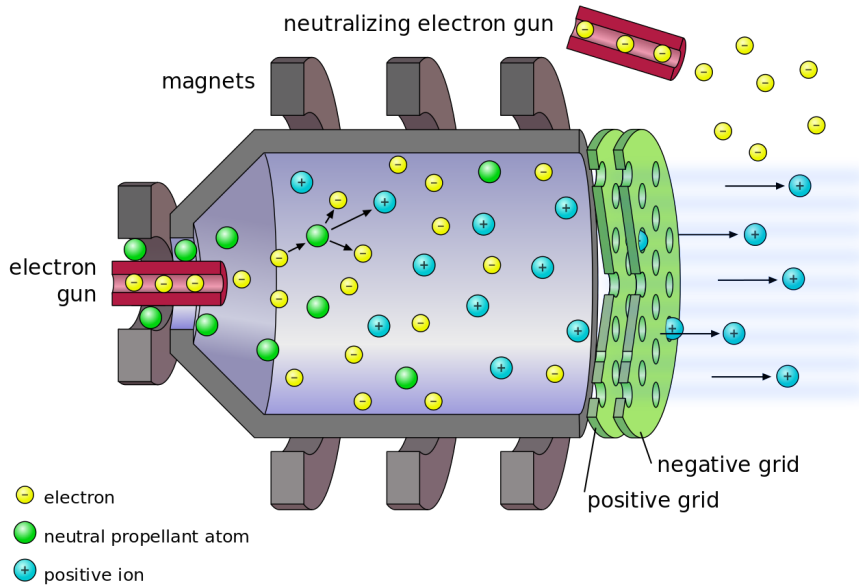


Figure 3.3: Gridded ion thruster's scheme

It is possible also to see the component used for the last action: neutralization. This is carried out with a *hollow cathode*, that extracts electrons from a fraction of the propellant flow. This process is necessary, but creates another loss in the propellant fraction that is ionized. In particular, the propellant flow  $\dot{m}_P$  is made up of the flow that is ionized  $\dot{m}_+$  and of two 'losses': the non ionized fraction  $\dot{m}_A$  and the fraction that goes to the hollow cathode  $\dot{m}_C$ . Thus:

$$\dot{m}_P = \dot{m}_+ + \dot{m}_A + \dot{m}_C$$

It is therefore possible to define an *efficiency of propellant utilization*:

$$\eta_u = \frac{\dot{m}_+}{\dot{m}_P}$$

If there are no other losses of electrical power, thus in an almost ideal case, the *global efficiency* is:

$$\eta_g = \eta_{id}\eta_u$$

This allows to define the fraction of the supplied electrical power that actually is converted in thrust power:

$$P_T = \frac{1}{2}Tc = \eta_g P_E$$

## Chapter 4

# Indirect Methods for Space Trajectories Optimization

*"The best is the enemy of the good"*  
— Voltaire

In this Chapter are described the global characteristics and the mathematical aspects of the method adopted for the optimization of the trajectories considered in this work. First the concepts of the Optimal Control Theory will be introduced in a general way, then the aspects of the deriving Boundary Value Problem will be described.

In general, optimization problems consist of the research of a particular control law which maximizes or minimizes a peculiar *performance index*. As far as space trajectories are concerned, the optimization problem is usually related to the maximization of the payload. Given the great importance of propellant consumption, which strongly affects the mission's cost, it is crucial to minimize it: minimizing consumption or maximizing the payload are, as a matter of fact, the same requirement.

The analytical solution of such a complex problem can be derived only if strong simplifications are adopted, which reduce the field to missions with little or no scientific interest. Thus, significant solutions need to be achieved exploiting approximated theories or numerical methods. Indirect methods belong to the latter category. These optimization techniques are characterized by a high numerical precision and a robust theoretical content. Furthermore, they rely on a limited amount of parameters, thus requiring little computational time. On the other hand, these methods are not robust and are usually characterized by a small convergence region, thus requiring a precise attempt solution.

### 4.1 Optimal Control Theory

The *Optimal Control Theory* — OCT — is based on the principles of variational calculus. It is used in different fields of expertise and is here summarized and described in the

form that best suits the application to space trajectories optimization.

The generic system, which the *Optimal Control Theory* can be applied to, can be described through the vector of the state variables  $\mathbf{x}$ . The differential equations, describing the evolution of the system's state between the initial and final time — *external boundary conditions* —, are a function of:

- $\mathbf{x}$ : state variables vector
- $\mathbf{u}$ : controls vector
- $t$ : time

Thus, they can be expressed in the following form:

$$\frac{d\mathbf{x}}{dt} = \mathbf{f}(\mathbf{x}, \mathbf{u}, t) \quad (4.1)$$

It is convenient, for the analyzed case, to divide the trajectory in a number  $n$  of subintervals, defined as *arches*. Within each arch the variables are continuous, but discontinuities can be present at the arches' interfaces. In fact, the division in arches allows to consider discontinuities — such as mass discontinuities connected to an impulsive manoeuvre or time discontinuities related to a planet fly-by — in a relatively simple way. If the  $j$ -th arch begins at time  $t_{(j-1)+}$  and ends at  $t_{j-}$ , the state vectors at the interval's edges is represented as  $\mathbf{x}_{(j-1)+}$  — beginning — and  $\mathbf{x}_{j-}$  — end —. In particular, the signs — and + refer to the values assumed before and after the considered point. The connection points of the arches are the *internal boundary conditions*. Following this strategy, the function representing the differential equations of the system can assume different expressions in each arch.

The boundary conditions are, in general, both mixed and non-linear. Thus, they involve non-linear relations between the state and time variables at the external and internal boundaries. In the generic form, they can be expressed as following:

$$\chi(\mathbf{x}_{(j-1)+}, \mathbf{x}_{j-}, t_{(j-1)+}, t_{j-}) = 0 \quad j = 1, \dots, n \quad (4.2)$$

The optimization problem consists of the research of the extremal values — relative maximum or minimum — of the *functional*:

$$J = \varphi(\mathbf{x}_{(j-1)+}, \mathbf{x}_{j-}, t_{(j-1)+}, t_{j-}) + \sum_j \int_{t_{(j-1)+}}^{t_{j-}} \Phi(\mathbf{x}(t), \mathbf{u}(t), t) dt \quad j = 1, \dots, n \quad (4.3)$$

The functional  $J$  is made up of two components:

- $\varphi$ : a function depending on the values of the variables vector and of the independent variable at the boundaries
- Integral of the  $\Phi$  function: which depends on the time and on the values assumed by the state and the controls at each instant

It is always possible, introducing particular auxiliary variables, to formulate the functional's expression in order to present:

- $\varphi = 0$ : *Lagrange's formulation*
- $\Phi = 0$ : *Mayer's formulation*, which is the one adopted in this thesis

It is then useful to reformulate the functional. In particular, introducing:

- $\boldsymbol{\mu}$ : *adjoint constants*, connected to the boundary conditions
- $\boldsymbol{\lambda}$ : *adjoint variables*, connected to the state equations

it is possible to write the expression of the modified functional:

$$J^* = \varphi + \boldsymbol{\mu}^T \boldsymbol{\chi} + \sum_j \int_{t_{(j-1)_+}^{t_{j-}^-}} (\Phi + \boldsymbol{\lambda}^T (\mathbf{f} - \dot{\mathbf{x}})) dt \quad j = 1, \dots, n \quad (4.4)$$

where the point  $\cdot$  means the derivative with respect to the time. Both functionals  $J$  and  $J^*$  depend on the time, the state vector and its derivative and the controls  $\mathbf{u}$ . In particular, the values of time and state variables which affect the functionals, are the ones related to each arch's edges. Needless to say, if the boundary conditions and the state equations are satisfied, the two functionals — and therefore their extremal values — coincide.

By integrating by parts, it is possible to eliminate the dependence of the functional  $J^*$  from the derivatives of the state vector:

$$\begin{aligned} J^* = \varphi + \boldsymbol{\mu}^T \boldsymbol{\chi} + \sum_j (\boldsymbol{\lambda}_{(j-1)_+}^T \mathbf{x}_{(j-1)_+} - \boldsymbol{\lambda}_{j_-}^T \mathbf{x}_{j_-}) + \\ + \sum_j \int_{t_{(j-1)_+}^{t_{j-}^-}} (\Phi + \boldsymbol{\lambda}^T \mathbf{f} - \dot{\boldsymbol{\lambda}}^T \mathbf{x}) dt \quad j = 1, \dots, n \end{aligned} \quad (4.5)$$

Furthermore, it is possible to differentiate the resulted expression in order to obtain the differential of the functional itself:

$$\begin{aligned} \delta J^* = & \left( -H_{(j-1)_+} + \frac{\partial \varphi}{\partial t_{(j-1)_+}} + \boldsymbol{\mu}^T \frac{\partial \boldsymbol{\chi}}{\partial t_{(j-1)_+}} \right) \delta t_{(j-1)_+} + \\ & + \left( H_{j_-} + \frac{\partial \varphi}{\partial t_{j_-}} + \boldsymbol{\mu}^T \frac{\partial \boldsymbol{\chi}}{\partial t_{j_-}} \right) \delta t_{j_-} + \\ & + \left( \boldsymbol{\lambda}_{(j-1)_+}^T + \frac{\partial \varphi}{\partial \mathbf{x}_{(j-1)_+}} + \boldsymbol{\mu}^T \left[ \frac{\partial \boldsymbol{\chi}}{\partial \mathbf{x}_{(j-1)_+}} \right] \right) \delta \mathbf{x}_{(j-1)_+} + \\ & + \left( -\boldsymbol{\lambda}_{j_-}^T + \frac{\partial \varphi}{\partial \mathbf{x}_{j_-}} + \boldsymbol{\mu}^T \left[ \frac{\partial \boldsymbol{\chi}}{\partial \mathbf{x}_{j_-}} \right] \right) \delta \mathbf{x}_{j_-} + \\ & + \sum_j \int_{t_{(j-1)_+}^{t_{j-}^-} \left( \left( \frac{\partial H}{\partial \mathbf{x}} + \dot{\boldsymbol{\lambda}}^T \right) \delta \mathbf{x} + \frac{\partial H}{\partial \mathbf{u}} \delta \mathbf{u} \right) dt \quad j = 1, \dots, n \end{aligned} \quad (4.6)$$

where it has been introduced the *Hamiltonian* of the system:

$$H = \Phi + \boldsymbol{\lambda}^T \mathbf{f} \quad (4.7)$$

In order to infer the optimal condition, it is necessary to impose the stationariness of the functional. Thus, the derivative of the functional with respect to any possible variation —  $\delta \mathbf{x}, \delta \mathbf{u}, \delta \mathbf{x}_{(j-1)_+}, \delta \mathbf{x}_{j-}, \delta t_{(j-1)_+}, \delta t_{j-}$  — has to be null, as far as it is compatible with the differential equations and the boundary conditions. The introduction of adjoint variables and constants allows, with a convenient choice, to contemporarily cancel the coefficient of each variation in equation (4.6), thus assuring the stationariness of the functional expressed by the condition  $\delta J^* = 0$ .

In particular, cancelling the coefficients of  $\delta \mathbf{x}$  and  $\delta \mathbf{u}$  in the integral term, two important relations can be derived:

- *Euler-Lagrange differential equations* for adjoint variables:

$$\frac{d\boldsymbol{\lambda}}{dt} = - \left( \frac{\partial H}{\partial \mathbf{x}} \right)^T \quad (4.8)$$

- *Algebraic equations* for controls:

$$\left( \frac{\partial H}{\partial \mathbf{u}} \right)^T = 0 \quad (4.9)$$

An interesting property of the control laws is their formal independence from the stationary point searched. Seeking maximum or minimum of the functional  $J$  does not affect the algebraic equations (4.9).

It is important to highlight the importance of dealing with constrained controls. As a matter of fact, one or more controls could be limited to a particular admissible domain. For instance, the thrust provided by a propulsor has to be positive and can not exceed a value  $T_{max}$ , defined by the thruster category. In this analysis, will not be considered controls' constraints variable with time or dependent from the state vector variables. Thus, any boundary condition on the controls is constant and explicit. If such a constraint is present, the optimal value of the bound control in any point of the trajectory is the one that, belonging to the admissibility domain, maximizes — if maximum are seeked — or viceversa minimizes the Hamiltonian in that point. This peculiarity is expressed by the *Pontryagin Maximum Principle*, which leads to two possibilities:

- The optimal value for control is the one derived from equation (4.9) if it belongs to the admissibility domain. In that point the constraint does not affect the system, resulting in a locally non-constrained control
- The optimal value for control is at the domain extremes. Thus, if the optimal control derived from equation (4.9) falls outside the domain, the control assumes its maximum or minimum value. In this case, the control is constrained

If the Hamiltonian is linear with respect to one of the constrained controls, the system presents a peculiarity. As a matter of fact, in the related equation (4.9) the control does not appear directly, therefore it can not be determined. In this case there are again two possibilities:

- In equation (4.7) the constrained control coefficient is not null. This means that the Hamiltonian is maximized assuming the maximum value for the control if it is positive, or the minimum one if its negative. This is often referred to as *bang-bang* control, and derives from the Pontryagin Maximum Principle
- In equation (4.7) the constrained control coefficient is null within a singular arch. It is then necessary to impose the cancellation of every derivative of the coefficient itself, with respect to the time, until one of them does not explicitly contain the control. The optimal control is then determined by imposing the last derivative equal to null. It is established that the derivative degree necessary is always even. Naming the derivative's degree  $n$ , the order of the singular arch is  $n/2$

As far as the missing boundary conditions are concerned, it is convenient to refer to the  $j$ -th extreme. It is possible to write down, for the considered boundary, the conditions deriving from considering it as the final edge of the  $(j - 1)$ -th sub-interval or as the initial point of the  $j$ -th sub-interval. By cancelling the coefficient of  $\delta\mathbf{x}_{j-}$ ,  $\delta\mathbf{x}_{j+}$ ,  $\delta t_{j-}$  and  $\delta t_{j+}$  in equation (4.6), the following conditions can be derived:

$$-\boldsymbol{\lambda}_{j-}^T + \frac{\partial\varphi}{\partial\mathbf{x}_{j-}} + \boldsymbol{\mu}^T \left[ \frac{\partial\boldsymbol{\chi}}{\partial\mathbf{x}_{j-}} \right] = 0 \quad j = 1, \dots, n \quad (4.10)$$

$$\boldsymbol{\lambda}_{j+}^T + \frac{\partial\varphi}{\partial\mathbf{x}_{j+}} + \boldsymbol{\mu}^T \left[ \frac{\partial\boldsymbol{\chi}}{\partial\mathbf{x}_{j+}} \right] = 0 \quad j = 0, \dots, n - 1 \quad (4.11)$$

$$H_{j-} + \frac{\partial\varphi}{\partial t_{j-}} + \boldsymbol{\mu}^T \frac{\partial\boldsymbol{\chi}}{\partial t_{j-}} = 0 \quad j = 1, \dots, n \quad (4.12)$$

$$-H_{j+} + \frac{\partial\varphi}{\partial t_{j+}} + \boldsymbol{\mu}^T \frac{\partial\boldsymbol{\chi}}{\partial t_{j+}} = 0 \quad j = 0, \dots, n - 1 \quad (4.13)$$

where  $j_-$  and  $j_+$  are the values assumed right before and right after the point  $j$ . As already introduced, it is crucial to distinguish the two instants, as a discontinuity could happen at the arches' conjunction points. Clearly, equations (4.10) and (4.12) can not be considered for the starting point of the trajectory —  $j = 0$  —, and equations (4.11) and (4.13) are not significant at the end, where  $j = n$ . Eliminating the adjoint constants  $\boldsymbol{\mu}$  from the set of equations above, the *Optimum Boundary Conditions* can be defined as:

$$\boldsymbol{\sigma}(\mathbf{x}_{(j-1)+}, \mathbf{x}_{j-}, \boldsymbol{\lambda}_{(j-1)+}, \boldsymbol{\lambda}_{j-}, t_{(j-1)+}, t_{j-}) = 0 \quad j = 1, \dots, n \quad (4.14)$$

The final system of differential equations is made up of equations: (4.1) (4.2) (4.8) (4.14).

Considering the generic state variable  $x$ , if subjected to particular boundary conditions, equations (4.10) and (4.11) give peculiar optimal values for the relative adjoint variable  $\lambda_x$ . In particular:

- If the state variable  $x$  value is given at the initial instant — which means that the imposed boundary conditions vector  $\chi$  contains the equation  $x_0 - a = 0$ , with  $a$  explicit value —, on the corresponding adjoint variable  $\lambda_x$  there are no conditions. Therefore, the adjoint variable's initial value  $\lambda_{x_0}$  is free. The same property can be inferred for the final instant, if a state variable is explicitly defined in that point. Mathematically:

$$\text{if } x_0 - a = 0 \quad \longrightarrow \quad \lambda_{x_0} \quad \text{is free}$$

- If the initial value of the state variable  $x_0$  does appear neither in the function  $\varphi$  nor in the boundary conditions, the relative adjoint variable is null at the initial instant:  $\lambda_{x_0} = 0$ . Also in this case, the consideration can be extended to the final instant. Mathematically:

$$\text{if } \varphi \neq f(x_0) \quad \wedge \quad \chi \neq f(x_0) \quad \longrightarrow \quad \lambda_{x_0} = 0$$

- If a state variable is continuous but not explicitly defined at an internal point  $j$  — which means that the vector  $\chi$  contains the equality  $x_{j+} = x_{j-}$  —, the corresponding adjoint variable is continuous as well in that point:  $\lambda_{x_{j+}} = \lambda_{x_{j-}}$ . Mathematically:

$$\text{if } x_{j+} = x_{j-} \quad \longrightarrow \quad \lambda_{x_{j+}} = \lambda_{x_{j-}}$$

- If a state variable is continuous and given at a defined internal interface — which means that  $\chi$  contains the equations  $x_{j-} = a$  and  $x_{j+} = a$  —, the corresponding adjoint variable in that point presents a free discontinuity. This means that its value after the point  $j$  is independent from the value it assumed before, and has to be determined through the optimization algorithm. Mathematically:

$$\text{if } x_{j+} = x_{j-} = a \quad \longrightarrow \quad \lambda_{x_{j+}} \neq f(\lambda_{x_{j-}})$$

With the same considerations, can be inferred that if the Hamiltonian does not explicitly depends on the time, also equations (4.12) and (4.13) give some peculiar boundary conditions. In particular:

- If the initial time  $t_0$  does not explicitly appear in the boundary conditions or in the function  $\varphi$ , the Hamiltonian of the system is null at the initial point:  $H_0 = 0$ . As always, the same conclusions can be inferred for the final time of the trajectory
- If the internal time  $t_j$  does non explicitly appear in the function  $\varphi$  — which means that the only condition in which it is involved is the continuity of the time at the internal boundary  $t_{j+} = t_{j-}$  —, the Hamiltonian of the system is continuous in  $j$ :  $H_{j+} = H_{j-}$

- If the internal time  $t_j$  is explicitly defined — which means that in  $\chi$  appears the equations  $t_{j-} = a$  and  $t_{j+} = a$  —, the Hamiltonian of the system in that point has a free discontinuity

## 4.2 Boundary Value Problem

The indirect method, used to optimize orbital transfers and space missions in general, relies on the application of the Optimal Control Theory at the system of differential equations. This is made up of the following systems:

$$\frac{d\mathbf{x}}{dt} = \mathbf{f}(\mathbf{x}, \mathbf{u}, t) \quad \text{State Differential Equations}$$

$$\frac{d\boldsymbol{\lambda}}{dt} = - \left( \frac{\partial H}{\partial \mathbf{x}} \right)^T \quad \text{Euler-Lagrange Equations}$$

$$\boldsymbol{\chi}(\mathbf{x}_{(j-1)+}, \mathbf{x}_{j-}, t_{(j-1)+}, t_{j-}) = 0 \quad \text{Imposed Boundary Conditions}$$

$$\boldsymbol{\sigma}(\mathbf{x}_{(j-1)+}, \mathbf{x}_{j-}, \boldsymbol{\lambda}_{(j-1)+}, \boldsymbol{\lambda}_{j-}, t_{(j-1)+}, t_{j-}) = 0 \quad \text{Optimum BC}$$

to which can be attached:

$$\left( \frac{\partial H}{\partial \mathbf{u}} \right)^T = 0 \quad \text{Controls Algebraic Equations}$$

The OCT traduces this problem in a *Boundary Values Problem* — BVP —, where some of the variables' initial values are unknown. The solution of the BVP consists in finding the initial values which satisfy contemporarily all the boundary conditions: both imposed and optimal. Such a method relies on the numerical integration of the system of differential equations.

The Optimal Control Theory, as explained in Section 4.1, formulates the optimization problem as a mathematical problem subjected to both differential and algebraic bounds. The described problem is characterized by some peculiarities:

- The integration domain is divided into subintervals called arches. Within each arch the formulation of the the differential equations is constant, but may be different from one arch to another
- The duration of each arch is, in general, unknown
- the boundary conditions may be non-linear, as well they can involve the values of the variables both at the external boundaries and the external
- The variables may be discontinuous at the internal boundaries and their values after such singularity might be unknown

The main challenge, dealing with indirect optimization techniques, is the solution of the Boundary Values Problems which derives from their application to physical systems. Therefore, the method for the BVP solution is one of the most important instruments. The solution is achieved by reducing the BVP to a sequence of sub-problems, which is then taken to convergence exploiting the *Newton method*.

In order to solve the problem related to indefiniteness of the duration of the arches, the independent variable  $t$  is replaced, only for the integration, with a new variable  $\varepsilon$ . This new variable is defined in the  $j$ -th arch as follows:

$$\varepsilon = j - 1 + \frac{t - t_{j-1}}{t_j - t_{j-1}} = j - 1 + \frac{t - t_{j-1}}{\tau_j}$$

where  $\tau_j$  is the duration — in general not known — of the subinterval. Thus, internal and external boundaries are fixed. In fact, thanks to the introduction of the unknown parameters  $\tau_j$ , the interface points are represented by the natural values of the new independent variable  $\varepsilon$ .

In order to describe the method, the differential equations are reformulated introducing the new variables vector which takes into account both the state variables and the adjoint variables:  $\mathbf{y} = (\mathbf{x}, \boldsymbol{\lambda})$ . Thus, the differential problem becomes:

$$\frac{d\mathbf{y}}{dt} = \mathbf{f}^*(\mathbf{y}, t) \quad (4.15)$$

It is worth highlighting the fact that, in the considered problem, some parameters — such as the arches' duration  $\tau$  — are constant. Thus, it is convenient to introduce another vector  $\mathbf{z} = (\mathbf{y}, \mathbf{c})$  which comprehends: state variables, adjoint variables and constant parameters.

Considering this last change, and the change of the independent variable, the system of differential equations can be expressed in the following form:

$$\frac{d\mathbf{z}}{d\varepsilon} = \mathbf{f}(\mathbf{z}, \varepsilon) \quad (4.16)$$

It is then possible to express the second member of the equation. As far as the state and adjoint variables vector is concerned, the derivative with respect to the new independent variable is:

$$\frac{d\mathbf{y}}{d\varepsilon} = \tau_j \frac{d\mathbf{y}}{dt} \quad (4.17)$$

while for the constants' vector can be easily derived:

$$\frac{d\mathbf{c}}{d\varepsilon} = 0 \quad (4.18)$$

The boundary conditions can be merged in a single vector that takes into account both the imposed ones and the optimal ones. They are usually expressed in the form:

$$\boldsymbol{\Psi}(\mathbf{s}) = 0 \quad (4.19)$$

where it has been introduced the vector  $\mathbf{s}$ . This new vector includes the values that the variables — both state and adjoint — assume at every boundary — external as well as internal — and the unknown constant parameters:

$$\mathbf{s} = (\mathbf{y}_0, \dots, \mathbf{y}_n, \mathbf{c}) \quad (4.20)$$

The initial values of some variables are usually unknown, thus the research of the solution coincides with the determination, through an iterative process, of which values they have to assume to satisfy the boundary conditions in equation (4.19). The methodology is here described considering all of the initial values as unknown. If one or more are explicitly defined, the method is simplified. Each iteration begins with the numerical integration of equations (4.16). If the  $r$ -th iteration is running, the initial values  $\mathbf{p}^r$  are the ones retrieved at the end of the previous iteration. This means that the following equality is imposed:

$$\mathbf{z}(0) = \mathbf{p}^r \quad (4.21)$$

then, the differential equations are integrated throughout the whole trajectory, taking into account the discontinuities at the internal boundaries. Needless to say, in order to spark the process it is necessary to choose the values of the first attempt vector:  $\mathbf{p}^1$ . At each internal boundary is determined the values of the state variables and, at the end of the integration process, the error on the boundary conditions is computed. This is referred to as:  $\Psi^r$  for the  $r$ -th iteration.

The variation  $\Delta\mathbf{p}$ , brings changes to the error on the boundary conditions. This error  $\Delta\Psi$ , considering only the first order terms, can be expressed as:

$$\Delta\Psi = \left[ \frac{\partial\Psi}{\partial\mathbf{p}} \right] \Delta\mathbf{p} \quad (4.22)$$

In order to fulfill the boundary conditions (4.19), such error has to be null. Thus, it is necessary that  $\Delta\Psi = -\Psi^r$ , resulting in a modification of the initial values at each iteration of:

$$\Delta\mathbf{p} = \mathbf{p}^{r+1} - \mathbf{p}^r = - \left[ \frac{\partial\Psi}{\partial\mathbf{p}} \right]^{-1} \Psi^r \quad (4.23)$$

this correction is applied until the boundary conditions are respected, with the desired accuracy. The matrix in the second term of equation (4.23), is calculated through the product of two matrices:

$$\left[ \frac{\partial\Psi}{\partial\mathbf{p}} \right] = \left[ \frac{\partial\Psi}{\partial\mathbf{s}} \right] \left[ \frac{\partial\mathbf{s}}{\partial\mathbf{p}} \right] \quad (4.24)$$

where the first one can be easily obtained derivating the boundary conditions with respect to the variables they depend on. The second matrix takes into account the derivative of the variables at the boundaries with respect to their initial values. This means that the second matrix represents the values assumed at the boundaries by the matrix:

$$\left[ \frac{\partial \mathbf{z}}{\partial \mathbf{p}} \right] = [\mathbf{g}(\varepsilon)] \quad (4.25)$$

which is obtained from the integration of the main system of differential equations (4.16) with respect to each of the initial values:

$$[\dot{\mathbf{g}}] = \frac{d}{d\varepsilon} \left[ \frac{\partial \mathbf{z}}{\partial \mathbf{p}} \right] = \left[ \frac{\partial}{\partial \mathbf{p}} \left( \frac{d\mathbf{z}}{d\varepsilon} \right) \right] = \left[ \frac{\partial \mathbf{f}}{\partial \mathbf{p}} \right] \quad (4.26)$$

where now the point  $\dot{\phantom{x}}$  represents the derivative with respect to the new independent variable  $\varepsilon$ . The *Jacobian* of the principal system (4.16) can be expressed, finding the following form for equation (4.26):

$$[\dot{\mathbf{g}}] = \left[ \frac{\partial \mathbf{f}}{\partial \mathbf{z}} \right] \left[ \frac{\partial \mathbf{z}}{\partial \mathbf{p}} \right] = \left[ \frac{\partial \mathbf{f}}{\partial \mathbf{z}} \right] [\mathbf{g}] \quad (4.27)$$

One of the peculiarities of the described method, for the solution of indirect optimization problems, is the symmetry of some terms of the Jacobian. Here such properties are not described since they fall out from the scope of the thesis.

The initial values of the homogeneous system (4.27) can be retrieved through the derivative of relation (4.22). This way, the identity matrix can be found:

$$[\mathbf{g}(0)] = \left[ \frac{\partial \mathbf{z}(0)}{\partial \mathbf{p}} \right] = [\mathbf{I}] \quad (4.28)$$

It is worth underlining that this method allows to deal also with discontinuities in the variables. As a matter of fact, in order to take into account a discontinuity at point  $i$ , it is sufficient to update both the vector of variable  $\mathbf{z}$  and the matrix  $\mathbf{g}$ . This operation can be realized through the relation  $\mathbf{h}$  which connects the values of the variables before and after the discontinuity:

$$\mathbf{z}_{i+} = \mathbf{h}(\mathbf{z}_{i-}) \quad (4.29)$$

$$[\mathbf{g}_{i+}] = \left[ \frac{\partial \mathbf{h}}{\partial \mathbf{z}} \right] [\mathbf{g}_{i-}] \quad (4.30)$$

This explains why the vector  $\mathbf{s}$  has been defined without a clear distinction between  $y_{i+}$  and  $y_{i-}$ . In fact, one is a known function of the other and of the vector  $\mathbf{c}$ , through the relation  $\mathbf{h}$ .

As already introduced, if some of the initial values are known, the problem is simpler. In fact, the vector  $\mathbf{p}$  is reduced to the estimate only of the unknown components of the vector  $\mathbf{z}(0)$  and the vector  $\Psi$  consists only of the boundary conditions which are unknown at the initial instant.

The matrix in the left term of equation (4.23) can be calculated numerically instead than analytically. In fact, its  $i$ -th row can be obtained slightly changing the  $i$ -th component of the vector  $\mathbf{p}$ , through the addition of a certain  $\Delta p$ . It is important to keep the other components fixed when proceeding with the integration. Thus, it is possible to

calculate the related change in the boundary conditions  $\Delta\Psi(\Delta p)$  and, through linearization, to obtain the corresponding row with the expression:  $\Delta\Psi/\Delta p$ . This method allows to cut down the computational time in some cases. On the other hand, the convergence of such a procedure is not granted. As a matter of fact, the numerical determination of the matrix in equation (4.23) is way less precise than its calculation through the solution of the system (4.27). Considering the sensibility of the problem, even adopting the most suitable value of  $\Delta p$  — that, relying on empirical knowledge, lies usually between  $10^{-7}$  and  $10^{-6}$  — the introduced numerical approximation can compromise the convergence of the solution.

Anyway, in spite of the higher precision of the analytical method, the numerical procedure is adopted in this work in order to calculate the Jacobian of the system and the matrix  $\left[\frac{\partial\Psi}{\partial s}\right]$  to reduce the computational times.

The linearization, introduced in order to calculate the correction  $\Delta\mathbf{p}$  — given by equation (4.23) — of the first attempt initial values, brings to errors that can invalidate the method's convergence. In fact, the linearization can bring the error on the boundary conditions to grow instead then decreasing. In order to solve this problem, the following strategy is carried out:

- In order to prevent the method from distancing too much from the solution of the problem, the correction applied is only a fraction of the one determined using equation (4.23). In particular:

$$\mathbf{p}^{r+1} = \mathbf{p}^r + K_1\Delta\mathbf{p} \quad (4.31)$$

where  $K_1 \in [0.1, 1]$ . These values are determined empirically during the first implementations of the codes, and depend on the distance of the first solution from the one searched

- Each iteration follows the same logic operations:
  1. The new vector of the attempt initial values  $\mathbf{p}^{r+1}$  is determined through equation (4.31)
  2. The motion differential equations are integrated
  3. The error on the boundary conditions  $E_{max}^{r+1}$  is compared to the one retrieved from the previous iteration step  $E_{max}^r$ . Then if:

$$E_{max}^{r+1} < K_2 E_{max}^r$$

the next iteration can be carried out. It is worth highlighting that, in order to converge to the solution, the error on the boundary conditions may grow in the first iterations. Thus, the value of  $K_2$  shall be greater than one. In particular, a value  $K_2 \in [2, 3]$  brings satisfying results.

- If the error connected to the latest iteration is too high with respect to the previous, the method proceeds with the bisection of the correction. That is to say that half

of the determined change is brought to the vector  $\mathbf{p}$  for the integration of the motion equations. Mathematically:

$$\mathbf{p}^{r+1} = \mathbf{p}^r + K_1 \Delta \mathbf{p} / 2 \quad (4.32)$$

The new error is then compared to the one of the previous iteration step. If necessary, the bisection can be applied to the correction value up to 5 times. If even after such a procedure the new iteration determines an error greater than the previous one, the computation is stopped. This means that the chosen attempt solution is not compatible with the convergence of the method and has to be modified.

## Chapter 5

# Problem Definition

*"This world's a treasure, but it's telling us to leave for a while now"*  
— Interstellar

In this Chapter will be presented the equations describing the analyzed problem, to which the *Optimal Control Theory* is applied, thus specifying the notions and general equations introduced in the preceding Chapter to the missions considered in this work. In the end, the strategy for the identification of the most suitable targets will be introduced, as well as the characteristics of the reference spacecraft for the mission.

The optimal trajectories that will be studied are defined in a heliocentric reference system. Thus, given the considerations highlighted in Chapter 2, it is possible to study the problem adopting the approximation of the *Two-Body Problem*. The vectorial differential equations describing the motion of the satellite are:

$$\frac{d\mathbf{r}}{dt} = \mathbf{V} \quad (5.1)$$

$$\frac{d\mathbf{V}}{dt} = -\frac{\mu_{\odot}}{r^2} \frac{\mathbf{r}}{r} + \frac{\mathbf{T}}{m} \quad (5.2)$$

$$\frac{dm}{dt} = -\frac{T}{c} \quad (5.3)$$

where  $\mathbf{r}$  is the position vector of the satellite with respect to the Sun,  $\mathbf{V}$  is the velocity vector of the spacecraft and  $\mathbf{T}$  is the thrust vector. Clearly,  $\mu_{\odot}$  is the Sun's gravitational parameter.

From the *Theory of Optimal Control* it is known that:

$$H = \Phi + \boldsymbol{\lambda}^T \mathbf{f}$$

that, combined with the vectorial expression of the *State Equations* brings to:

$$H = \boldsymbol{\lambda}_r^T \mathbf{V} + \boldsymbol{\lambda}_V^T \left( -\frac{\mu_{\odot}}{r^2} \frac{\mathbf{r}}{r} + \frac{\mathbf{T}}{m} \right) - \lambda_m \frac{T}{c} \quad (5.4)$$

Such expression can be reformulated introducing the *Switching Function*:

$$S_F = \frac{\boldsymbol{\lambda}_V^T \mathbf{T}}{mT} - \frac{\lambda_m}{c} \quad (5.5)$$

that brings to the following expression for the Hamiltonian:

$$H = \boldsymbol{\lambda}_r^T \mathbf{V} + \boldsymbol{\lambda}_V^T \mathbf{g} + TS_F \quad (5.6)$$

where  $g = -\frac{\mu_{\odot}}{r^2} \frac{r}{r}$ .

The optimal control imposes the maximization of the Hamiltonian, thus the thrust to be parallel to the *primer vector*:  $\lambda_V$ . This consideration brings to the definition of:

$$S_F = \frac{\lambda_V}{m} - \frac{\lambda_m}{c} \quad (5.7)$$

Thus, the switching function, and in particular its sign, define the strategy to maximize the Hamiltonian:

$$S_F < 0 \quad \longrightarrow \quad T = 0 \quad (5.8)$$

$$S_F > 0 \quad \longrightarrow \quad T = T_{max} \quad (5.9)$$

## 5.1 Spherical Coordinates

The trajectory of the spacecraft that performs the mission is described by a set of vectorial equations, that shall be projected on a convenient reference system of coordinates.

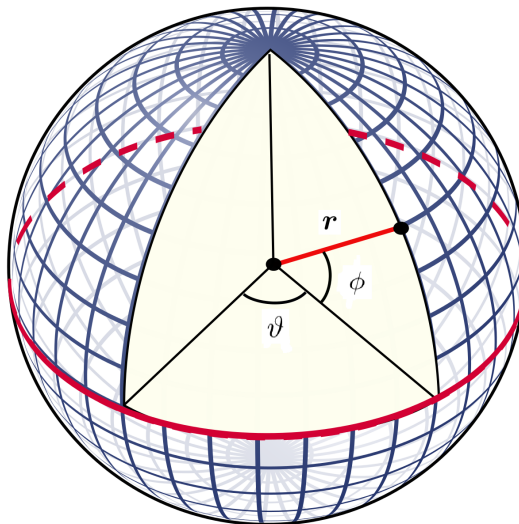


Figure 5.1: Spherical coordinates

The optimal choice is an inertial reference frame, given the absence of Coriolis and inertial accelerations. Thus, a spherical set of coordinates is adopted to describe the satellite position and velocity vectors, in the inertial frame based on the equatorial plane of the central body — in this case, the Sun—.

The *position vector* of the spacecraft is:

$$\mathbf{r} = \begin{bmatrix} r \\ \vartheta \\ \phi \end{bmatrix} \quad (5.10)$$

where  $r$  is the distance from the Sun,  $\vartheta$  is the longitude and  $\phi$  is the latitude. A graphical representation of the entities described above is presented in Fig. 5.1.

The *velocity vector* of the spacecraft is made up of the following components:

$$\mathbf{V} = \begin{bmatrix} u \\ v \\ w \end{bmatrix} \quad (5.11)$$

being  $u$ ,  $v$  and  $w$  respectively the radial, tangential and normal components.

Perhaps, it is easier to understand the physical orientation of the velocity components looking at their graphical representation in the horizon plane, reported in Fig. 5.2.

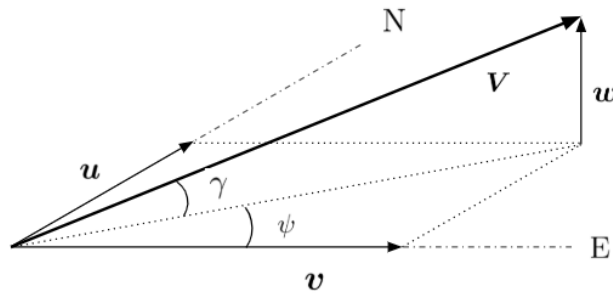


Figure 5.2: Velocity components in the horizon plane

## 5.2 State and Adjoint Variables

Projecting the *State Equations* in the chosen reference frame, being the state vector  $\mathbf{x} = [r \ \vartheta \ \phi \ u \ v \ w \ m]$ , the following expressions are obtained:

$$\frac{dr}{dt} = u \quad (5.12)$$

$$\frac{d\vartheta}{dt} = \frac{v}{r \cos \phi} \quad (5.13)$$

$$\frac{d\phi}{dt} = \frac{w}{r} \quad (5.14)$$

$$\frac{du}{dt} = -\frac{1}{r^2} + \frac{v^2}{r} + \frac{w^2}{r} + \frac{T}{m} \sin \gamma_T \quad (5.15)$$

$$\frac{dv}{dt} = -\frac{uv}{r} + \frac{vw}{r} \tan \phi + \frac{T}{m} \cos \gamma_T \cos \psi_T \quad (5.16)$$

$$\frac{dw}{dt} = -\frac{uw}{r} - \frac{v^2}{r} \tan \phi + \frac{T}{m} \cos \gamma_T \sin \psi_T \quad (5.17)$$

$$\frac{dm}{dt} = -\frac{T}{c} \quad (5.18)$$

where  $\gamma_T$  and  $\psi_T$  are the *flight path angle* and the *heading angle* of the thrust respectively. Their physical meaning can be easily inferred looking again at Fig. 5.2, where the same angles referred to the velocity vector are displayed.

It is then possible to formulate the expression of the *Hamiltonian*:

$$\begin{aligned} H = & \lambda_r u + \lambda_\vartheta \frac{v}{r \cos \phi} + \lambda_\phi \frac{w}{r} + \\ & + \lambda_u \left( -\frac{\mu}{r^2} + \frac{v^2}{r} + \frac{w^2}{r} + \frac{T}{m} \sin \gamma_T \right) + \\ & + \lambda_v \left( -\frac{uv}{r} + \frac{vw}{r} \tan \phi + \frac{T}{m} \cos \gamma_T \cos \psi_T \right) + \\ & + \lambda_w \left( -\frac{uw}{r} - \frac{v^2}{r} \tan \phi + \frac{T}{m} \cos \gamma_T \sin \psi_T \right) - \lambda_m \frac{T}{c} \end{aligned} \quad (5.19)$$

The thrust flight path angle and heading angle are, as a matter of fact, the controls that define the direction of the thrust itself. Relying on what has been said in the Chapter 4, it is possible to derive the optimal values of  $\gamma_T$  and  $\psi_T$ , imposing equal to null the partial derivatives of the Hamiltonian. Mathematically:

$$\left( \frac{\partial H}{\partial \mathbf{u}} \right)^T = 0$$

being  $\mathbf{u} = [\gamma_T \ \psi_T]$  the *Controls*.

This yields to the *Algebraic Equations of Control*:

$$\sin \gamma_T = \frac{\lambda_u}{\lambda_V} \quad (5.20)$$

$$\cos \gamma_T \cos \psi_T = \frac{\lambda_v}{\lambda_V} \quad (5.21)$$

$$\cos \gamma_T \sin \psi_T = \frac{\lambda_w}{\lambda_V} \quad (5.22)$$

where:

$$\lambda_V = \sqrt{\lambda_u^2 + \lambda_v^2 + \lambda_w^2} \quad (5.23)$$

is the primer vector's module. As mentioned before, the primer vector is parallel to the optimal direction of the thrust.

The only set of equations left to be defined are the differential equations for the adjoint variables:  $\boldsymbol{\lambda} = [\lambda_r \ \lambda_\vartheta \ \lambda_\phi \ \lambda_u \ \lambda_v \ \lambda_w \ \lambda_m]$ . These are the *Euler-Lagrange Equations*:

$$\frac{d\boldsymbol{\lambda}}{dt} = - \left( \frac{\partial H}{\partial \boldsymbol{x}} \right)^T$$

that for the analyzed problem becomes:

$$\begin{aligned} \dot{\lambda}_r = \frac{1}{r^2} \left[ \lambda_\vartheta \frac{v}{\cos \phi} + \lambda_\phi w + \lambda_u \left( -\frac{2}{r} + v^2 + w^2 \right) + \right. \\ \left. + \lambda_v (-uv + vw \tan \phi) + \lambda_w (-uw - v^2 \tan \phi) \right] \end{aligned} \quad (5.24)$$

$$\dot{\lambda}_\vartheta = 0 \quad (5.25)$$

$$\dot{\lambda}_\phi = \frac{1}{r \cos^2 \phi} \left( -\lambda_\vartheta v \sin \phi - \lambda_v v w + \lambda_w v^2 \right) \quad (5.26)$$

$$\dot{\lambda}_u = \frac{1}{r} (-\lambda_r r + \lambda_v v + \lambda_w w) \quad (5.27)$$

$$\dot{\lambda}_v = \frac{1}{r} \left[ -\lambda_\vartheta \frac{1}{\cos \phi} - 2\lambda_u v + \lambda_v (u - w \tan \phi) + 2\lambda_w v \tan \phi \right] \quad (5.28)$$

$$\dot{\lambda}_w = \frac{1}{r} (-\lambda_\phi - 2\lambda_u w - \lambda_v v \tan \phi + \lambda_w u) \quad (5.29)$$

$$\dot{\lambda}_m = \frac{T}{m^2} \lambda_V \quad (5.30)$$

## 5.3 Dimensionless Quantities

Before entering the core of the problem definition and of the adopted methodology it is useful to describe some reference quantities. In particular, these are used to formulate the problem in a dimensionless, and therefore more general, form.

### 5.3.1 Dimensionless Distance

Instead of using distances in kilometers to define spatial variables —such as  $r$ —, all the distances are defined as a multiple of the astronomical unit:

$$1 \text{ AU} = 149597870.7 \text{ km}$$

which is roughly the distance between the Earth and the Sun. The adoption of astronomical units as the measure of distance allows to operate with numbers which are of the order of units, instead of several millions. As a matter of fact, studying missions towards NEAs, rarely the distance of the spacecraft from the Sun exceeds  $3 \text{ AU}$  or falls under  $0.7 \text{ AU}$ . Thus, the reference distance is exactly:

$$r_{conv} = 1 \text{ AU}$$

### 5.3.2 Dimensionless Time

Also the time is expressed in a dimensionless form. In particular, time is related to the revolution of the Earth around the Sun. Thus, instead of using years, radians are used to measure time. This means that one year, being the equivalent of a complete revolution of Earth, corresponds to a turn:

$$1 \text{ year} = 2\pi \text{ rad}$$

On the basis of the preceding considerations, the reference time is:

$$t_{conv} = \frac{365 \text{ days}}{2\pi} = 58.13244088 \text{ days}$$

It is then necessary to define a starting date from which time is measured. As in most space mission analysis  $J2000$  is used as the reference date. Thus:

$$\text{if } t = 125.66 \quad \longrightarrow \quad \text{date} = J2000 + \frac{t}{2\pi} = 1/1/2020$$

### 5.3.3 Dimensionless Velocity

On the basis of what has been said concerning the dimensionless form of distances, it is easy to guess that also the velocities will be referred to a characteristic velocity of the Earth's orbit. As a matter of fact, all the velocities are expressed as a multiple of the circular velocity of the Earth:

$$V_{conv} = \sqrt{\frac{\mu_{\odot}}{r_{conv}}} = 29.78469183 \text{ km/s}$$

The motivation that brings to express velocities in a dimensionless form is the same that drives the use of dimensionless distances. With this operation all the velocities are near 1, beside being the dimensionless approach more general.

### 5.3.4 Dimensionless Acceleration and Mass

Again, it is possible to refer to the Earth's orbit to find the reference acceleration. This is:

$$a_{conv} = \frac{\mu_{\odot}}{r_{conv}^2} = 5.930083517 \cdot 10^6 \text{ km/s}^2$$

As far as mass is concerned, the reference one is the initial mass of the spacecraft. Thus, at the beginning of the mission the mass will be equal to 1, while the final mass will be equal to the ratio of the final and initial masses.

## 5.4 Boundary Conditions

After the definition of the set of differential equations and the dimensionless parameters, it is necessary to introduce the boundary conditions of the problem. As it has already been introduced, the mission considered has a departure from one between the Lagrangian points  $L4$  and  $L5$ , leverages an Earth gravity assist and then reaches the target asteroid. Thus, it is possible to set some boundary conditions in the relevant moments of the mission. In particular, the following numeration is adopted to indicate the various points of the mission:

- Departure:  $\longrightarrow$  **0**
- Before fly-by:  $\longrightarrow$  **1**
- After fly-by:  $\longrightarrow$  **2**
- Arrival:  $\longrightarrow$  **3**

### 5.4.1 Departure

At the moment of the departure, the spacecraft is either in  $L4$  or in  $L5$ , thus:

- If the departure is from  $L4$ :

$$\mathbf{r}(t_0) = \mathbf{r}_{Earth}(t_0 + \frac{\pi}{3})$$

$$\mathbf{V}(t_0) = \mathbf{V}_{Earth}(t_0 + \frac{\pi}{3})$$

- If the departure is from  $L5$ :

$$\begin{aligned}\mathbf{r}(t_0) &= \mathbf{r}_{Earth}(t_0 - \frac{\pi}{3}) \\ \mathbf{V}(t_0) &= \mathbf{V}_{Earth}(t_0 - \frac{\pi}{3})\end{aligned}$$

Clearly, at the beginning of the mission:

$$m(t_0) = 1$$

### 5.4.2 Fly-By

In order to perform an Earth fly-by, to leverage the gravity assist, the spacecraft and the Earth must be in the same position at the same time.

$$\mathbf{r}(t_1) = \mathbf{r}_{Earth}(t_1)$$

Since the fly-by manoeuvre is negligible, both in terms of space and time, if compared to the characteristic distances and durations of the heliocentric phases, there is no difference in position and time before and after the gravity assist. Mathematically:

$$t_1 = t_2 \quad \longrightarrow \quad \mathbf{r}(t_1) = \mathbf{r}(t_2)$$

Needless to say, the spacecraft shall have a non-null velocity with respect to Earth to perform the gravity assist — $V_\infty \neq 0$ —. Furthermore, on the basis of what has been said in Chapter 2, the fly-by is a discontinuity in velocity. As a matter of fact, it is used to change the velocity direction and module.

On the other hand, the module of the hyperbolic excess velocity shall not change across the fly-by. Thus, it is necessary to formulate the following boundary condition:

$$[\mathbf{V}_1 - \mathbf{V}_{Earth}(t_1)]^2 = [\mathbf{V}_2 - \mathbf{V}_{Earth}(t_1)]^2 = V_\infty^2$$

This means that the fly-by can be seen as an instant rotation of the hyperbolic excess velocity —while the heliocentric velocity changes both in module and direction—.

Moreover, as will be further explained, the fly-by must be effectuated near the intersection between the orbit of the NEA and the Earth. This is not a boundary condition properly said, but has been a crucial driving aspect of the mission design.

The minimum height of the fly-by manoeuvre is fixed at  $h = 500 \text{ km}$  above the Earth's surface. Nonetheless, it may happen that the optimal trajectory leverages a gravity assist with a lower altitude. In such cases, it is necessary to bound the fly-by altitude at the imposed minimum, hence changing the free fly-by in a constrained one. Constrained fly-by rely on the following additional condition:

$$[\mathbf{V}_1 - \mathbf{V}_{Earth}(t_1)] [\mathbf{V}_2 - \mathbf{V}_{Earth}(t_1)] = 2 \cos \delta V_\infty^2$$

where  $\delta$  is the rotation of the hyperbolic excess velocity, and is defined as:

$$\sin\left(\frac{\delta}{2}\right) = \frac{\frac{\mu_{\odot}}{(R_{\odot}+h)}}{V_{\infty}^2 + \frac{\mu_{\odot}}{(R_{\odot}+h)}}$$

### 5.4.3 Arrival

At the arrival the spacecraft shall have the same orbit as the target asteroid, thus the same position and velocity vectors. Mathematically:

$$\mathbf{r}(t_3) = \mathbf{r}_{NEA}(t_0)$$

$$\mathbf{V}(t_3) = \mathbf{V}_{NEA}(t_0)$$

## 5.5 Initial Conditions

Once the boundary conditions are defined it is necessary to carry out one last step. As a matter of fact, the adopted indirect method needs an initial guess of some conditions to carry out the analysis. Such initial conditions are contained in the already described vector  $\mathbf{p}$ , which for the analyzed case is:

$$\mathbf{p} = \begin{bmatrix} t_0 & t_1 & \lambda_{\vartheta 0} \\ t_3 & \lambda_{\vartheta 2} & t^* \\ u_2 & v_2 & w_2 \\ \lambda_{r2} & \lambda_{\phi 2} & \lambda_{u2} \\ \lambda_{v2} & \lambda_{w2} & V_{\infty 0} \\ r_0 & \vartheta_0 & \phi_0 \\ u_0 & v_0 & w_0 \\ \lambda_{r0} & \lambda_{\phi 0} & \lambda_{u0} \\ \lambda_{v0} & \lambda_{w0} & m_0 \end{bmatrix} \quad (5.31)$$

where:

- $[t_0 \ t_1 \ t_3 \ t^*]$ : are respectively the departure time, the time of fly-by, the arrival time and the 'optimal' duration of the fly-by. As a matter of fact, the influence of this last quantity is almost negligible, as far as it is very low: for example  $10^{-20}$ .
- $[\lambda_{\vartheta 0} \ \lambda_{\vartheta 2}]$ : are the value of  $\lambda_{\vartheta}$  at the departure and after the fly-by. Equation (5.23) highlights that in each arch this adjoint variable is constant, thus:

$$\lambda_{\vartheta 0} = \lambda_{\vartheta 1}$$

$$\lambda_{\vartheta 2} = \lambda_{\vartheta 3}$$

- $[r_0 \vartheta_0 \phi_0 u_0 v_0 w_0 \lambda_{r0} \lambda_{\phi0} \lambda_{u0} \lambda_{v0} \lambda_{w0}]$ : are the state and adjoint variables at the departure.
- $[u_2 v_2 w_2 \lambda_{r2} \lambda_{\phi2} \lambda_{u2} \lambda_{v2} \lambda_{w2}]$ : are the state and adjoint variables after the gravity assist.
- $[V_{\infty0} m_0]$ : are the departure hyperbolic excess velocity, which is null being the satellite in a Lagrangian point and therefore outside the Earth's sphere of influence, and the initial mass, which is  $m_0 = 1$ .

The vector  $\mathbf{p}$  is the starting point for the integration of the differential equations. In order to attain the desired solution, the initial attempt of  $\mathbf{p}$  shall be built up with care and attention. As a matter of fact, the numerical method is sensible to the variation of initial conditions.

At each iteration the conditions in  $\mathbf{p}$  are updated on the basis of the distance of the obtained solution from the boundary conditions imposed. Once that the desired accuracy — i.e. an error equal to  $10^{-7}$  on the boundary conditions — is obtained the iterations stop, since the optimal solution has been found.

If the initial guess is not precise enough, the numerical method does not converge and the error constantly grows: thus the iteration chain is stopped.

Since the mission leverages a gravity assist, on the basis of what has been said in Paragraph 2.3.1, also the height of the fly-by must be monitored. If the optimal solution found needs a too low fly-by to be carried out, for obvious reasons it is not considered. Nonetheless, it is possible to find a solution with a constrained fly-by. In the numerical code is imposed the height of the fly-by, and the optimal mission with this adjoint constraint is sought. Perhaps, the so found solution is not as good as the one with free fly-by in terms of payload fraction, but it is feasible —which of course is the most important aspect—.

### 5.5.1 Tentative Solution Definition

As mentioned, the definition of the initial guess is crucial for the convergence of the method. Fortunately, the strategy of the mission allows to define most of the variables of the vector  $\mathbf{p}$ .

Given the considerations in Section 5.4, it is possible to define the position and the velocity of the spacecraft at the departure, once that the initial time  $t_0$  has been fixed. The initial time itself is defined with respect to the fly-by time  $t_{1-2}$ . In fact, the fly-by is carried out when the Earth passes at the point of MOID. If, ideally, both the Earth and the NEA passed in this point at the same time, the rendezvous could be carried out instantaneously, attaining after the gravity assist the same velocity of the NEA. Actually, a phase between the Earth and the asteroid always exists, thus the fly-by time and the arrival time  $t_3$  do not coincide.

Anyway, once the fly-by time is fixed, it is possible to define the initial time, and therefore the initial position and velocity vectors. As will be further described, the

initial time is imposed to be one year —departure from L5— or one and a half years —departure from L4— before the fly-by date.

The velocity components after the fly-by can be imposed to be equal to the asteroid's velocity components at the close encounter. As a matter of fact, even if a phase exists between the Earth and the NEA, the fly-by is used to reach a heliocentric velocity close to the asteroid's one, so that only minor adjustments are necessary afterwards. It is possible to refine such a first initial guess considering the phase between the two bodies. In particular, it is necessary to change the in plane component  $v$  that defines the major semiaxis of the spacecraft's orbit after the fly-by. In general, little changes are sufficient.

As far as the final time is concerned, it is possible to impose it to be roughly one year after the fly-by. Thus, it is possible for the spacecraft to phase with the target asteroid. Needless to say, this variable strongly depends on the phase between the Earth and the asteroid at the close encounter. If this is little, a shorter time is sufficient to perform the phasing. On the other hand, it may be necessary to extend the second leg if the phase is not favourable.

Concerning the adjoint variables, these are imposed to be small, but are not precisely defined. Nonetheless, the sign of the primer vector's components have to be properly defined at the departure. As a matter of fact, the direction of  $\lambda_V$  defines the direction of the thrust at the beginning. As will be broadly described in the next Chapter, depending on the departure point the strategy changes, and the satellite needs either to accelerate —L4 departure— or decrease its velocity —L5 departure— at the beginning.

## 5.6 Choice of the Target Asteroids

In order to carry out the mission it is crucial to define the target. On the basis of what has been said in Chapter 1, it is clear that the number of possible targets is huge. Thus, it is necessary to narrow the field to the asteroids which present characteristics suitable and convenient for the conceived mission.

First of all, the target asteroids shall have at least one intersection point with the Earth's orbit. This is necessary for two main reasons:

- The first is related again to the considerations in Chapter 1. Only the asteroids that cross the orbit of Earth represent a threat and are therefore interesting for studies and analysis.
- The second is related to orbital mechanics considerations. In order to pass from one orbit to another, these have to be at least one common point. Now, it is not necessary for the intersection to be precise, but the orbit of Earth and NEA must get very close in at least one point. From the point of view of the strategy of the mission, in this point the gravity assist manoeuvre will be effectuated. This way, it is possible to inject the spacecraft in an orbit close to the NEA's one, leveraging the fly-by manoeuvre, and not relying on thrust: thus saving propellant.

Since the considered database of NEAs —retrieved from the *JPL Small Body Objects Database*— presents asteroids with major semiaxis greater than the one of the Earth's

orbit, the common point of the two orbits will be the NEA's perihelion. Moreover, if the NEA's perihelion was precisely 1  $AU$ , it would be possible for the spacecraft to acquire after the fly-by a hyperbolic excess velocity which lies in the horizon plane, to perform the rendezvous. Thus, since no radial component would be needed, the spacecraft would have to reach a lower module of  $V_\infty$ , saving propellant in the first leg.

Hence, the first condition imposed is that the NEA's orbit shall be near 1  $AU$ . Such a condition is not binding, but missions towards NEAs with this orbital property are more convenient. At first, the possibility to narrow the field to asteroids which have the perihelion between 0.9  $AU$  and 1.1  $AU$  was sought. However, this condition was too broad and too many asteroids resulted adequate. Thus it was necessary to impose a tighter requirement, that in the end resulted in the following statement:

$$0.98 \text{ AU} < r_P < 1.02 \text{ AU} \quad (5.32)$$

where  $r_P$  is the perihelion of the NEA.

In the second place, NEAs do not only have different major semiaxis if compared to Earth, they also have different inclination. Thus, the gravity assist shall not only bring the heliocentric velocity module —and therefore the orbit's mechanical energy, which is connected to the major semiaxis as stated in equation (2.6)— of the satellite close to the NEA's one, but it also have to bring the inclination of the spacecraft's orbit near the one of the target, rotating the heliocentric velocity. As a matter of fact, this last consideration is even more important than the first. In fact, the manoeuvres that change the orbital plane are the most expensive from a propulsive point of view.

Without entering the detail of these manoeuvres, their maximum effectiveness is reached if the velocity direction —heading angle— is changed at the nodes of the orbit. In fact, if the velocity is rotated in the ascending or descending node, all the propulsive effort of the thruster is used to change inclination, because the heading change is exactly equal to the inclination change. On the other hand, if the velocity is rotated in another point of the trajectory, the propulsive effort is shared between two effects: a change in inclination and a change in RAAN — since  $\Delta i \neq \Delta \psi$ —. Since, in the analyzed mission, there is no will to change  $\Omega$ , the fly-by has to be performed near a node of the asteroid's orbit. Clearly, the fly-by happens on the Earth's orbit. Thus, one node of the NEA's orbit shall be in the nearby of 1  $AU$ . Mathematically, the second constraint is:

$$0.98 \text{ AU} < r_{AN} < 1.02 \text{ AU} \quad \text{or} \quad 0.98 \text{ AU} < r_{DN} < 1.02 \text{ AU} \quad (5.33)$$

where  $r_{AN}$  and  $r_{DN}$  respectively are the distance of the ascending node and of the descending node of the asteroid's orbit from the Sun.

Imposing the previously described conditions, the field is narrowed to 62 asteroids. Clearly, not all will be analyzed, but it is a far more manageable number than the initial one that included several thousands of NEAs.

## 5.7 Spacecraft Characteristics

As mentioned, the analysis has been carried out relying on dimensionless quantities. Nonetheless, for sake of consistency, the general characteristics of the spacecraft have to be defined. As a matter of fact, it is crucial for the properties of the satellite that carries out the mission to match with the characteristics of the mission itself, and of course to be realistic. The satellites shall be CubeSats, that are left at the departure Lagrangian points as piggyback of a bigger primary spacecraft. Indeed, CubeSats characteristics perfectly fit the requirements of NEA's orbit and physical properties analysis. As a matter of fact, there is no need to use bigger satellites that would result in not justified excessive costs.

Since, as mentioned, the equilateral Lagrangian points are characterized by stable equilibrium, the CubeSats may be left in these sweet spots, with no need of station-keeping manoeuvres to maintain the position. There they could wait the most favourable moment for departure, maybe using the waiting time to carry out space observation activities.

The reference satellite is the Lunar IceCube. It is a 6U CubeSat characterized by a 14 kg global mass and a 3.5 kg payload capacity. It is propelled by a BIT-3 — Busek Ion Thruster - 3 cm grid—: a gridded radiofrequency ion thruster. In spite of most ion thrusters using Xenon as a propellant, the BIT-3 is regarded as the first gridded ion thruster using *iodine* — $I_2$ — propellant. The advantage of an iodine-fueled thruster relies on the storage characteristics of this propellant. The main advantage is due to the capability of iodine to be stored as a solid. Thus, there is no need for the heavy and expensive high pressure tanks used to store Xenon. This allows great savings in terms of weight, and therefore cost. The propulsive characteristics of iodine are not far from the ones of Xenon. As a matter of fact, further development in the technology may allow  $I_2$  to overcome the performances of  $Xe$ . BIT-3 is characterized by a total wet mass of 3 kg, that includes 1.5 kg of propellant. As far as the propulsive performance are concerned:

$$I_s = 2100 \text{ s} \quad T = 1.24 \text{ mN} \quad P = 70 \text{ W}$$

As mentioned, the Lunar IceCube is used as a reference model to study feasible and realistic trajectories. Nonetheless, the results obtained and showed in the next Chapter are obtained with slightly different propulsive performances. In particular, the characteristic acceleration, defined as the ratio of thrust and mass, has been considered a bit higher than the one of the Lunar IceCube. For such satellite:

$$\frac{T}{m} = 0.08857 \frac{mm}{s^2}$$

For the analyzed case, it has been considered:

$$\frac{T}{m} = 0.09967 \frac{mm}{s^2}$$

This means that if the same mass as the Lunar IceCube —14 kg— is considered, the thrust has to be 1.4 mN. As far as the current technology is concerned, these values are

not feasible yet, but further improvement can make them real. Viceversa, if the same thrust as the one produced by BIT-3 is implemented, the total mass has to be 12.44 kg. This solution may be feasible, if a payload of 2 kg —instead of the nominal 3.5 kg— is implemented and can still fulfill the mission requirements and activities.

# Chapter 6

## Results

*"Eureka!"*

In this Chapter will be presented the results obtained from the trajectory optimization towards seven asteroids, chosen following the criteria explained above. The designated target asteroids are:

Asteroid	$a$ (AU)	$e$	$i$ (deg)	$\omega$ (deg)	$\Omega$ (deg)
2014 FZ	1.3699	0.2652	2.4157	176.1851	18.2759
2004 FN8	1.1689	0.1447	5.2588	159.7901	4.0793
2012 UE34	1.1054	0.0993	9.6576	18.3640	198.4632
2008 TS10	1.2584	0.2026	1.4684	345.3689	5.6386
2015 XA379	1.2876	0.2183	1.3460	349.4535	148.5370
2016 YE	1.1296	0.1082	8.4836	7.4413	83.6439
2017 BN93	1.0445	0.0514	2.1204	23.3681	315.7962

Table 6.1: Chosen asteroids

Before entering the particulars of the solutions, it is necessary to describe some aspects of the methodology followed.

Given the inherent cyclical nature of orbital mechanics phenomena, it is clear that does not exist only one single optimal mission. As a matter of fact, fixed the strategy — mission with gravity assist— and the target, there are several windows that correspond to one —or more— optimal trajectory.

It goes without saying that each of these missions will be the optimal one for its launch window, but among them there will be one which is better than the others. The superiority of the best mission is due to the phasing of the bodies involved, in this case: the Earth and the target NEA. In fact, the phasing between these two celestial bodies changes from one moment to the other, thus there is one particular phasing that minimizes the mission's cost, thus maximizing the payload fraction.

In order to find the optimal trajectory, different periods in times are explored for the starting of the mission. One example, referred to the mission towards 2012 UE34 with departure from L5, is reported in Tab. 6.2.

	Mission 1	Mission 2	Mission 3	Mission 4
$\frac{m_f}{m_i}$	0.8828	0.8563	0.8748	0.8606
Duration (days)	968	926	1308	1399
Departure date	1/ 4/2026	31/ 3/2027	2/ 4/2027	31/ 3/2028
Fly-by date	12/ 4/2027	11/ 4/2028	12/ 4/2028	11/ 4/2029
Arrival date	24/11/2028	12/10/2029	30/10/2030	30/ 1/2032
Fly-by type	Constrained	Constrained	Constrained	Constrained
Phase* (deg)	13	69	69	117
	Mission 5	Mission 6	Mission 7	Mission 8
$\frac{m_f}{m_i}$	0.9169	0.8852	0.8841	0.8617
Duration (days)	1391	1028	619	906
Departure date	1/ 4/2032	31/ 3/2033	28/ 3/2033	31/ 3/2034
Fly-by date	12/ 4/2034	12/ 4/2034	9/ 4/2034	12/ 4/2035
Arrival date	22/ 1/2036	23/ 1/2036	7/12/2034	22/ 9/2036
Fly-by type	Constrained	Constrained	Constrained	Constrained
Phase* (deg)	3	3	3	60

Table 6.2: Missions towards 2012 UE34, departure from L5

\* between the Earth and the asteroid at the fly-by

As it can be seen, the same mission can be carried out in different periods, resulting in different durations and payload fractions.

Mission 1 and Mission 2 have almost the same duration, but are characterized by different payload fractions. Being the ratio  $\frac{m_f}{m_i}$  higher for Mission 1, it is clear that this is characterized by a more favourable phasing of the bodies.

Furthermore, Tab. 6.2 allows to introduce other concepts that have been crucial for the definition of the best trajectory.

Comparing Mission 2 and Mission 3, it is possible to note that these have almost the same departure and fly-by dates, but the arrival is shifted by roughly one year. Mission 3 is longer, but it is also characterized by a higher  $\frac{m_f}{m_i}$  ratio. This highlights the fact that, for any mission, there is a longer version and a shorter one. The first is connected to a smaller propellant output, since relying on much time to be carried out, there is a lower use of thrust. The second, on the other hand, has to be carried out in a shorter time, thus is connected to a broader use of thrust, resulting in a higher need of propellant.

At a first glance, it may seem that the same concept may motivate the difference between Mission 5 and Mission 6. But at a more careful analysis, it is possible to see

that the arrival date of these two missions, which effectuate the fly-by in the very same moment, is the same as well. The difference is indeed in the first leg, the one between departure and fly-by. While Mission 6 takes one year roughly to carry out this phase, Mission 5 needs double the time. Again, the longer mission is connected to a lower propulsive cost.

The presence of such similar, but anyway different, missions is due to the characteristics of the method used for the analysis. The numerical code maximizes the payload, but it is left to the analyst to optimize the initial and final times. As a matter of fact, even if the longer missions are more efficient, their duration is not justified by the advantages in terms of payload fraction. Indeed, between the couple of missions which have the same fly-by date but different departure or arrival time, the shortest is chosen.

Besides this optimization of final and initial times, which translates the dates of roughly one year, there is another, more technical and subtle refinement to carry out.

Sometimes the solution found, presents one —or both— of these two flaws:

- $S_F(t_0) < 0$ : thus meaning that, at the found departure time, the spacecraft is not thrusting. Clearly this means that the first part of the trajectory is useless: the optimal trajectory starts when the spacecraft begins to use thrust.
- $S_F(t_f) < 0$ : thus meaning that, at the found final time, the spacecraft is not thrusting. This means that the last part of the trajectory is a simple coasting arch that has no utility. Thus, the final time has to be refined.

These two aspects are considered and the solutions found are refined, smoothing the initial and final times to find the optimal —that is to say minimum— duration. Clearly, these changes are connected to minimal or null changes in the payload fraction, since they simply imply the elimination of useless segments of the trajectory.

Mathematically, the conditions searched are:

- *Departure*:  $S_F = 0$  and  $t \uparrow \longrightarrow S_F > 0$

The mission starts with a null switching function, but as the time increases the switching function becomes positive. Thus, the mission begins exactly when the satellite begins to use thrust.

- *Arrival*:  $S_F = 0$  and for  $t = t_f - dt \longrightarrow S_F(t) > 0$

The mission ends exactly when the satellite stops thrusting.

On the basis of the criteria described above, the optimal solution is Mission 7. Although it is not the one with the higher payload fraction, it is the shorter —Mission 6 has a longer second leg and Mission 5 has both first and second phases of the mission longer— among the ones with the most favourable phasing. As will be further described, for favourable phasing is implied a small —or ideally null— phase shift between the two bodies at the close encounter, i.e. the fly-by position.

## 6.1 Asteroid 2014 FZ

Asteroid 2014 FZ has been the first one, in chronological order, to be analyzed. Therefore, it is described as a case study: as a matter of fact, many characteristics of the optimal missions towards this NEA are common to the others. This means that, while describing the missions designed to reach 2014 FZ, will be described the common features that are shared with all the other missions. Clearly, some asteroids present some peculiarities that will be highlighted at the proper moment. Nonetheless, for sake of brevity, the considerations that are explained in this Section will not be repeated for each asteroid.

The characteristics of the optimal missions towards 2014 FZ are summarized in the synoptic Tab. 6.3. In this table it is possible to appreciate an immediate comparison between the mission with departure from L4 and the one that has L5 as starting point.

	Departure from L4	Departure from L5
$\frac{m_f}{m_i}$	0.9209	0.9106
Duration (days)	1207	974
Departure date	8/ 8/2028	26/ 3/2029
Fly-by date	9/ 4/2030	9/ 4/2030
Arrival date	28/11/2031	25/11/2031
Fly-by type	Free	Constrained
$V_\infty$ at fly-by	0.1372	0.1373

Table 6.3: Asteroid 2014 FZ, optimal mission characteristics

First of all it is possible to note the difference in terms of duration between the two missions. This is due to the difference, in terms of strategy, imposed by the starting point of the trajectory.

The Lagrangian point L4 is  $60^\circ$  before the Earth while L5 occupies the symmetrical position with respect to the blue planet. This implies a different strategy for the first phase of the mission: the one between the departure and the fly-by. When the departure is from L4 the satellite is injected on an orbit characterized by higher energy —thus higher major semiaxis— and, therefore, slower. Following this strategy, the satellite waits for the Earth, which is faster, to arrive in the correct position for the fly-by. On the other hand, when the departure is from L5, the spacecraft must chase the Earth, which is ahead its position on the same orbit. Thus, the spacecraft is injected on a faster orbit, characterized by lower energy. This way is the spacecraft to chase the planet in order to reach it in the right position for the gravity assist.

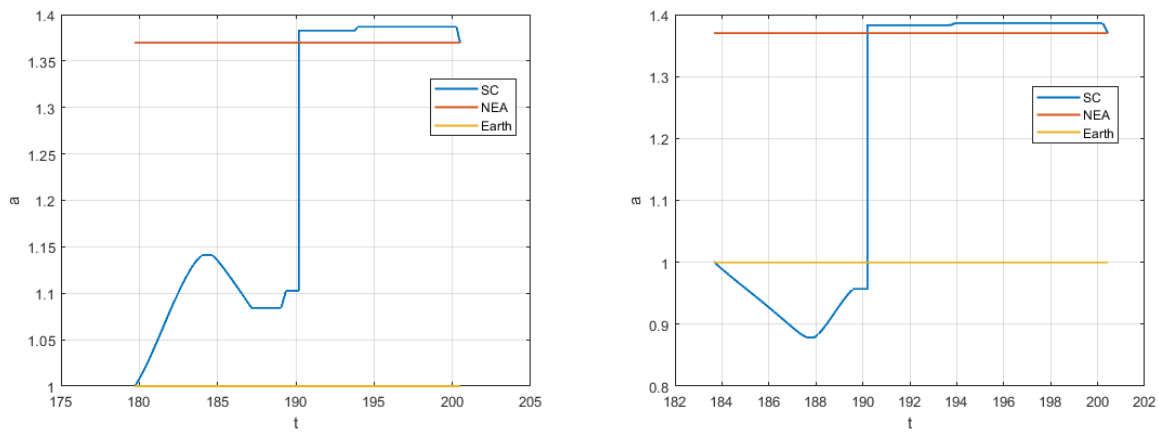


Figure 6.1: Asteroid 2014 FZ, major semiaxis evolution:  
 SX departure from L4, DX departure from L5

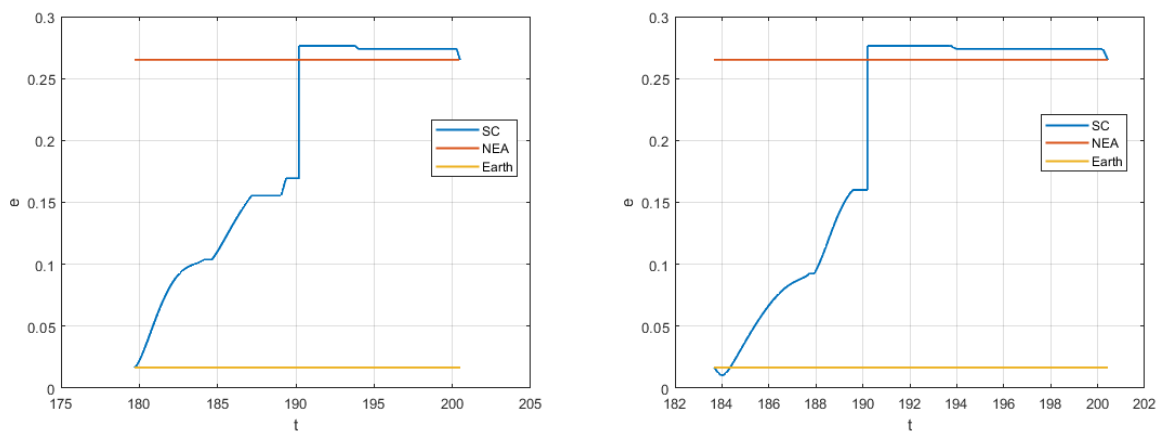


Figure 6.2: Asteroid 2014 FZ, eccentricity evolution:  
 SX departure from L4, DX departure from L5

What has been described above can be inferred looking at Fig. 6.1 and 6.2, that show the evolution of the major semiaxis of the satellite's orbit throughout the whole mission.

This difference in strategy, results in a difference in duration of the first leg of the trajectory. As a matter of fact, while the phase between the gravity assist and the arrival has almost the same length, both for the departure from L4 and L5, the first one strongly depends on the starting point. In particular, missions with departure from L4 needs 18-20 months to reach the right position for the fly-by, while the one starting from L5 only takes roughly one year. This is why the missions with departure from L5 are, in general, more than 200 days shorter than their counterpart that set-off from L4.

The drawback of having a shorter duration, is a smaller payload fraction. This difference is not so pronounced —usually limited to few percentile points— but still exists. Thus, in general, missions with departure from L4 are longer but also more efficient from a propulsive point of view. This difference is again shown in Tab. 6.3.

Looking at Fig 6.1-6.2, 6.3-6.4 and 6.5-6.6, it is possible to see the discontinuity corresponding to the fly-by manoeuvre. As a matter of fact, the fly-by is characterized by great changes in the orbital elements of the satellite's orbit in a short time —negligible if compared to the duration of the heliocentric phases—. The gravity assist is used to modify the velocity and therefore the orbital elements, taking the spacecraft's orbit close to the asteroid's one. It is possible to appreciate that the greatest change in the orbital elements happens at the fly-by: this allows great saves in terms of propellant throughput. In particular, this is true if referring to inclination. In fact, on the basis of what has been said, the major semiaxis is changed also leveraging thrust in the first phase of the mission, to take the satellite in the right position for the fly-by.

As forecastable, the fly-by date is the same for both the missions. Indeed, the optimal fly-by is leveraged at the MOID point, so there is no reason for the missions to effectuate such manoeuvre at different times, since one of the two would be sub-optimal. Nonetheless, some exceptions still exist, and will be highlighted at the proper moment. Anyway, the difference in time is always limited to few days. The perfect —and therefore ideal— fly-by is carried out when the Earth and the NEA are in the very same position, and the target orbit is obtained simply relying on the instant rotation of  $V_\infty$  provided by the gravity assist, with no need for further thrusting arches.

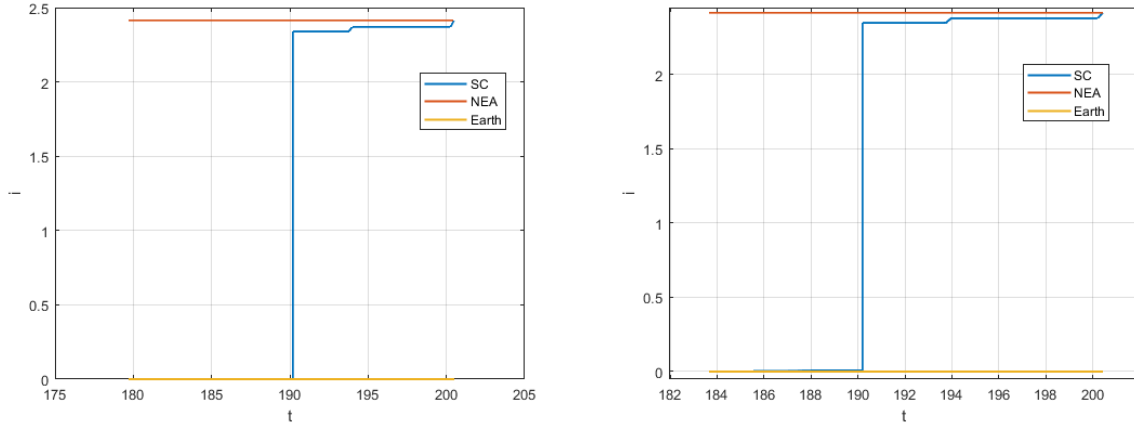


Figure 6.3: Asteroid 2014 FZ, inclination evolution:  
SX departure from L4, DX departure from L5

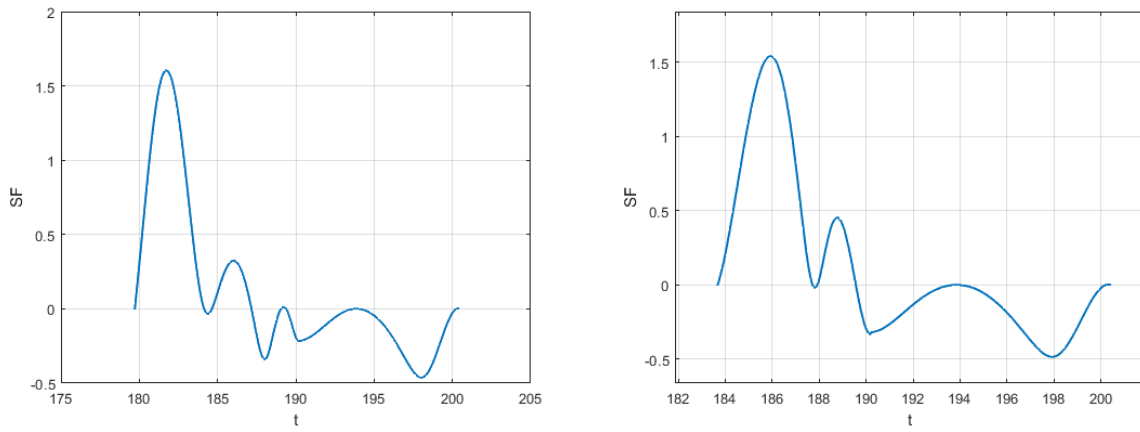


Figure 6.4: Asteroid 2014 FZ, switching function evolution:  
SX departure from L4, DX departure from L5

As far as inclination is concerned, it is not changed until the fly-by. As a matter of fact, inclination changing manoeuvres are the most expensive from a propulsive point of view. Although the considered asteroids have relatively limited inclination, it would be anyway inefficient to change this parameter using thrust. Therefore, the first phase is carried out on the Earth's orbital plane, and the velocity is rotated only at the fly-by. Clearly, it is not possible to precisely reach the values of the asteroid's orbital elements just leveraging the fly-by. Thus, as can be inferred from the figures, some little adjustment firings are necessary, to take the value of the orbital elements to the desired value in the right moment, thus performing the approach to the NEA.

The considerations introduced above, have the same validity both for the mission from L4 and L5. Moreover, the two missions share other common points.

The first, as it has already been introduced, is the phase between the fly-by and the arrival. On the basis of what has been said, it is crucial to have the fly-by near the intersection of the orbits of the Earth and the asteroid. Thus, the fly-by date is the same—or almost the same—for the two missions. Also the  $V_\infty$  is pretty much the same: this results in an arrival date which is almost equal.

Furthermore, there is a similarity concerning the first leg of the trajectory. In spite of being different in terms of strategy and duration between the trajectory starting from L4 and the one with departure from L5, this phase presents a common point shared by the two missions. As a matter of fact, the trajectory segment from the departure to the fly-by is almost always—with some asteroids representing an anomaly—characterized by two arches leveraging thrust, independently on the starting point. It is possible to appreciate this aspect from Fig. 6.9 and 6.10.

When the switching function is greater than zero, the spacecraft is thrusting, while it is not when the same parameter is negative.

Thus, at the departure the satellite starts thrusting—clearly in a different direction depending on the starting point—in order to change its phase with respect to the Earth. As it has been broadly explained, this manoeuvre implicates the injection on a slower orbit for departure from L4 and viceversa for the dual mission.

Then the satellite stops thrusting for a relatively short period. After that, there is the second thrusting arch which is used in order to meet the Earth at the proper moment for the gravity assist. It is worth highlighting that, in order to perform the gravity assist, it is not sufficient to acquire the right position. In fact, the satellite must enter the Earth's sphere of influence with a suitable  $V_\infty$  in order to carry out an effective gravity assist to reach—or almost reach—the asteroid's orbit.

In the end, it is possible to summarize all these aspects in Fig. 6.11 and 6.12, which represent the optimal trajectories' projections on the Earth's orbital plane. The orbits are described by the legend, while the highlighted points represent:

- *Departure*  $\longrightarrow$   $\bigcirc$
- *Fly-by*  $\longrightarrow$   $\triangle$
- *Arrival*  $\longrightarrow$   $\square$

It is possible to appreciate the difference in strategy and the contemporaneity of the fly-by between the two missions, while clearly all the aspects related to the thrust utilization are hidden.

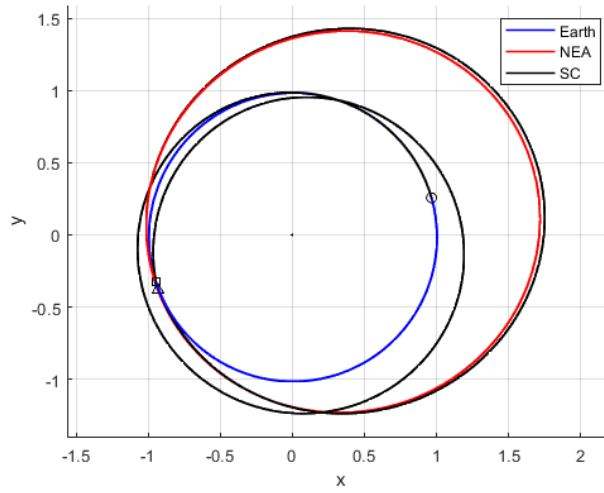


Figure 6.5: Asteroid 2014 FZ, trajectory: Departure from L4

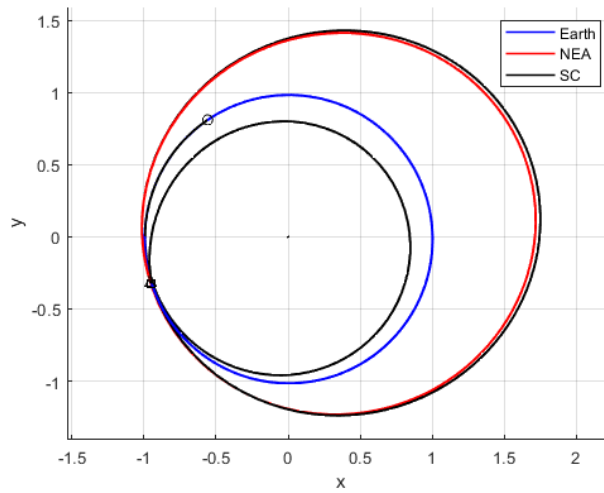


Figure 6.6: Asteroid 2014 FZ, trajectory: Departure from L5

It is possible to highlight another aspect common to almost all the missions. To introduce such a concept, it is necessary to plot the evolution of the aphelion distance of the satellite's orbit and to compare it with the aphelion of the asteroid —as shown in Fig. 6.11 and 6.12—.

As can be inferred from the previous considerations, the bigger the orbit the slower it is. Thus, a higher aphelion distance is connected to an orbit with smaller circular velocity. This aspect is crucial when referring to the fly-by. If, at the close encounter —thus near the fly-by, which is in correspondence of the two orbits intersection— the asteroid is ahead with respect to the Earth —thus it passes from the conjunction point before the blue planet—, the satellite has to chase it. In fact, the satellite is in the same position as the Earth, since it is performing the fly-by manoeuvre. This means that after the fly-by the spacecraft will inject on a faster orbit than the asteroid's one: thus, with a smaller aphelion distance.

On the other hand, if the asteroid is behind the Earth, the satellite has to inject on a slower orbit after the fly-by. Thus, it waits for the asteroid to perform the final approach. This is related to an aphelion distance greater than the asteroid's one, after the fly-by. Summing up:

- If the asteroid is before the Earth at the close encounter, the satellite shall chase the NEA:

$$r_A^{SC} < r_A^{NEA}$$

where  $r_A^{SC}$  and  $r_A^{NEA}$  are respectively the aphelion distances of the spacecraft's orbit and of the asteroid's one.

- If the asteroid is behind the Earth at the close encounter, the satellite shall wait for the NEA:

$$r_A^{SC} > r_A^{NEA}$$

It happens that, for almost all the optimal missions, the second scenario occurs. Thus, for this and the other asteroids, it can be appreciated a higher aphelion distance of the satellite's orbit, after the fly-by, if compared to the asteroid's one.

For completeness, also the evolution of the perihelion distance is shown — Fig. 6.13 and 6.14—. Clearly, the considerations on the behaviour of this parameter are not that important. In fact, to choose the asteroids the constraint in equation (1.2) has been imposed on the perihelion distance. Thus, after the fly-by, the satellite's orbit  $r_P$  goes near the value of the Earth or directly the one of the NEA.

The characteristics described above have almost general validity. Thus, they refer also to the following missions and not only to the one toward 2014 FZ.

It is now possible to introduce a peculiarity of this particular asteroid. Chronologically speaking, the mission with departure from L4 has been analyzed first. It relies on a free fly-by and presents all the aspects described.

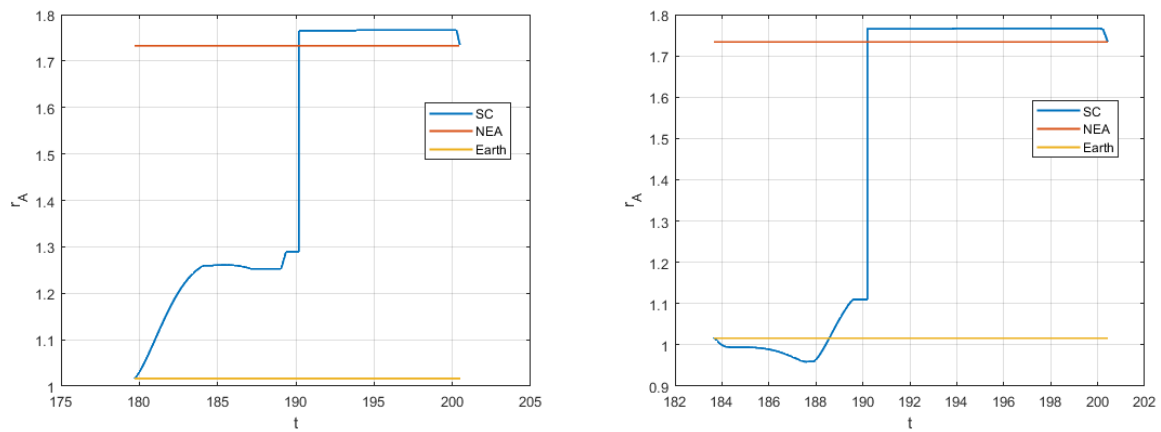


Figure 6.7: Asteroid 2014 FZ, apohelion distance evolution:  
 SX departure from L4, DX departure from L5

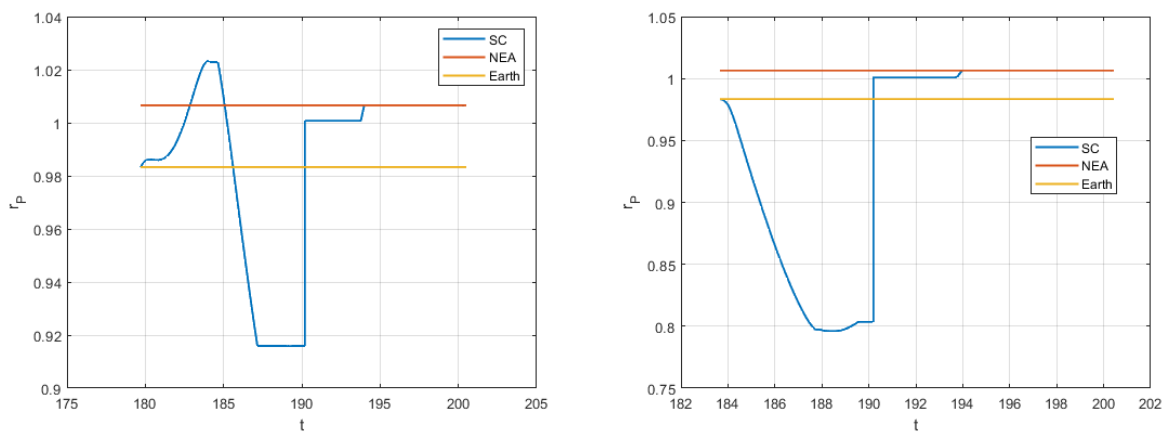


Figure 6.8: Asteroid 2014 FZ, perihelion distance evolution:  
 SX departure from L4, DX departure from L5

However, a peculiarity occurred while searching the optimal mission starting from L5. As a matter of fact, this presented all the typical aspects of the missions of its kind but, in order to be carried out, it leveraged a too low fly-by. This means that the free fly-by was characterized from an altitude lower than the imposed limit of 500 *km*.

Therefore, it has been necessary to implement a constrained fly-by to find an admissible mission. This is the only case for which the two missions towards the same asteroid require a different fly-by approach.

## 6.2 Asteroid 2004 FN8

Asteroid 2004 FN8 has a smaller orbit than 2014 FZ, but its inclination is roughly the double. This difference results in a global cost of the mission, in terms of propellant throughput, which is almost the same for the two missions. The relevant aspects of the optimal mission are summarized in Tab. 6.4.

	Departure from L4	Departure from L5
$\frac{m_f}{m_i}$	0.9290	0.9166
Duration (days)	1104	876
Departure date	28/ 7/2026	6/ 3/2027
Fly-by date	23/ 3/2028	24/ 3/2028
Arrival date	5/ 8/2029	30/ 7/2029
Fly-by type	Free	Free
$V_\infty$ at fly-by	0.1170	0.1191

Table 6.4: Asteroid 2004 FN8, optimal mission characteristics

It can be appreciated that the missions towards 2004 FN8 present all the general characteristics common to almost all the asteroids —without anomalies and peculiarities— highlighted in the preceding section, and here shortly summarized:

- The strategy for the first leg is imposed by the departure point. Looking at Fig. 6.15-6.16 it is possible to see that starting from L4 the spacecraft injects an orbit with a higher major semiaxis to wait for the Earth to gain the right position. viceversa, starting from L5 the satellite enters an orbit with a lower major semiaxis to reach the blue planet at the fly-by position.
- The mission with departure from L5 is roughly 200 days shorter than the one starting from L4. The diversity is due to the difference in the first phase of the trajectory. The fly-by and arrival dates are almost the same for the two missions.
- The mission with departure from L4 is slightly more efficient, in terms of propellant consumption, than the dual one.
- Looking at Fig. 6.21-6.22 it is possible to appreciate the two thrusted arches in the first phase.
- The evolution of eccentricity, inclination and major semiaxis prove that the fly-by is used to acquire the orbital elements of the target asteroid. After the gravity assist, only minor adjustments are effectuated.
- In Fig. 6.23-6.24 it is possible to behold the effects of the phasing —between the Earth and the asteroid— at the fly-by. The asteroid is behind the Earth, thus after the fly-by the satellite enters a slower orbit than the asteroid one. This is proved by the higher aphelion distance.

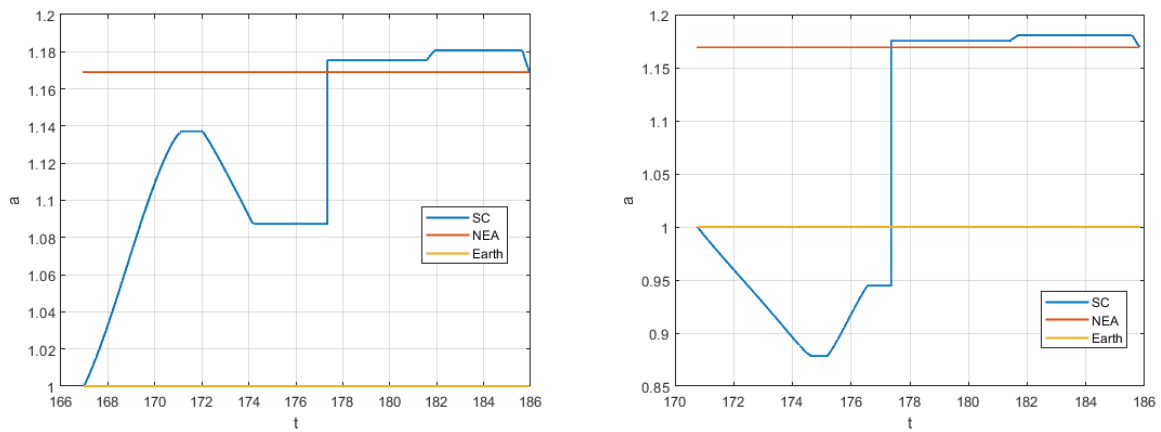


Figure 6.9: Asteroid 2004 FN8, major semiaxis evolution:  
 SX departure from L4, DX departure from L5

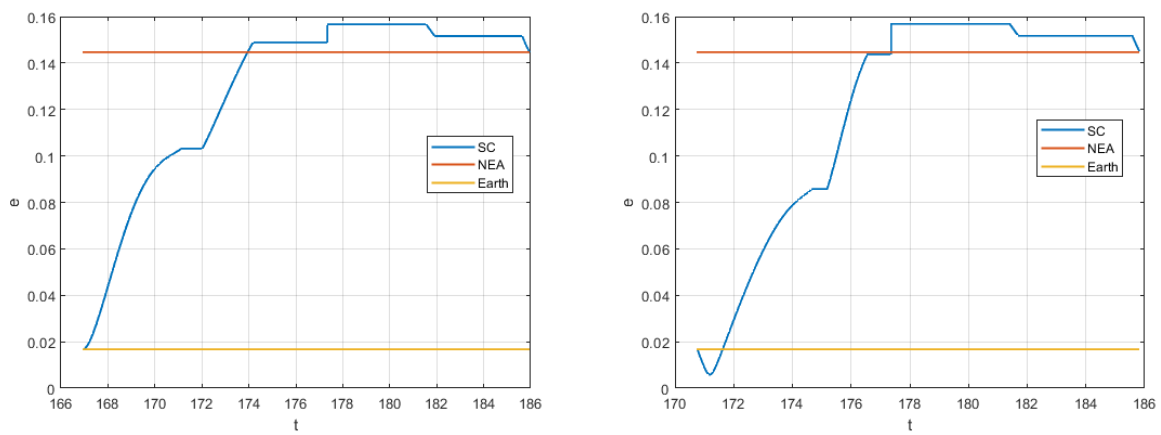


Figure 6.10: Asteroid 2004 FN8, eccentricity evolution:  
 SX departure from L4, DX departure from L5

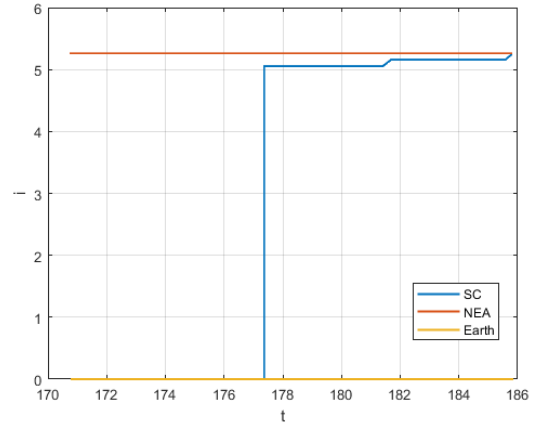
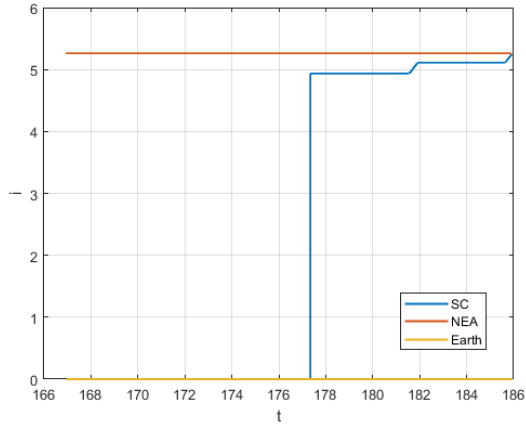


Figure 6.11: Asteroid 2004 FN8, inclination evolution:  
SX departure from L4, DX departure from L5

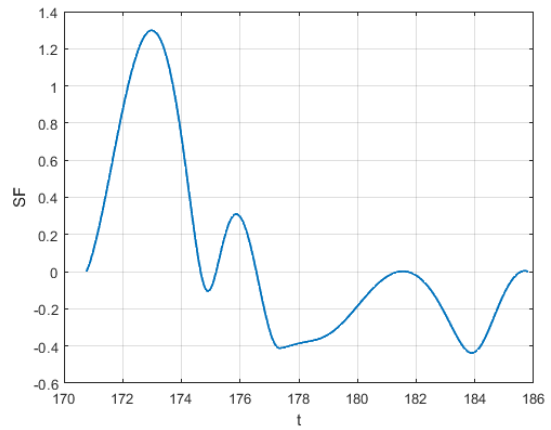
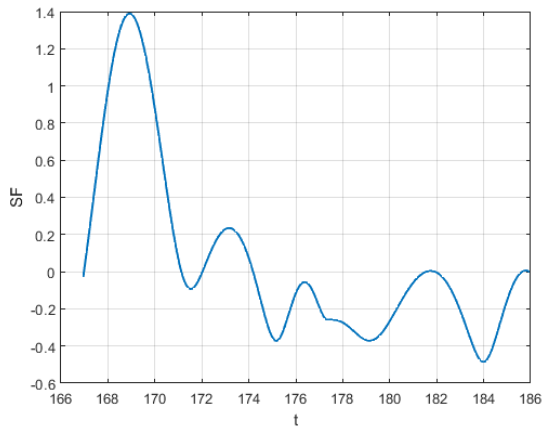


Figure 6.12: Asteroid 2004 FN8, switching function evolution:  
SX departure from L4, DX departure from L5

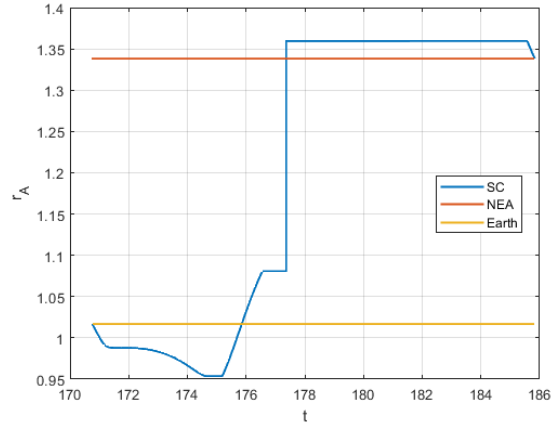
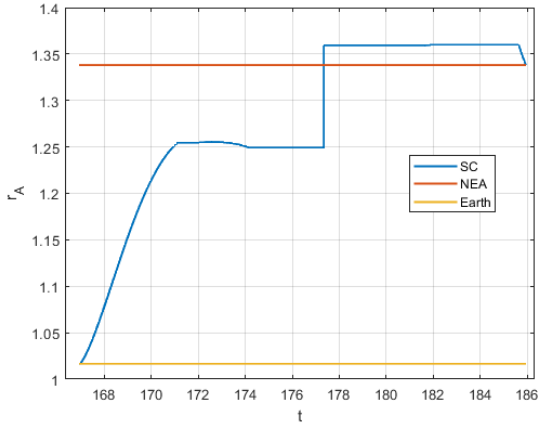


Figure 6.13: Asteroid 2004 FN8, aphelion distance evolution:  
SX departure from L4, DX departure from L5

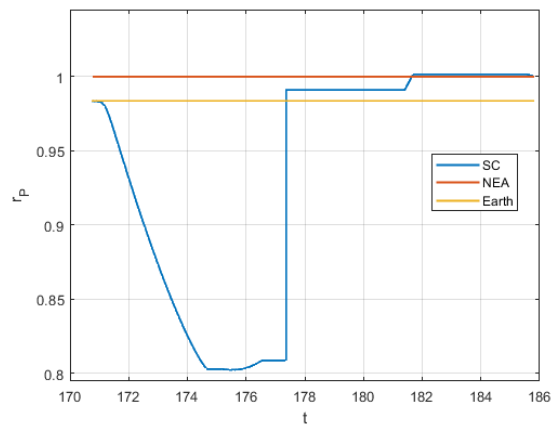
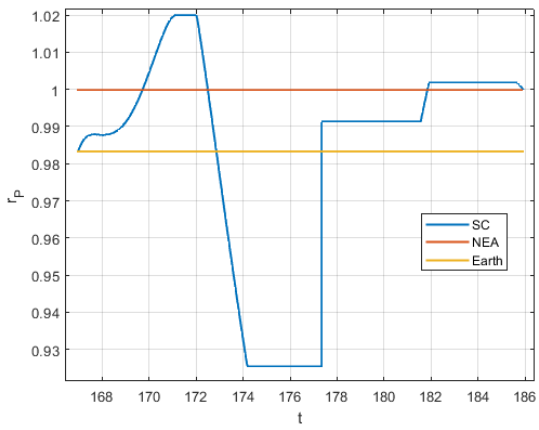


Figure 6.14: Asteroid 2004 FN8, perihelion distance evolution:  
SX departure from L4, DX departure from L5

In the end, the optimal trajectory and the bodies orbits are displayed.

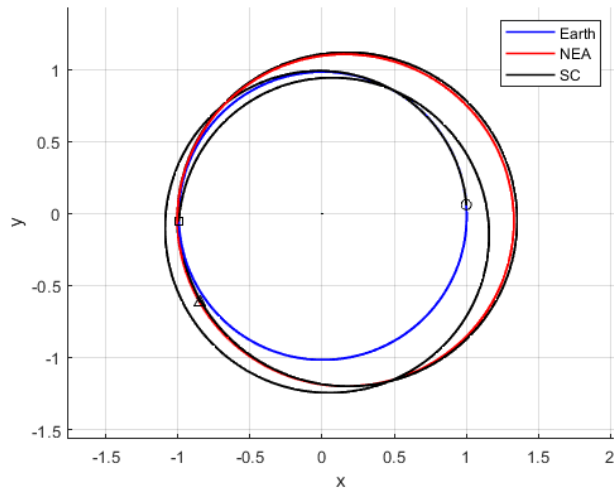


Figure 6.15: Asteroid 2004 FN8, trajectory: Departure from L4

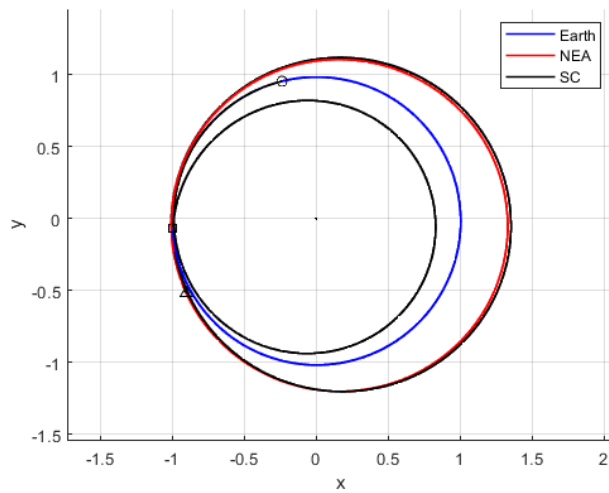


Figure 6.16: Asteroid 2004 FN8, trajectory: Departure from L5

### 6.3 Asteroid 2012 UE34

Asteroid 2012 UE34 is the one with the most inclined orbit among the ones studied. This results in some peculiar behaviours.

First of all, as can be retrieved from Tab. 6.5, the missions are characterized by a relatively low payload fraction. This is due to the necessity to use thrust also in the first phase, that is to say before the fly-by.

	Departure from L4	Departure from L5
$\frac{m_f}{m_i}$	0.8960	0.8841
Duration (days)	858	618
Departure date	7/ 8/2032	28/ 3/2033
Fly-by date	10/ 4/2034	9/ 4/2034
Arrival date	13/ 12/2034	7/ 12/2034
Fly-by type	Constrained	Constrained
$V_\infty$ at fly-by	0.1550	0.1470

Table 6.5: Asteroid 2012 UE34, optimal mission characteristics

As a matter of fact, the solution found is characterized by a favorable phasing of the two bodies —Earth and asteroid— that results in a relatively short second leg. In general, a good phasing also results in a high payload fraction. This is not true in this case, because of the first phase. The peculiarity of this leg can be inferred looking at the inclination evolution.

While the evolutions of eccentricity and major semiaxis respect the global trend of the missions, the inclination presents an anomaly. In fact, while the missions towards the other asteroids effectuate the first leg in the Earth’s orbital plane —thus not changing inclination—, this is not true for 2012 UE34.

To reach the asteroid’s inclination, the satellite can not rely only on the fly-by manoeuvre, but needs to change inclination also using thrust. This clearly results in a higher propellant consumption.

Thus, the first phase is completely thrust: there are not two separated thrust phases. This characteristic is clear looking at the switching function evolution.

These peculiarities may be all due to the implementation of the constrained altitude of the fly-by. This results in a limit on the inclination change acquirable with the gravity assist manoeuvre, since the rotation of  $V_\infty$  across the EGA is limited as well. Nonetheless, it is necessary to bound the fly-by, since a mission with a free gravity assist would have resulted in a too low fly-by, and would have been not realizable.

Another peculiarity of the missions towards 2012 UE34, is the phasing of the asteroid and the Earth. For this asteroid, the optimal mission is related to a position of the asteroid, at the fly-by, which is ahead with respect to the Earth. Thus, the orbit of the spacecraft after the gravity assist has a lower aphelion distance, if compared to the asteroid’s one.

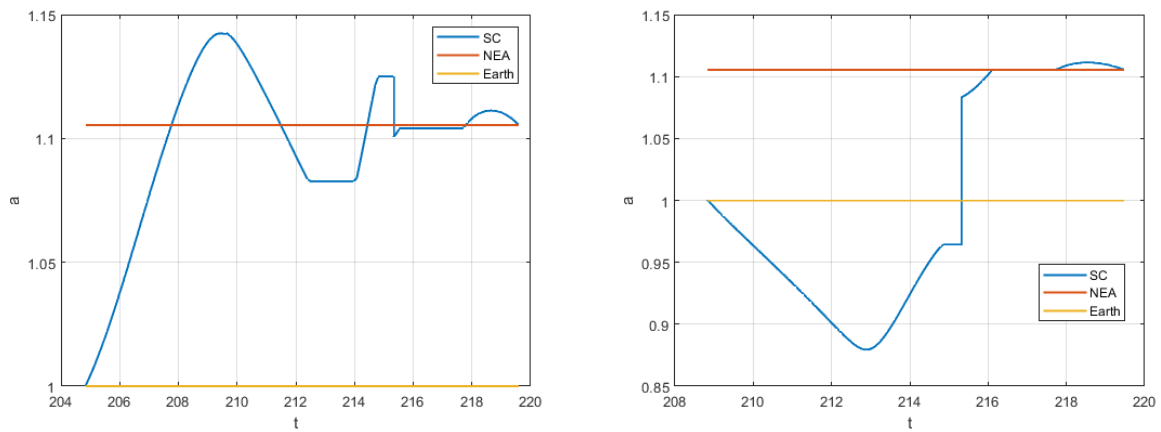


Figure 6.17: Asteroid 2012 UE34, major semiaxis evolution:  
 SX departure from L4, DX departure from L5

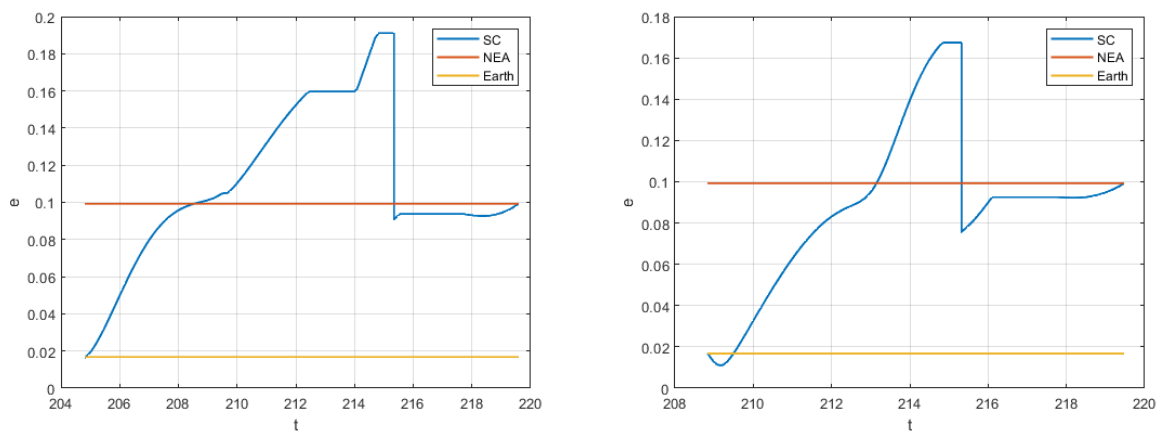


Figure 6.18: Asteroid 2012 UE34, eccentricity evolution:  
 SX departure from L4, DX departure from L5

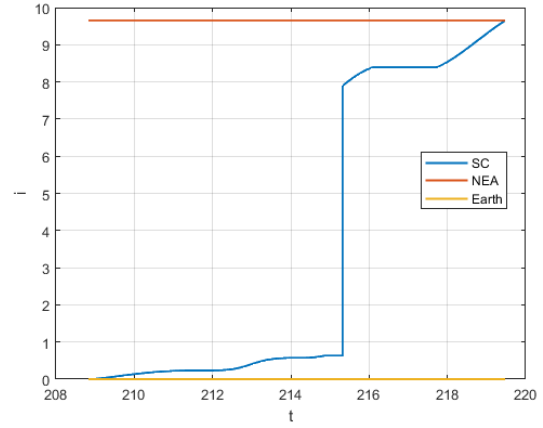
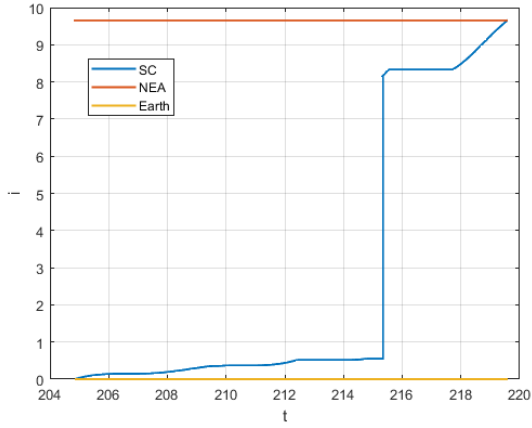


Figure 6.19: Asteroid 2012 UE34, inclination evolution:  
SX departure from L4, DX departure from L5

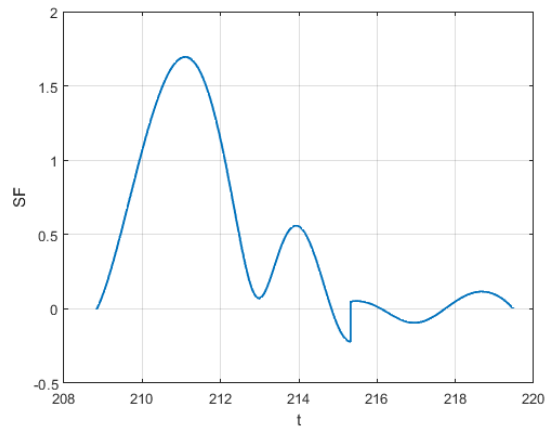
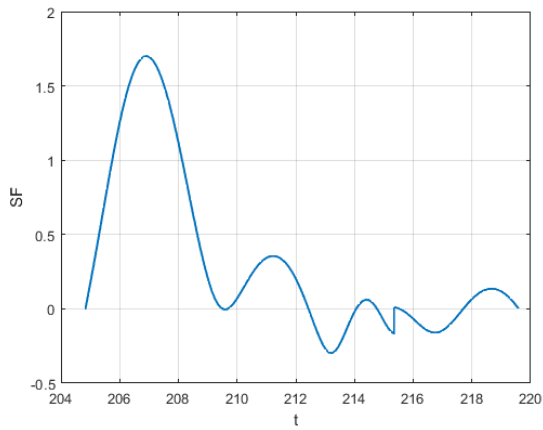


Figure 6.20: Asteroid 2012 UE34, switching function evolution:  
SX departure from L4, DX departure from L5

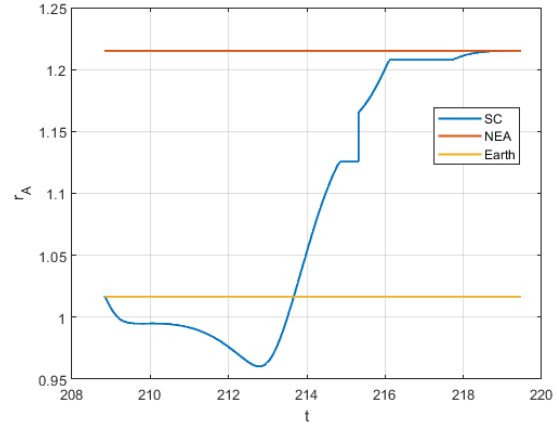
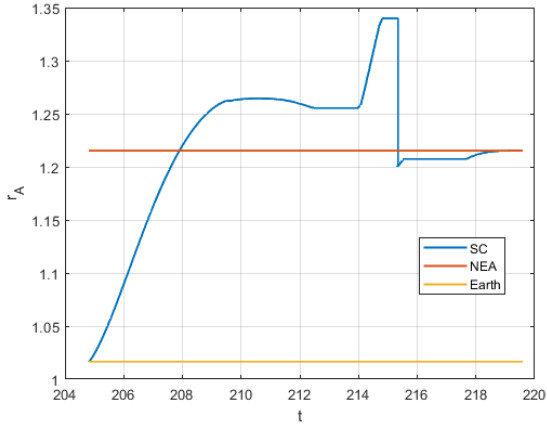


Figure 6.21: Asteroid 2012 UE34, aphelion distance evolution:  
 SX departure from L4, DX departure from L5

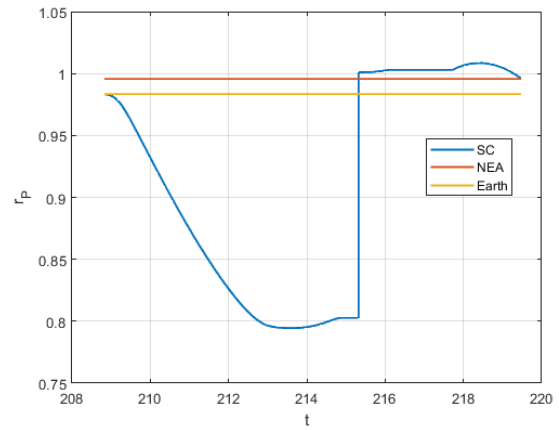
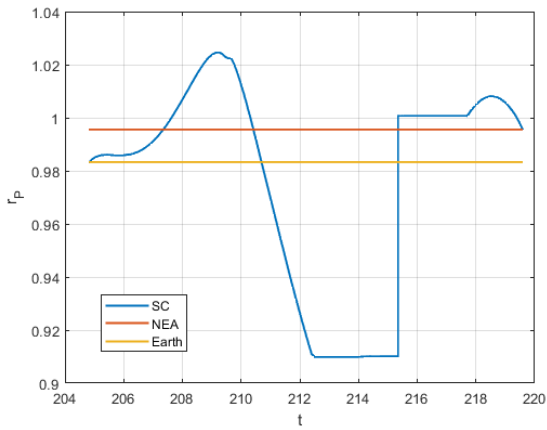


Figure 6.22: Asteroid 2012 UE34, perihelion distance evolution:  
 SX departure from L4, DX departure from L5

As far as the other aspects are concerned, the missions towards 2012 UE34 follow the global trends highlighted above.

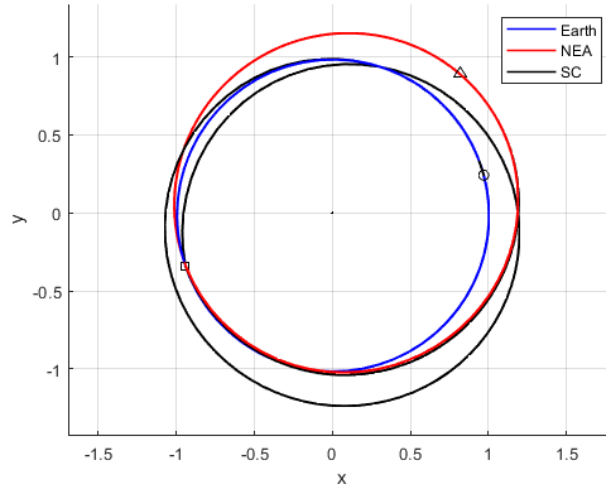


Figure 6.23: Asteroid 2012 UE34, trajectory: Departure from L4

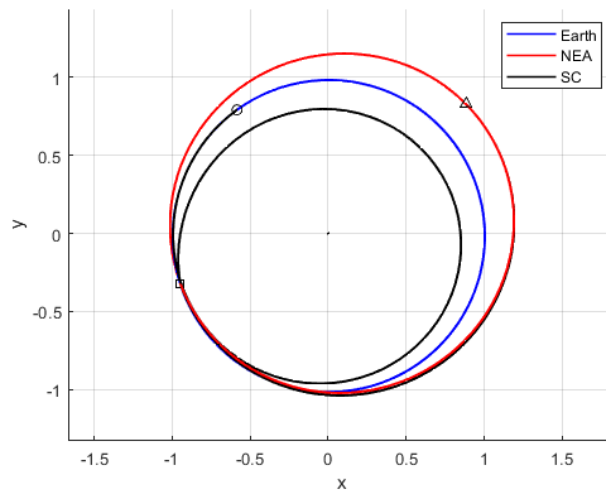


Figure 6.24: Asteroid 2012 UE34, trajectory: Departure from L5

## 6.4 Asteroid 2008 TS10

Asteroid 2008 TS10 does not present any peculiarity: all the considerations reported for 2004 FZ apply also to this NEA. The global characteristics of the optimal missions are reported in Tab. 6.6.

	Departure from L4	Departure from L5
$\frac{m_f}{m_i}$	0.9339	0.9237
Duration (days)	1007	798
Departure date	21/ 1/2031	27/ 8/2031
Fly-by date	14/ 9/2032	19/ 9/2032
Arrival date	24/10/2033	2/11/2033
Fly-by type	Free	Free
$V_\infty$ at fly-by	0.1040	0.1075

Table 6.6: Asteroid 2008 TS10, optimal mission characteristics

It is anyway possible to highlight some aspects concerning the missions towards this asteroid.

In first place, it is possible to appreciate that the payload fractions connected to both the missions towards 2008 TS10 are higher than the ones corresponding to the preceding asteroids. As a matter of fact, although the orbit of 2008 TS10 is relatively big —its major semiaxis is the third among the considered asteroids—, its inclination is limited. This results in a lower propellant throughput. But there is another aspect that concurs in reducing the propellant consumption. It is possible to appreciate that, after the fly-by, the spacecraft almost perfectly acquires the asteroid’s eccentricity and major semiaxis. Thus, only minimal secondary adjustments are needed to fix the value of these two orbital elements to the desired values.

Secondarily, while for almost all the other asteroids the fly-by occurs in the same date —or with one day of difference— for the two missions with different departure, for 2008 TS10 the fly-by for the mission starting from L5 occurs five days after the one leveraged by the mission with departure from L4. Given the low inclination of the NEA’s orbit this characteristic does not create any difference, but it was anyway worth highlighting.

Moreover, the evolution of the aphelion distance shows the good phasing also for this mission. As a matter of fact, at the fly-by the asteroid is roughly  $1^\circ$  behind the Earth.

The evolution of the orbital parameters is shown.

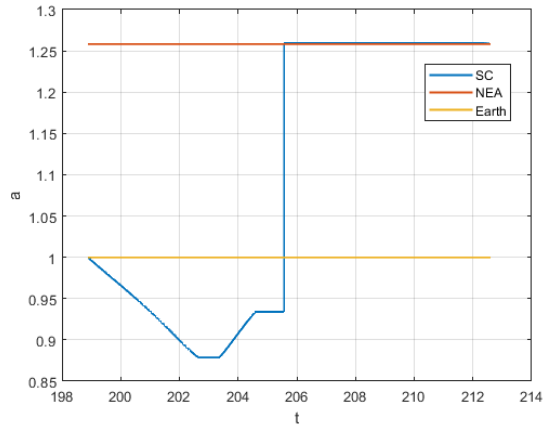
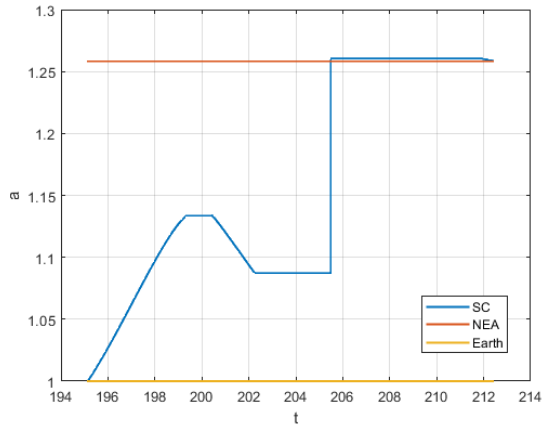


Figure 6.25: Asteroid 2008 TS10, major semiaxis evolution:  
SX departure from L4, DX departure from L5

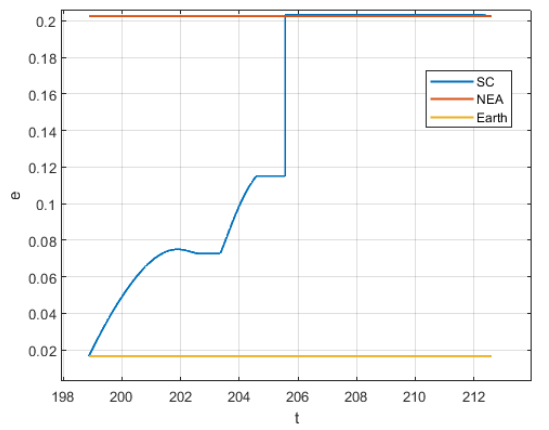
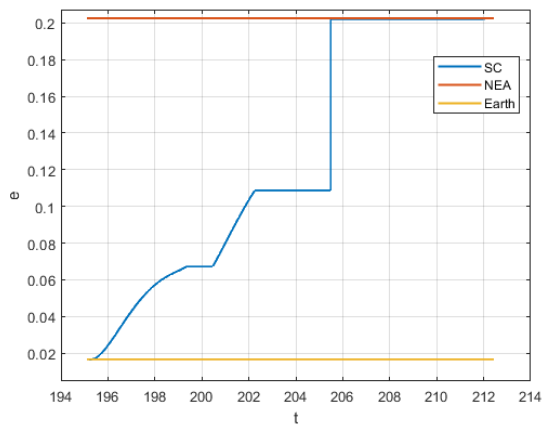


Figure 6.26: Asteroid 2008 TS10, eccentricity evolution:  
SX departure from L4, DX departure from L5

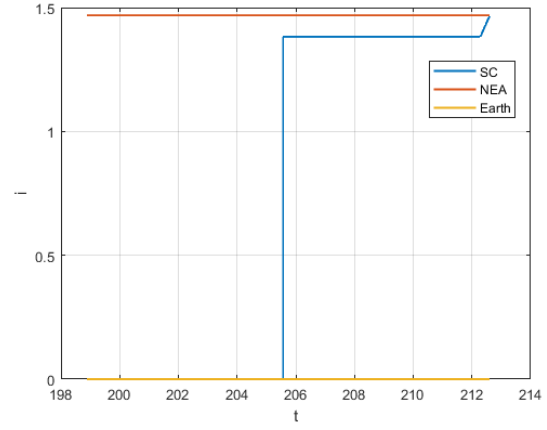
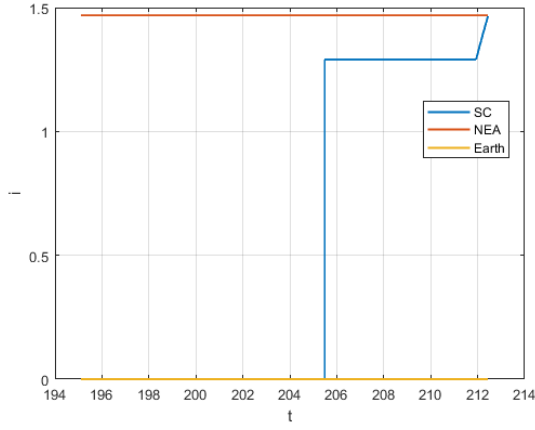


Figure 6.27: Asteroid 2008 TS10, inclination evolution:  
 SX departure from L4, DX departure from L5

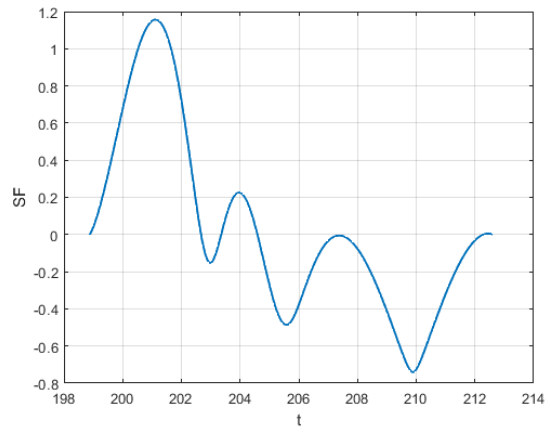
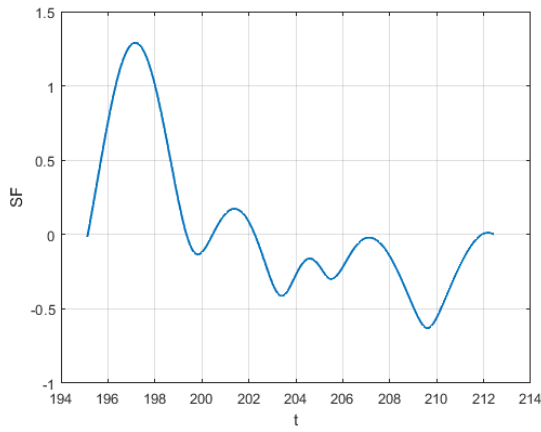


Figure 6.28: Asteroid 2008 TS10, switching function evolution:  
 SX departure from L4, DX departure from L5

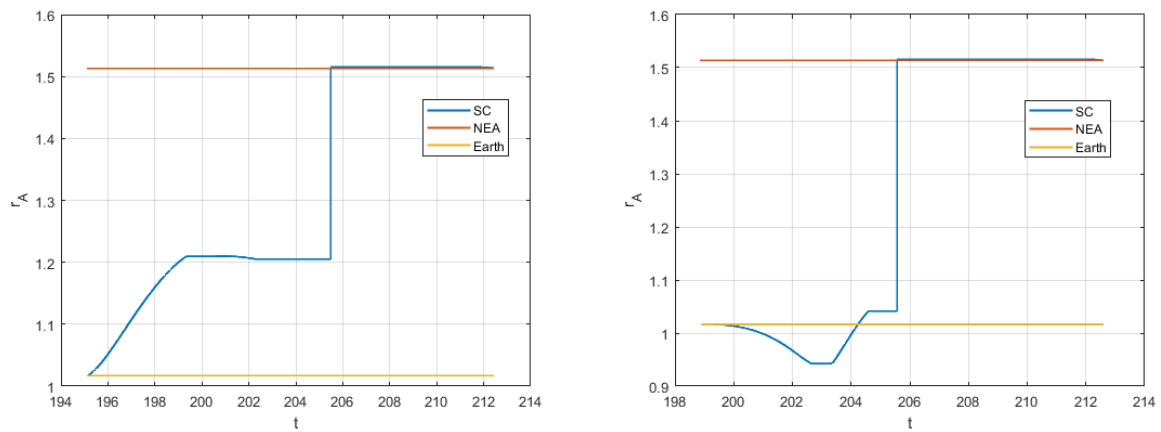


Figure 6.29: Asteroid 2008 TS10, aphelion distance evolution:  
SX departure from L4, DX departure from L5

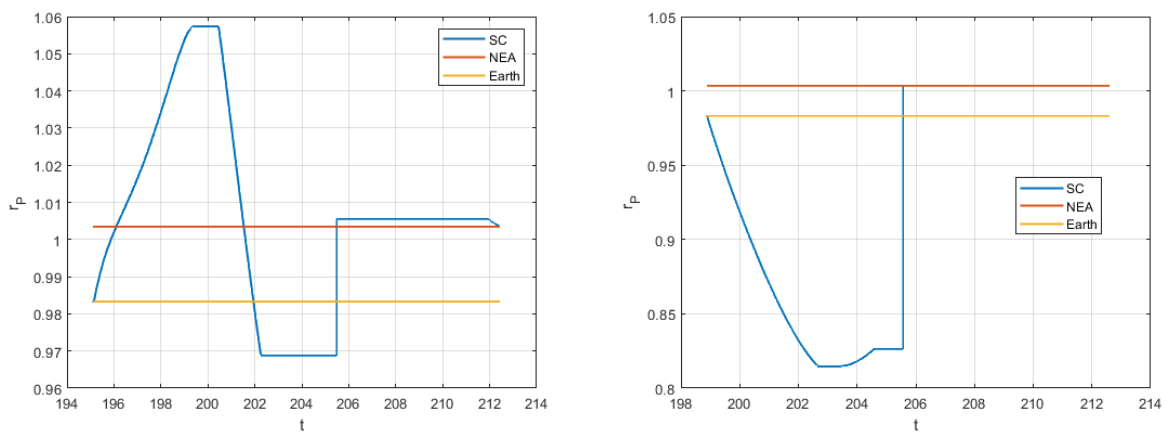


Figure 6.30: Asteroid 2008 TS10, perihelion distance evolution:  
SX departure from L4, DX departure from L5

Finally, it is possible to show the optimal trajectories.

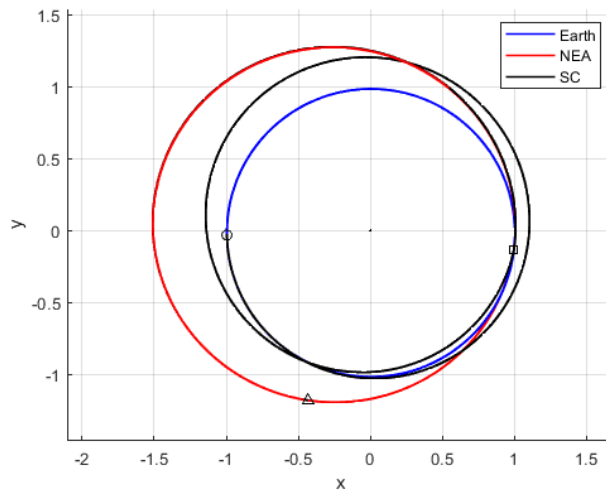


Figure 6.31: Asteroid 2008 TS10, trajectory: Departure from L4

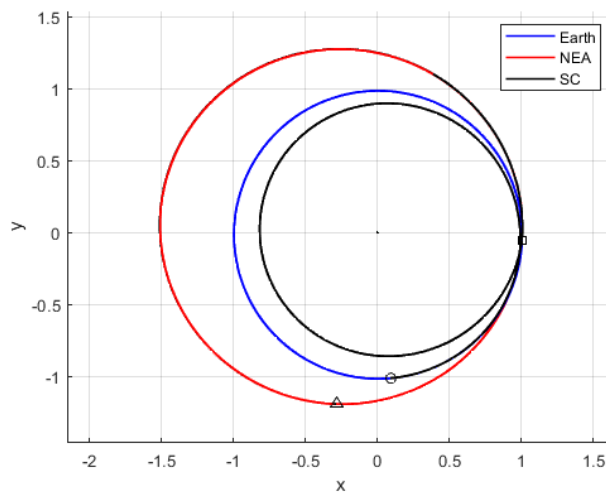


Figure 6.32: Asteroid 2008 TS10, trajectory: Departure from L5

## 6.5 Asteroid 2015 XA379

Asteroid 2015 XA379 is characterized by an orbit similar to 2008 TS10. As a matter of fact, their orbital elements —eccentricity, inclination and major semiaxis— are pretty much the same. This motivates the similarities in the optimal missions towards these two asteroids.

	Departure from L4	Departure from L5
$\frac{m_f}{m_i}$	0.9234	0.9119
Duration (days)	1196	972
Departure date	20/ 6/2030	26/1/2031
Fly-by date	12/ 2/2032	13/ 2/2032
Arrival date	28/ 9/2033	24/ 9/2033
Fly-by type	Free	Free
$V_\infty$ at fly-by	0.1152	0.1159

Table 6.7: Asteroid 2015 XA379, optimal mission characteristics

Asteroid 2015 XA379 presents the same peculiarity as 2008 TS10, as far as the fly-by date is concerned.

On the other hand, the payload fractions for the missions towards 2015 XA379 are lower than their counterparts connected to the trajectories towards 2008 TS10. In fact, in spite of being both characterized by a low inclination, there is a crucial difference. As far as asteroid 2015 XA379 is concerned, after the fly-by the spacecraft does not reach the values of eccentricity and major semiaxis of the NEA itself. Thus, with respect to the missions towards 2008 TS10, greater secondary adjustments are needed. This clearly results in a higher propellant consumption.

The evolution of the orbital parameters is shown.

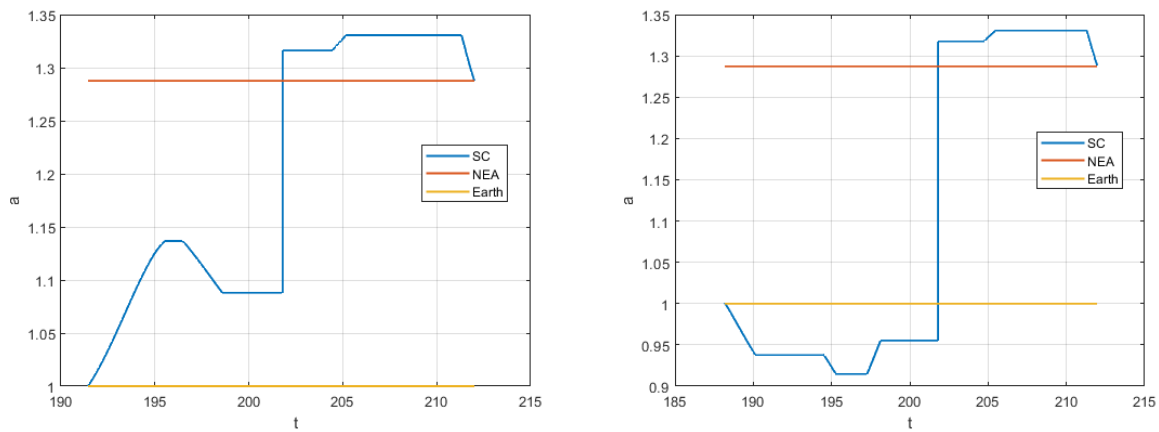


Figure 6.33: Asteroid 2015 XA379, major semiaxis evolution:  
 SX departure from L4, DX departure from L5

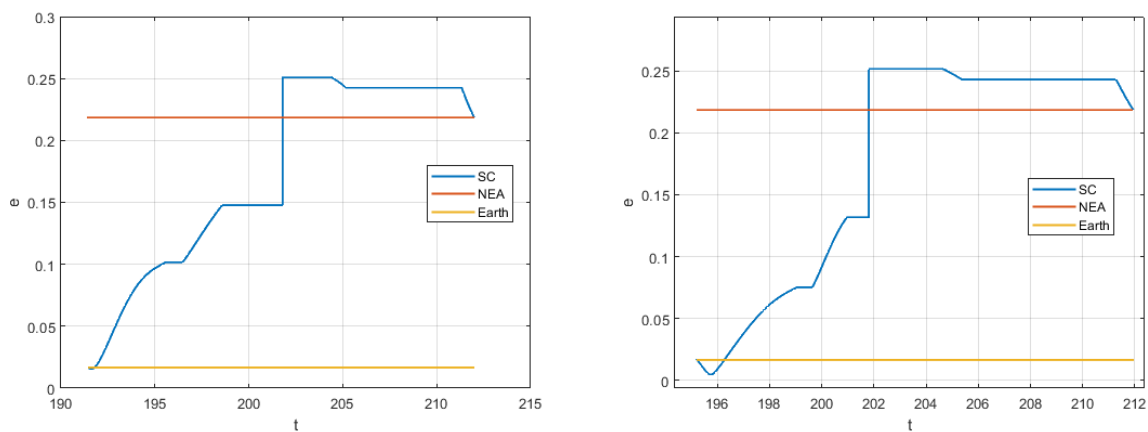


Figure 6.34: Asteroid 2015 XA379, eccentricity evolution:  
 SX departure from L4, DX departure from L5

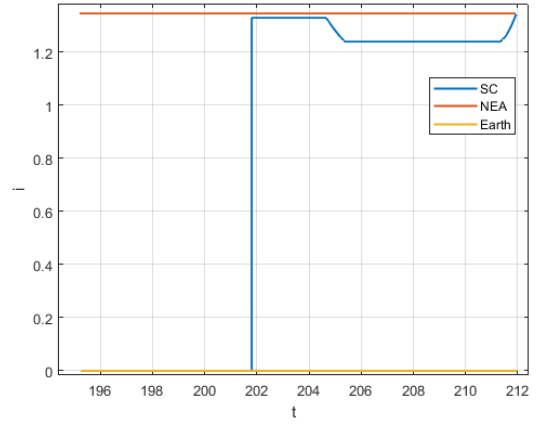
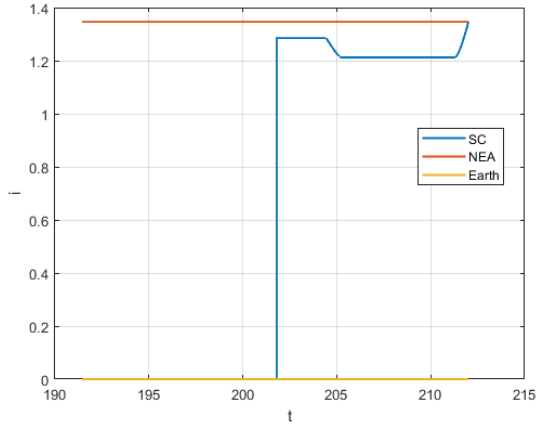


Figure 6.35: Asteroid 2015 XA379, inclination evolution:  
 SX departure from L4, DX departure from L5

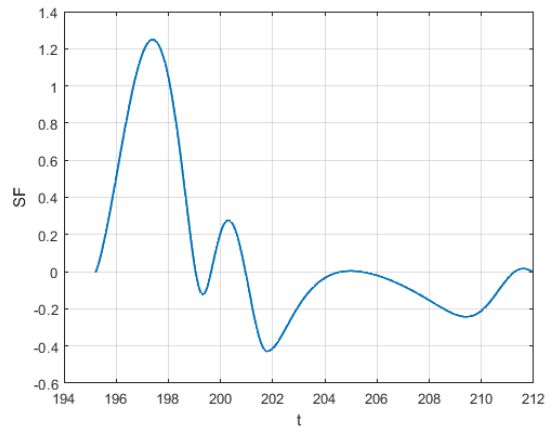
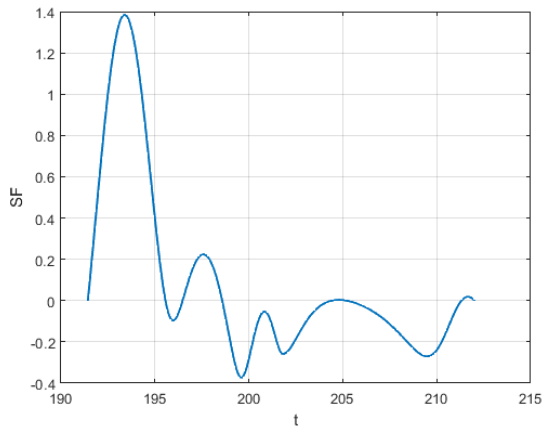


Figure 6.36: Asteroid 2015 XA379, switching function evolution:  
 SX departure from L4, DX departure from L5

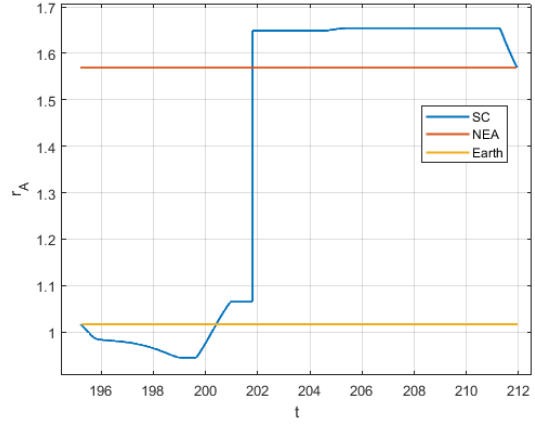
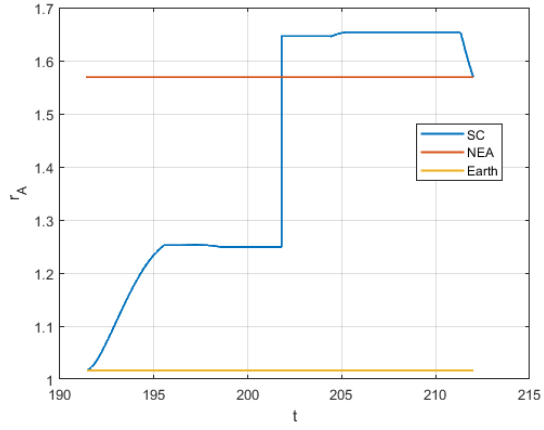


Figure 6.37: Asteroid 2015 XA379, aphelion distance evolution:  
SX departure from L4, DX departure from L5

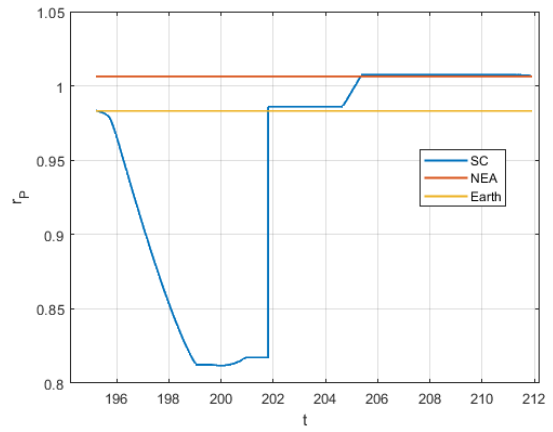
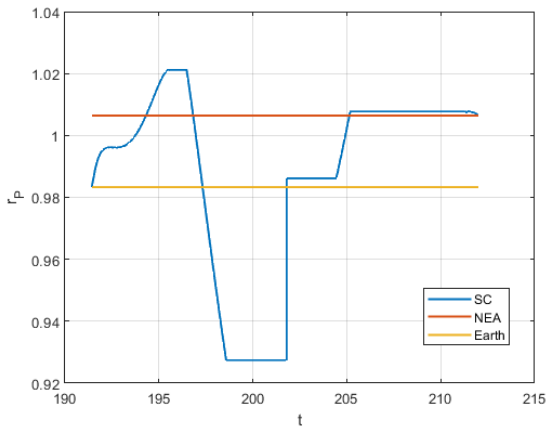


Figure 6.38: Asteroid 2015 XA379, perihelion distance evolution:  
SX departure from L4, DX departure from L5

Finally, it is possible to show the optimal trajectories.

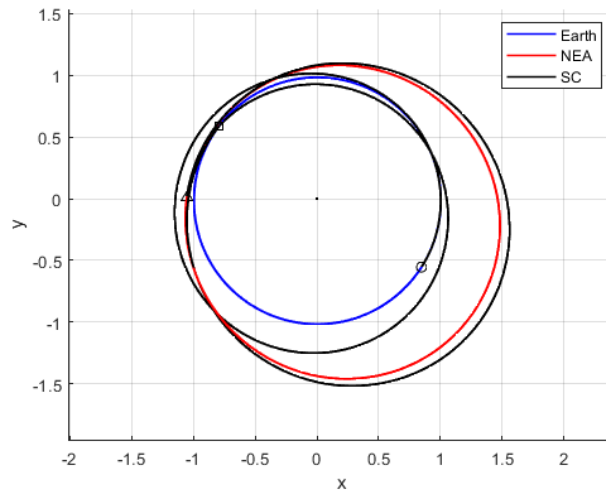


Figure 6.39: Asteroid 2015 XA379, trajectory: Departure from L4

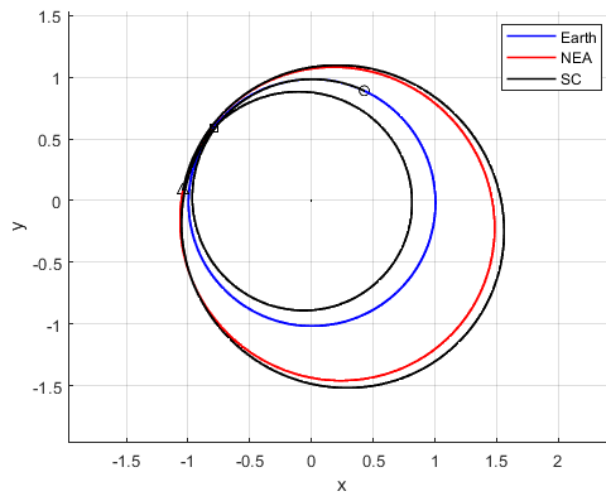


Figure 6.40: Asteroid 2015 XA379, trajectory: Departure from L5

## 6.6 Asteroid 2016 YE

The global properties of the missions towards 2016 YE are, as always, summarized in the following table.

	Departure from L4	Departure from L5
$\frac{m_f}{m_i}$	0.9204	0.9005
Duration (days)	889	816
Departure date	30/9/2027	11/12/2027
Fly-by date	16/12/2028	16/12/2028
Arrival date	6/ 3/2030	6/ 3/2030
Fly-by type	Free	Free
$V_\infty$ at fly-by	0.1519	0.1512

Table 6.8: Asteroid 2016 YE, optimal mission characteristics

The missions to reach this particular asteroid are characterized by some peculiarities:

- The first leg, for both the missions, is completely thrustless. Thus, there are not two different thrustless arches. The thrust is applied in the orbital plane, as it is used to change only  $a$  and  $e$ , without varying the inclination. This results in a not excessive penalization in terms of propellant consumption.
- The mission with departure from L5 is only 73 days shorter —instead of the typical 200 days difference— that the one starting from L4. This happens because the mission with departure from L4 only takes 13 months, and not 18-20, from the start to the fly-by.
- The trajectory presents two minima, relatively close to one another. Thus, it has been necessary to carry out a more careful analysis to find the global minimum, that is to say the real optimum.
- The orbit of the asteroid has a relatively high inclination: the second among the ones considered. Nonetheless, it has not been necessary to implement a constrained fly-by —as for 2012 UE34—, as the optimal missions do not result in too low altitude of the gravity assist manoeuvre. This results in a higher payload fraction, if compared to 2012 UE34.

The evolution of the orbital parameters is shown.

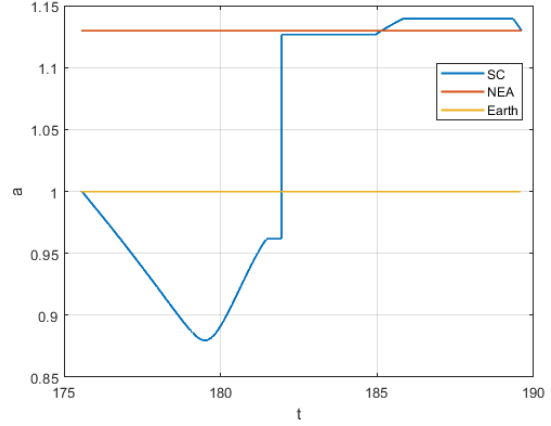
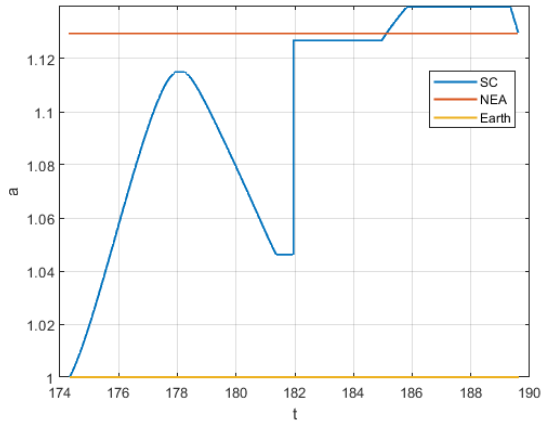


Figure 6.41: Asteroid 2016 YE, major semiaxis evolution:  
 SX departure from L4, DX departure from L5

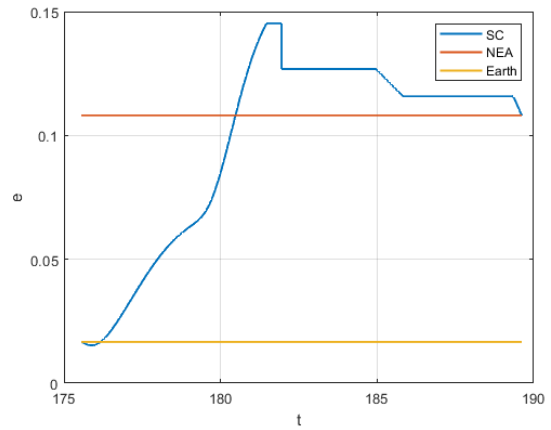
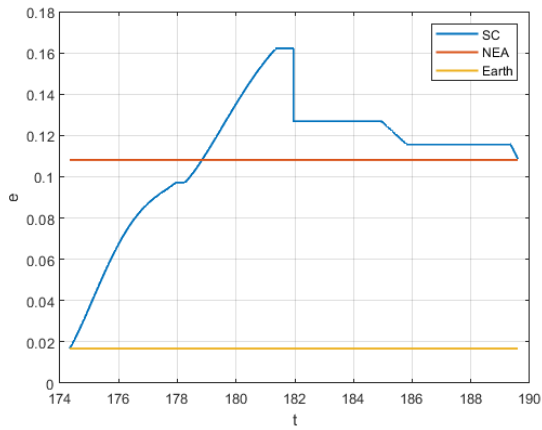


Figure 6.42: Asteroid 2016 YE, eccentricity evolution:  
 SX departure from L4, DX departure from L5

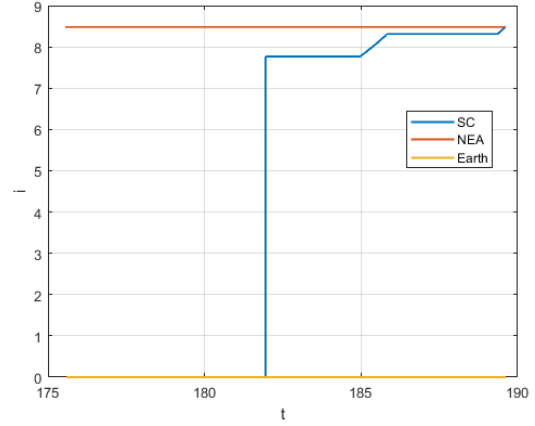
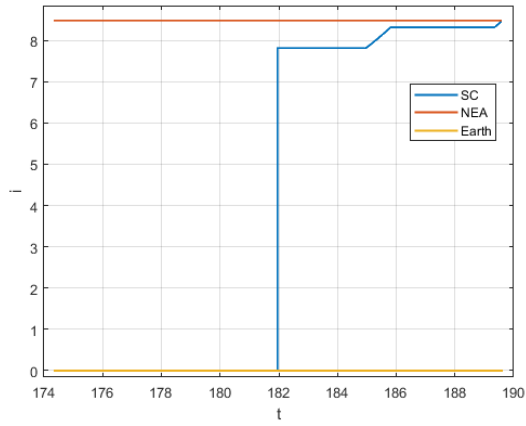


Figure 6.43: Asteroid 2016 YE, inclination evolution:  
 SX departure from L4, DX departure from L5

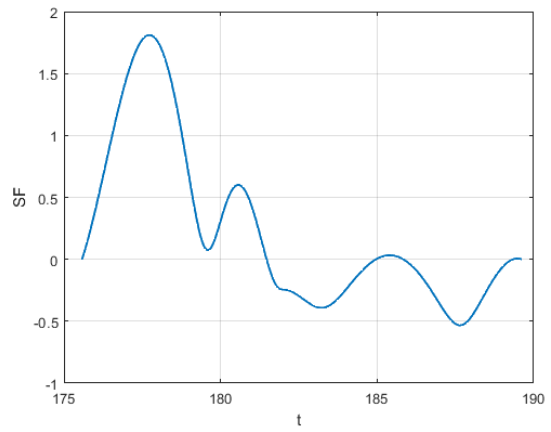
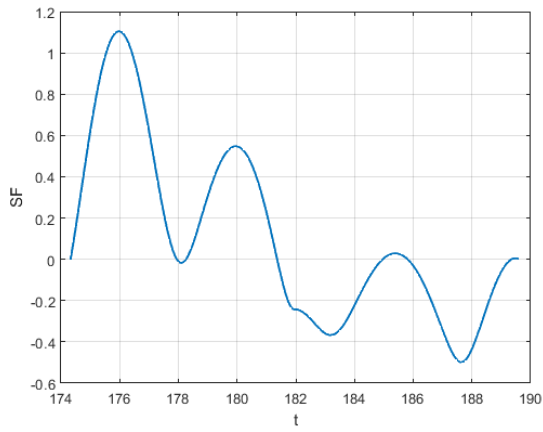


Figure 6.44: Asteroid 2016 YE, switching function evolution:  
 SX departure from L4, DX departure from L5

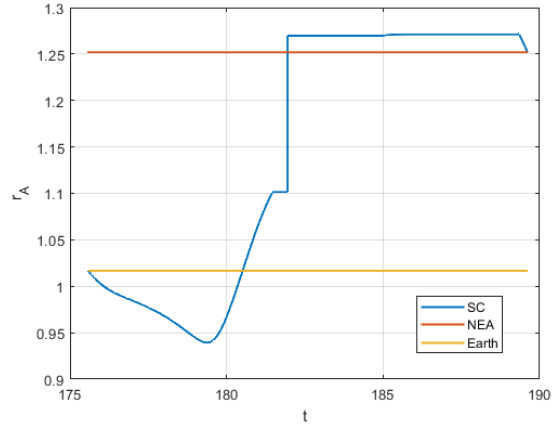
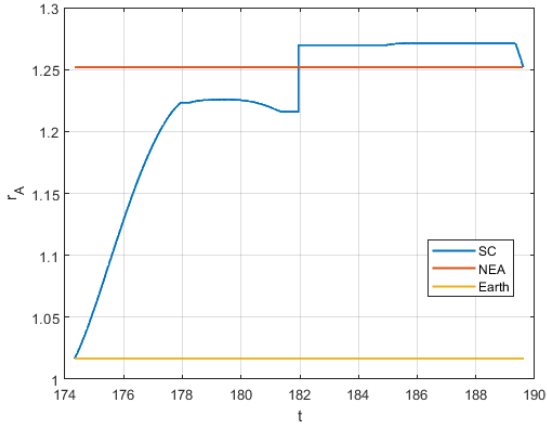


Figure 6.45: Asteroid 2016 YE, aphelion distance evolution:  
SX departure from L4, DX departure from L5

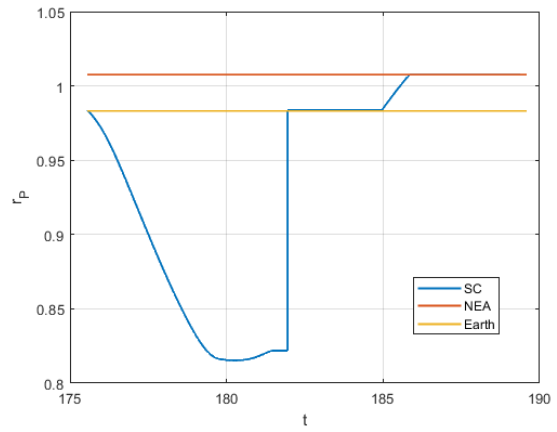
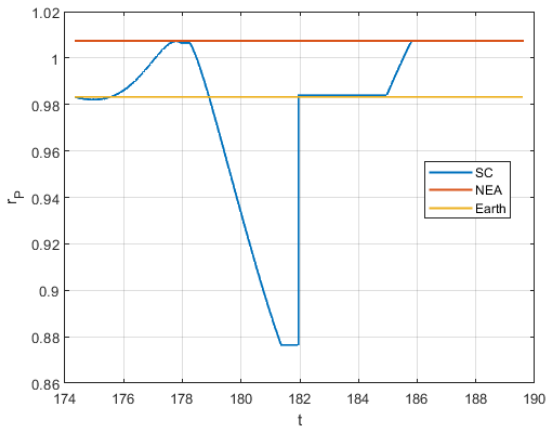


Figure 6.46: Asteroid 2016 YE, perihelion distance evolution:  
SX departure from L4, DX departure from L5

Finally, it is possible to show the optimal trajectories.

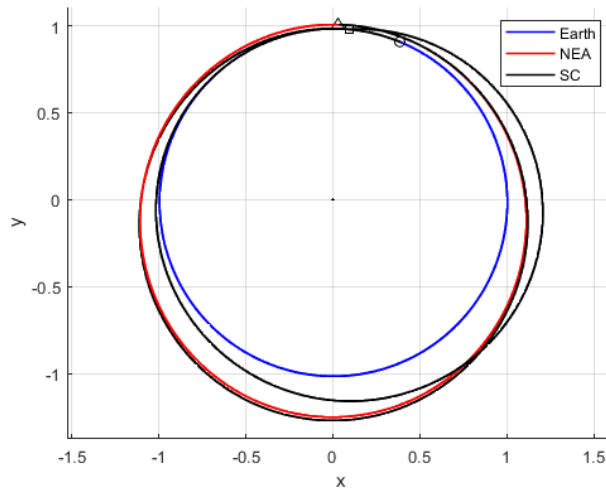


Figure 6.47: Asteroid 2016 YE, trajectory: Departure from L4

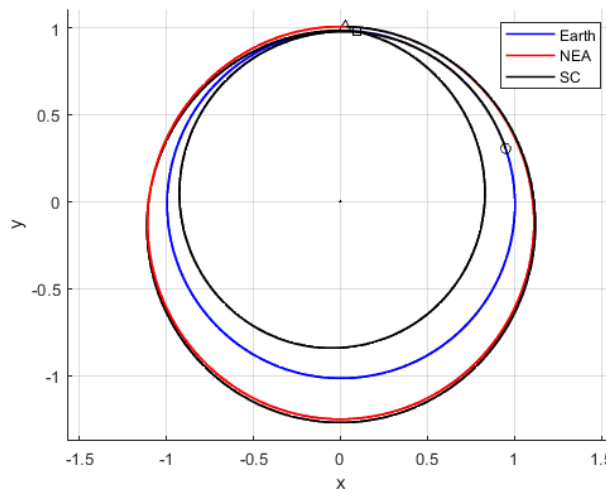


Figure 6.48: Asteroid 2016 YE, trajectory: Departure from L5

## 6.7 Asteroid 2017 BN93

Asteroid 2017 BN93 has an orbit which is really close to the Earth's one. Thus it is forecastable that the missions toward this NEA will be the less expensive —from a propulsive point of view— and the shortest among the ones studied. Looking at Tab. 6.9 it is possible to appreciate that this is exactly what occurs.

	Departure from L4	Departure from L5
$\frac{m_f}{m_i}$	0.9456	0.9256
Duration (days)	618	538
Departure date	13/ 3/2031	1/ 6/2031
Fly-by date	23/7/2032	23/ 7/2032
Arrival date	21/ 11/2032	20/ 11/2032
Fly-by type	Free	Free
$V_\infty$ at fly-by	0.0629	0.0629

Table 6.9: Asteroid 2017 BN93, optimal mission characteristics

The missions towards 2017 BN93 take less than two years to be accomplished. As a matter of fact, while the first leg is almost the same as the other missions, the second one is only 4 months long. This is due to the favorable phase between the Earth and the asteroid, that at the fly-by it is less than  $1^\circ$  behind the blue planet.

It is worth highlighting that, as for asteroid 2016 YE, the difference of duration between the two missions is relatively low. Again, this is due to the fact that the first leg for the mission with departure from L4 only takes roughly 16 months.

Being the orbit of the asteroid close to the one of the Earth, the value of  $V_\infty$  after the fly-by is way lower than the other missions.

As far as all the other aspects are concerned, the missions towards 2017 BN93 share the common characteristics of the other trajectories.

The evolution of the orbital parameters is shown.

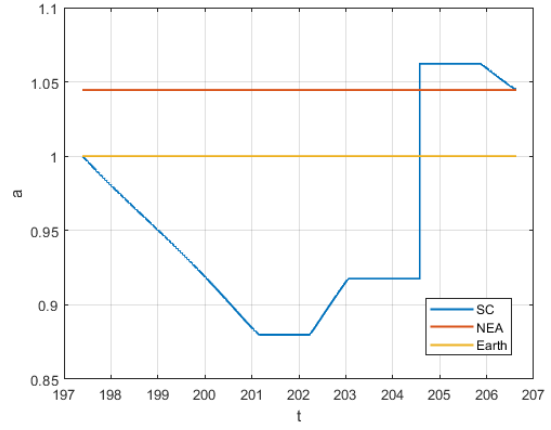
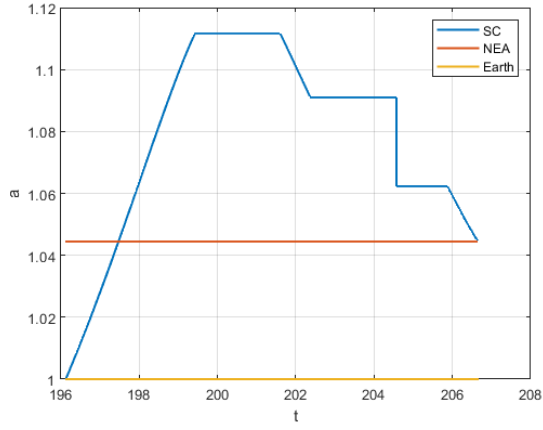


Figure 6.49: Asteroid 2017 BN93, major semiaxis evolution:  
SX departure from L4, DX departure from L5

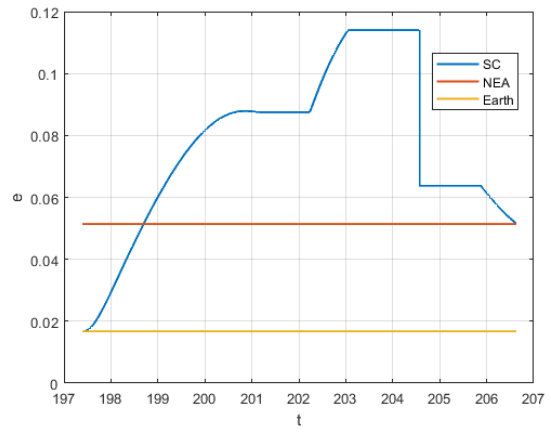
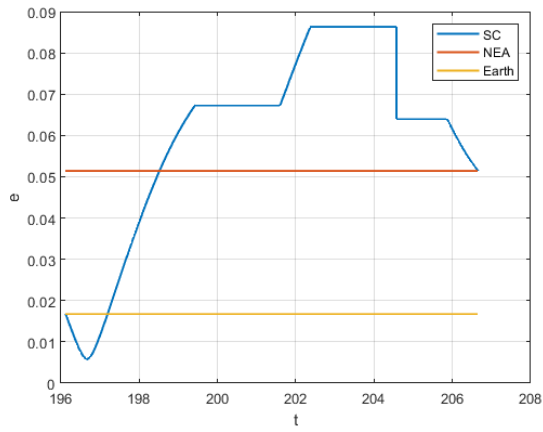


Figure 6.50: Asteroid 2017 BN93, eccentricity evolution:  
SX departure from L4, DX departure from L5

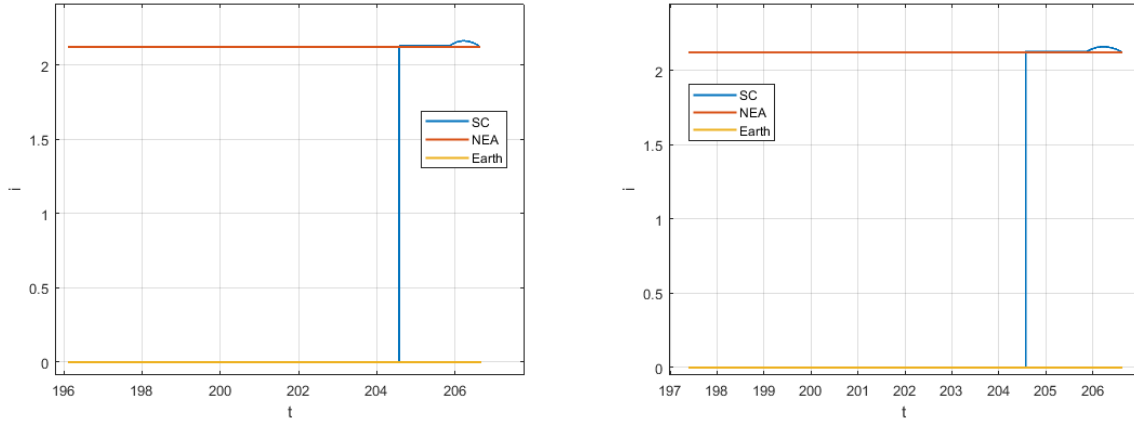


Figure 6.51: Asteroid 2017 BN93, inclination evolution:  
SX departure from L4, DX departure from L5

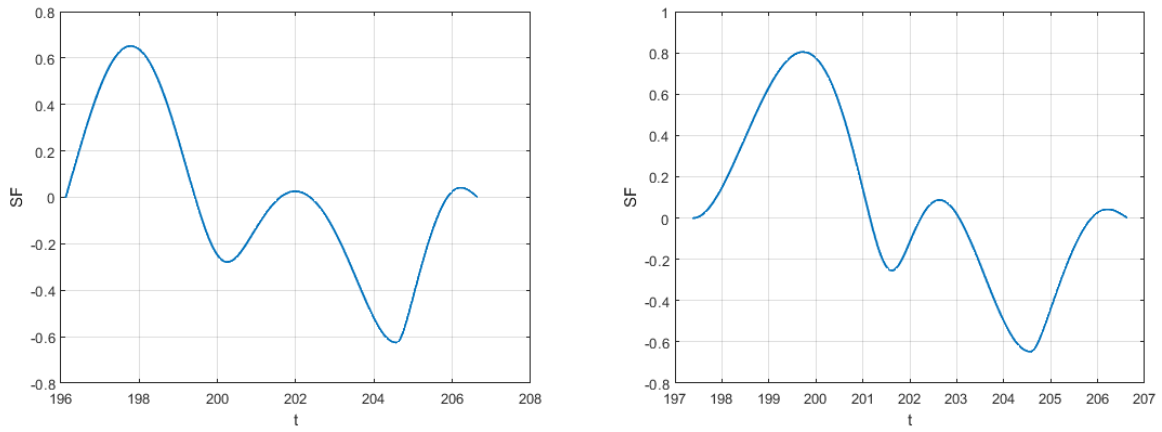


Figure 6.52: Asteroid 2017 BN93, switching function evolution:  
SX departure from L4, DX departure from L5

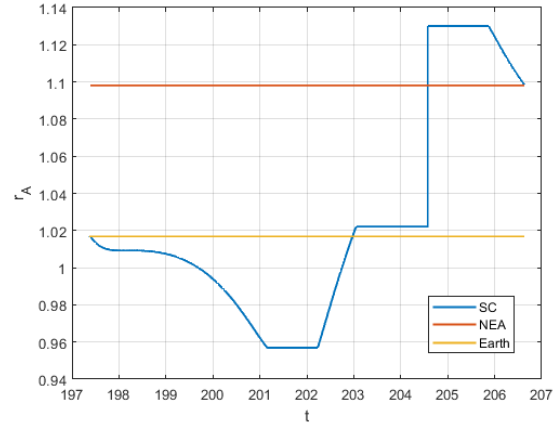
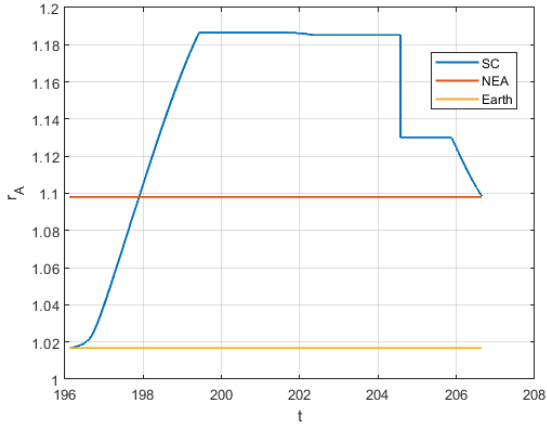


Figure 6.53: Asteroid 2017 BN93, aphelion distance evolution:  
SX departure from L4, DX departure from L5

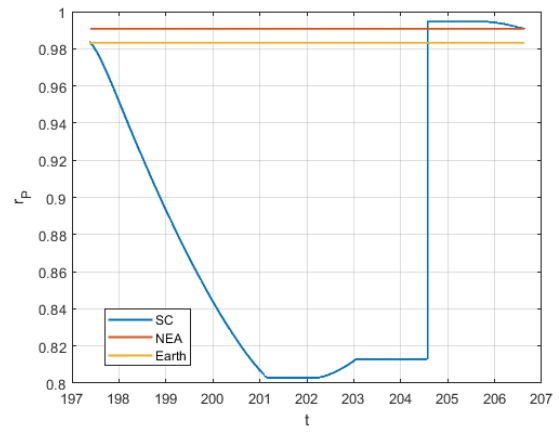
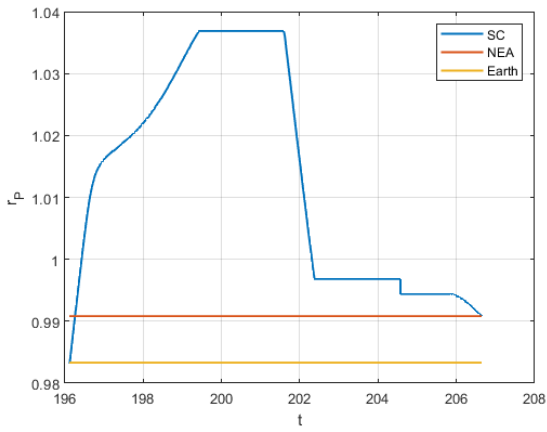


Figure 6.54: Asteroid 2017 BN93, perihelion distance evolution:  
SX departure from L4, DX departure from L5

Finally, it is possible to show the optimal trajectories.

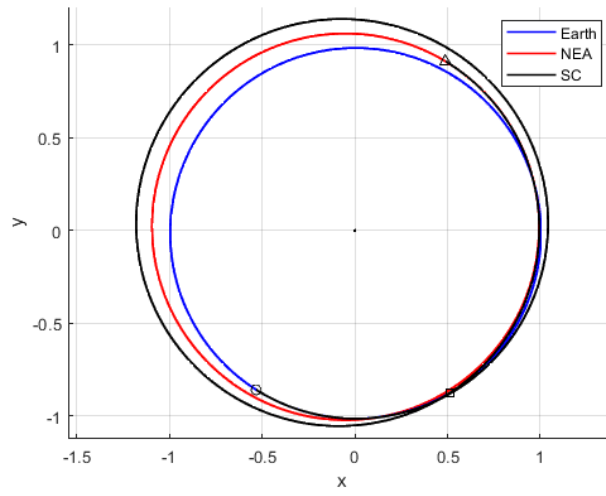


Figure 6.55: Asteroid 2017 BN93, trajectory: Departure from L4

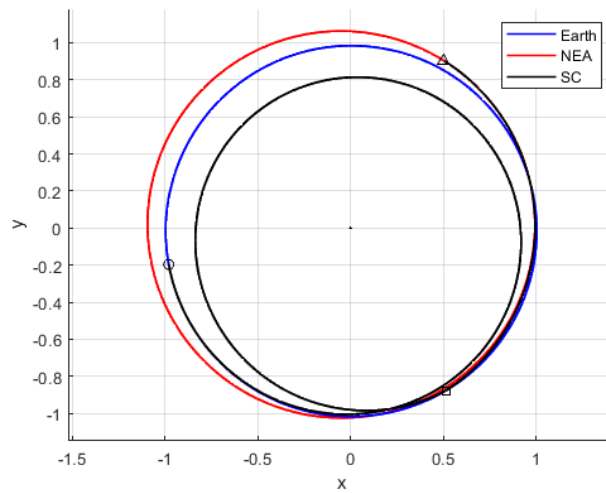


Figure 6.56: Asteroid 2017 BN93, trajectory: Departure from L5

## 6.8 Final Assessment

It is possible to summarize the results obtained in synoptic diagrams, showing the final mass of the missions, with respect to some particular quantities. In Fig. 6.57, are shown the final masses of the various missions with respect to the two asteroid's orbital parameters that mainly affect their value: major semiaxis and inclination. In Fig. 6.58, the same masses are reported as a function of the mission's duration and of the hyperbolic excess velocity at the fly-by.

If no *Earth-gravity-assist* —EGA— manoeuvre was leveraged, it would have been logic to forecast a smaller final mass for the shorter missions that rendezvous with the most inclined asteroids. As mentioned, inclination changing manoeuvre are propulsively inefficient — and therefore expensive — and longer durations result in a more limited use of thrust, thus reducing propellant consumption. A similar reasoning could have been carried out considering the dimension of the asteroid's orbit, thus the major semiaxis. It goes without saying that, the greater is the gap in mechanical energy between the departure orbit and the arrival one, the greater is the propulsive cost of the transfer. Nonetheless, such an argument presents two flaws.

Firstly, it does not take into account that the transfer is not between two orbits, but between two points on those orbits: thus the phasing is a crucial issue. The more favourable is the attainable phasing, the smaller is the propellant consumption used for minor phasing adjustment after the fly-by. This means that, if the asteroid and the Earth are near at the close encounter, the mission is less expensive. The bigger the distance in phase, the less favourable is the mission to be carried out. If the phase is unacceptable —e.g. the fly-by is effectuated at the asteroid perihelion where occurs the MOID, but at the fly-by time the asteroid is at its aphelion— the mission can not be carried out.

Second, but more important, the EGA changes the considerations. The cost of the manoeuvre is not defined by the target orbit characteristics, but by the effectiveness of the fly-by manoeuvre: the capacity of obtaining, just leveraging the EGA, the target's orbital elements. This is the reason why there is no significant dependence of the final mass from the asteroids' orbital elements and from the duration of the mission.

As a matter of fact what strongly affects the mission's efficiency is the attainable  $V_\infty$  at fly-by. If the phasing between the Earth and the target asteroid would be perfect —i.e. with Earth and asteroid in the same position at fly-by time— it would be possible to instantaneously rendezvous with the NEA, if a suitable hyperbolic excess velocity was gained before the fly-by. Indeed, the fly-by could be used to obtain the same heliocentric velocity as the target, which would be in the same position of the satellite. Same position and same velocity at a certain time mean same orbital elements, including the true anomaly. However, beside a perfect phasing which is practically infeasible, it is necessary for the spacecraft to obtain a suitable  $V_\infty$ .

The  $V_\infty$  necessary for the ideal instantaneous rendezvous after the fly-by is fixed, and defined by the target orbital elements.

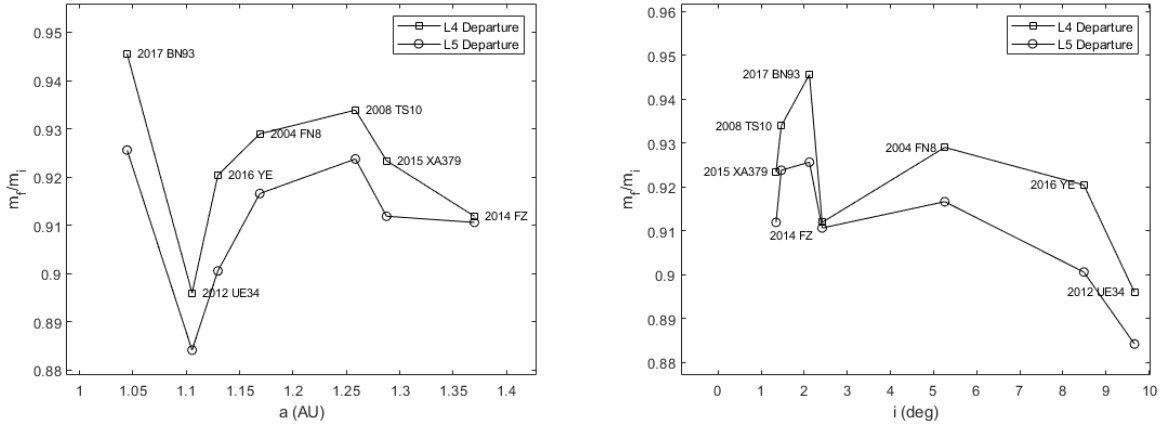


Figure 6.57: Final mass of the missions as a function of: SX major semiaxis, DX inclination

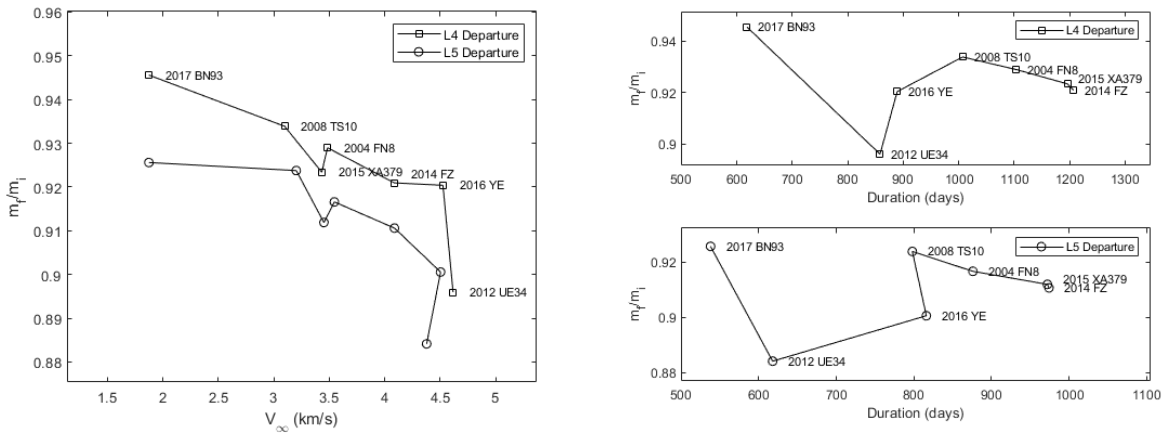


Figure 6.58: Final mass of the missions as a function of: SX  $V_\infty$  at fly-by, DX duration

The effectiveness of the EGA manoeuvre is defined by the capability of gaining a  $V_\infty$  as close as possible to the ideal one, both in terms of inclination and module. As mentioned, the hyperbolic excess velocity's modulus is constant across the fly-by, that can be seen as an instantaneous rotation of such an entity. Thus, the second burn before the fly-by, used to intercept the Earth with the necessary  $V_\infty$ , is crucial. The higher the ideal  $V_\infty$ , the more expensive the first leg is to obtain an hyperbolic excess velocity which is close to that value. This explains the dependence of the final mass from the value of  $V_\infty$ .

Clearly, the EGA is not effectuated at the ideal value of  $V_\infty$ , also because the perfect phasing is never obtained. Nonetheless, some missions perform effective EGAs —i.e. 2008 TS10 and 2017 BN93— resulting in almost null secondary adjustments and high final masses. On the other hand, other missions can not obtain a  $V_\infty$  close to the desired value or direction, and are characterized by a small payload fraction. The clearer example is 2012 UE34. The optimal rotation of the hyperbolic excess velocity is neither reached nor even approached by the spacecraft. Indeed, to gain a suitable rotation of  $V_\infty$ , it would have been necessary —as mentioned— a fly-by with too low altitude. Constraining the fly-by, the attained  $V_\infty$  is lower —although it remains the highest among the considered asteroids— and not inclined enough: hence the spacecraft needs to broadly use thrust both before and after the fly-by to perform the rendezvous. This motivates the anomaly, represented by 2012 UE34 in Fig. 6.57-6.58, where it is characterized by huge drops in final mass, with respect to similar asteroids.

In the end, the dimensional performances of the optimal missions can be shown in Tab. 6.10. It is possible to appreciate the conformity of the  $V_\infty$  gained at the fly-by between the missions with different departure points. As a matter of fact, since the last leg is similar for both the departure points it could not have been otherwise.

Two cases —introduced in Section 5.7— to which the dimensionless analysis effectuated can be applied, are considered. These are indicated with the apex:

- *I*: case with global mass  $m_{tot} = 14 \text{ kg}$  and thrust  $T = 1.4 \text{ mN}$ . This case is not realizable with the current technology.
- *II*: case with global mass  $m_{tot} = 12.44 \text{ kg}$  and thrust  $T = 1 \text{ mN}$ .

As mentioned, BIT-3 can store up to 1.5 kg of propellant. Thus, if it was implemented in a 12.44 kg spacecraft —obtainable sacrificing 1.56 kg of payload from the Lunar IceCube—, all the asteroids could be reached with the projected missions. On the other hand, if the weight of the spacecraft was not changed and a hypothetical thruster with 1.4 mN-thrust and same propellant mass was used, asteroid 2012 UE34 could not be reached starting from L5. Of course, this is a hypothetical consideration, since such a thruster does not exist, and guessing its characteristics makes little sense.

Asteroid	Departure	$m_P^I$ (kg)	$m_P^{II}$ (kg)	Duration (days)	$V_\infty$ (km/s)
2014 FZ	L4	1.107	0.984	1207	4.09
2014 FZ	L5*	1.252	1.112	974	4.09
2004 FN8	L4	0.995	0.884	1104	3.48
2004 FN8	L5	1.168	1.038	876	3.55
2012 UE34	L4*	1.457	1.294	858	4.62
2012 UE34	L5*	1.622	1.441	618	4.38
2008 TS10	L4	0.926	0.823	1007	3.10
2008 TS10	L5	1.068	0.949	798	3.20
2015 XA397	L4	1.073	0.953	1196	3.43
2015 XA397	L5	1.234	1.096	972	3.45
2016 YE	L4	1.115	0.990	889	4.53
2016 YE	L5	1.392	1.237	816	4.50
2017 BN93	L4	0.762	0.677	618	1.87
2017 BN93	L5	1.042	0.926	538	1.87

Table 6.10: Missions performance summary

\* denotes a constrained fly-by

# Conclusion

The methodology and the results of an indirect method of optimization for missions with departure from the *Sun-Earth equilateral Lagrangian points* to rendezvous with near-Earth asteroids have been presented and discussed. The missions refer to *CubeSats* left as piggyback of a primary larger spacecraft in either L4 or L5, being the Lunar IceCube the reference model. Being L4 and L5 stable equilibrium points the spacecraft can wait, without the need for station-keeping manoeuvres, at the starting point, effectuating secondary operations and activities while waiting for the most favourable departure time. The missions leverage an *Earth-gravity-assist manoeuvre*, performed in the nearby of the minimum orbit intersection distance of Earth and asteroid, to perform the rendezvous with the target with the smallest propellant consumption. Thus, the spacecraft performs, in general, two thrusted arches in the first leg —i.e. L4-Earth or L5-Earth— to properly phase with the blue planet and to gain a sufficient hyperbolic excess velocity for the fly-by. This is used to obtain, or almost obtain, the orbital elements of the target asteroid and can be seen as an instantaneous rotation of  $V_\infty$ . The second leg —i.e. Earth-NEA— is used for minor corrections and adjustment manoeuvres, necessary to effectuate the rendezvous. First, free height fly-by is sought, then if the optimal mission results in a not admissible altitude the option of a minimum eight fly-by is explored.

The geometry of the mission allows a relatively easy definition of the first guess of the tentative solution, necessary to provide the convergence of the method. This, being an indirect method based on the *Optimal Control Theory*, provides precise and reliable solutions, but is sensitive to the precision of the first guess solution. A set of possible favourable targets has been defined, taking into account the MOID. Asteroids with a MOID inferior to 0.02 AU have been considered for the analysis, given their inherent compatibility with the EGA manoeuvre and due to the impact threat they may represent.

Different solutions, in time, have been found for seven asteroids among the ones selected, for missions with departure from either L4 and L5. These missions have been optimized in terms of final and initial time, and then only the most favourable in terms of phasing has been considered. The orbital properties of the target, as forecastable, strongly affect both the duration and the efficiency of the mission. In general, missions starting from L4 are slightly more efficient and roughly 200 days longer than their counterparts departing from L5. The phasing between Earth and asteroids affects both duration and final mass as well: closer the two bodies are at the close encounter the globally better is the mission. The results show the feasibility of the missions with the

current technology, accepting the disadvantage of a reduced payload or—but this option has not been considered in the present work—an increase in duration. Further developments in the considered technology may allow the fulfillment of the missions without constraints, and perhaps improving their efficiency or duration.

Possible future developments and refinements of the present work may include:

- Analysis of missions with the real characteristics of the Lunar IceCube, thus considering a longer initial leg. This would be necessary to provide the phasing and the gaining of the suitable  $V_\infty$  for the fly-by, with a lower  $T/m$  ratio than the one considered.
- Analysis of missions towards the targets not yet studied. As mentioned, only seven asteroids out of the sixty designated have been analysed, for clear time reasons. Moreover, future developments in the reference technology may make attainable targets now too demanding. Such broadening of the analysis is dynamic, since the number of discovered NEAs is constantly updated with new discoveries.
- Analysis of the proximity operations. Once the rendezvous has been carried out, it could be possible to study the evolution of the spacecraft orbit near the asteroid, analyzing its stability. Moreover, it could be interesting the analysis of close operations necessary to study the characteristics of the body, or even to deflect its trajectory.

# Bibliography

- [1] NASA, Jet Propulsion Laboratory, *Small-Body Orbital Elements*.  
[https://ssd.jpl.nasa.gov/?sb\\_elem](https://ssd.jpl.nasa.gov/?sb_elem)
- [2] NASA, Jet Propulsion Laboratory, *Near Earth Objects*.  
<https://cneos.jpl.nasa.gov/about/basics.html>
- [3] NASA, Jet Propulsion Laboratory, *Torino Impact Hazard Scale*.  
[https://cneos.jpl.nasa.gov/sentry/torino\\_scale.html](https://cneos.jpl.nasa.gov/sentry/torino_scale.html)
- [4] NASA, Jet Propulsion Laboratory, *Torino Technical Impact Hazard Scale*.  
[https://cneos.jpl.nasa.gov/sentry/palermo\\_scale.html](https://cneos.jpl.nasa.gov/sentry/palermo_scale.html)
- [5] Curtis, H., *Orbital Mechanics for Engineering Students*, Elsevier, Oxford, 2005.
- [6] Jahn, R. G., *Physics of Electric Propulsion*, McGraw-Hill, New York, 1968.
- [7] Casalino, L., *Ottimizzazione Indiretta di traiettorie Spaziali*.
- [8] Kirk, D. E., *Optimal Control Theory: An Introduction*, Dover Publications, Mineola, New York, 2004.
- [9] Casalino, L., *Equazioni in coordinate sferiche*.
- [10] eoPortal, *Lunar IceCube*, 2020.  
<https://directory.eoportal.org/web/eoportal/satellite-missions/1/lunar-icecube>
- [11] BUSEK, *BIT-3 RF Ion Thruster Datasheet*, 2019.  
[http://busek.com/index\\_htm\\_files/70010819F.pdf](http://busek.com/index_htm_files/70010819F.pdf)
- [12] Fasano, G. and János, D. P. Editors, *Modeling and Optimization in Space Engineering*, Springer, New York, 2013,  
Chapter 6, pp. 141-158, Colasurdo, G. and Casalino, L., *Indirect Methods for the Optimization of Spacecraft Trajectories*
- [13] Casalino, L., and Pastrone, D., *Efficient Missions to Potentially Hazardous Object 2013 TV135*, Journal of Spacecraft and Rockets, 2014, 10.2514/LA32890.

- [14] Casalino, L., Colasurdo, G. and Pastrone, D., *Optimal Low-Thrust Escape Trajectories Using Gravity Assist*, Journal of Guidance, Control, and Dynamics, 1999, 10.2514/2.4451